# POLITECNICO DI MILANO

Scuola di Ingegneria Industriale e dell'Informazione

Corso di Laurea Magistrale in Ingegneria Energetica

POLITECNICO
MILANO 1863

Hydrogen refueling stations:
Thermodynamic modeling and operational performance analysis
from the 3Emotion Project

Relatore: Prof. Gianluca VALENTI

Co-relatori: Prof. Enrico BOCCI

Dott. Andrea MONFORTI FERRARIO

Tesi di Laurea di:

Roberta CAPONI Matr. 906008

Anno Accademico 2019-2020

*Il tempo presente e il tempo passato*
*Sono forse entrambi presenti nel tempo futuro,*
*E il tempo futuro è contenuto nel tempo passato.*

T.S.Eliot

# Acknowledgments

I would like to thank Prof. Enrico Bocci and Andrea for giving me the opportunity to be part of this project from which I have learned so much and for the useful suggestions that guided me in the development of the thesis.
A sincere thank goes to Prof. Gianluca Valenti for his support and for the trust placed in me.
Thanks to all the partners of the 3Emotion Project with whom I have been in an ongoing correspondence and that gave me the possibility to analyze and present their data.
To my mum and dad, a huge thank for always supporting me, for giving me freedom in my choices and for guiding me throughout all these years. To my sister, I would like to say that without you, I would have much more space but certainly the time spent would have been much more boring. Thanks also to all my family, grandparents, uncles, aunts, and cousins. I love you.
Domenico, there are no words to describe how grateful I am for your help, love, for being close to me in the last years and for all the experiences that we lived together.
Finally, I would like to thank two dearest friends: Agnese it's over, we made it! Jessica, the last years were the best and I am very glad we met, and all the people that have accompanied me through these years.

# Sommario

Fra gli elementi cardine della transizione energetica globale, l'idrogeno è certamente uno dei protagonisti in grado di offrire, in molteplici settori, soluzioni valide. Senza dubbio esso giocherà un ruolo significativo nel processo di decarbonizzazione dei veicoli per il trasporto su strada che non potrà prescindere dalla creazione di una adeguata infrastruttura. Lo scopo di questo lavoro è quello di sviluppare un modello termodinamico in grado di valutare le prestazioni delle stazioni di rifornimento ad idrogeno. In particolare, il loro uso al fine di rifornire una flotta di autobus a celle a combustibile (350 bar). Il modello, implementato in MATLAB, simula un rifornimento "tank-to-tank" nel quale il processo è guidato dalla differenza di pressione fra uno stoccaggio ad alta pressione, dove è immagazzinato l'idrogeno, ed il serbatoio del veicolo, a più bassa pressione.

A causa dell'incremento di temperatura del gas durante il rifornimento la "Society of Automotive Engineers" ha sviluppato un protocollo, denominato SAE TIR J2601/2, che stabilisce i requisiti tecnici ed i parametri operativi atti a prevenire il raggiungimento di condizioni non sicure. Tuttavia, nonostante la SAE J2601/2 fornisca alcune raccomandazioni, una procedura standardizzata per veicoli pesanti non è ancora stata definita. Lo scopo di questo lavoro è quello di tentare di colmare questa importante lacuna. Per raggiungere questo obiettivo varie condizioni iniziali, come differenti temperature ambientali, pressioni iniziali del serbatoio dei veicoli e incrementi di pressione, sono state testate al fine di studiarne l'influenza sulle dimensioni cardine sul processo. Particolare attenzione è stata posta sul tempo di rifornimento ed un ulteriore algoritmo è stato sviluppato al fine di determinare l'incremento di pressione più adeguato a rifornire i veicoli nel minor tempo possibile rispettando i limiti.

Dalla simulazione del rifornimento della durata di 10 minuti con incremento di pressione uguale a 0.03 MPa/s si osserva che la quantità di idrogeno erogato è di 17.75 kg. Tale valore rispecchia le prestazioni delle stazioni di rifornimento del Progetto 3Emotion. In conclusione, l'analisi sui vari incrementi di pressione mostra come sia possibile ridurre in sicurezza del 62% la durata del rifornimento da vuoto a pieno del serbatoio passando da 0.03 a 0.06 MPa/s.

***Parole chiave**: Stazioni di rifornimento ad idrogeno, SAE J2601, APRR, rifornimento di veicoli pesanti, analisi termodinamica*

# Abstract

Among the participants of the global energy transition, hydrogen is certainly one of the protagonists that could offer in multiple sectors viable solutions. Undoubtedly, it would have a significant role in decarbonizing road vehicle transportation that cannot be reached unless an adequate hydrogen infrastructure is put in place. The aim of this work is to develop a thermodynamic model that assesses the operational performances of Hydrogen Refueling Stations (HRSs). In particular, their application for the refueling of fuel cell buses (350 bar) has been investigated. The model, implemented in MATLAB, simulates a tank-to-tank refueling where the pressure difference between a high-pressure tank, in which the hydrogen is stored, and a tank at lower pressure drives the process.

Due to the increase in the gas temperature during the refueling, the Society of Automotive Engineers has developed a protocol, denoted SAE TIR J2601/2, that establishes the performance requirements for the stations to ensure that unsafe conditions are not reached. However, although the SAE J2601/2 provides refueling recommendations, a standardized procedure for heavy-duty vehicles is far from being defined. This work is intended to address this lack of valuable knowledge. Furthermore, various operating conditions such as different ambient temperature, vehicle tank initial pressure, and Average Pressure Ramp Rates (APRRs) have been examined to assess their influence on the process parameters. Considerable attention is given to refueling time, and a further algorithm is presented with the objective of determining the most suitable APRR at which the vehicle tank is filled in the quickest time possible, within the allowable limits.

From the simulation of 10 minutes refueling with an APRR=0.03 MPa/s, was found that the amount of hydrogen dispensed is 17.75 kg. This value is aligned with the performances of the 3Emotion hydrogen station sites. In conclusion, the analysis of the effect of different APRR shows that is possible to safely reduce the duration of empty-to-full fuel cell bus refueling by 62% increasing the APRR value from 0.03 to 0.06 MPs/s.

***Keywords:*** *Hydrogen Refueling Stations, SAE J2601, APRR, heavy-duty vehicle refueling, thermodynamic modeling*

# Extended abstract

## Introduction

Hydrogen could play a vital role in tackling climate change and become a protagonist in the global energy transition. The reason for this is in its vast potential, as an energy carrier, to connect multiple sectors contributing deeply to their decarbonization.

An application in which compressed gaseous hydrogen is gaining much attention is for fueling fuel cell electric vehicles. Indeed, fuel cell vehicles offer long driving ranges, short refueling time, and together with the necessity of just one daily refill, high flexibility. The overall filling process is regulated by a strict protocol denoted SAE J2601 that provides performance requirements for gaseous hydrogen stations. These requirements ensure a costumer-acceptable and safe refueling since, during the process, the gas heats up may lead to potential hazards.

Two physical phenomena are responsible for this behavior: first, the heat of compression inside the tank occurring during the refueling. Second, the reverse Joule-Thomson effect that verifies when hydrogen is throttled since it is characterized by a negative Joule-Thomson coefficient in the temperature and pressure working conditions.

Therefore, being able to evaluate the temperature evolution in the tank correctly is of extreme importance. Previous scientific studies focused on determining the temperature distribution within a compressed gas cylinder during refueling. Multi-dimensional heat transfer analysis based on Computational Fluid Dynamics (CFD) were carried out by Dicken and Mérida [1-2] that investigated the temperature distribution in a compressed gas cylinder during refueling. Their results, validated by a set of experimental data obtained placing 63 thermocouples in a type III tank, showed a non-uniform temperature distribution during the filling. In contrast, Monde et al. [3-5] demonstrated that there is a consistent trend in the gas temperature distribution, and that can be accepted the uniformity assumption. Measured temperatures during fast fill up to 35 and 70 MPa well predicted the estimated values of their model. Zhao et al. [6] also performed CFD calculations on temperature rise with good accordance between the numerical simulation and empirical tests.

In other studies, a zero-dimensional modeling approach was adopted with the goal of estimating the overall performance of hydrogen storage systems [7-12]. However, the majority of the efforts made so far have been invested into the numerical and experimental investigation of the refueling process for a small-scale application like the one for personal transportation, while a less in-depth investigation has been addressed to the

refueling of heavy-duty vehicles, such as buses or freight vehicles. Additionally, although the protocol establishes safety limitations, a standardized procedure that regulates the overall process is far from being defined.

In this framework, in the present study, a thermodynamic model that analyzes the operational performances of the refueling of fuel cell buses is developed. To predict the process parameters evolution a zero-dimensional thermodynamic model based on mass and energy balance equations is proposed.

Variation of the ambient temperature, initial vehicle tank pressure, and Average Pressure Ramp Rate (APRR), which defines the desired pressure rise in the vehicle, are also carried out to verify their influence on the process parameters.

This thesis aims also to determine the most suitable APRR at which the tank system can be filled as fast as possible, within the constraints imposed. The results of the model are then compared with aggregate data from real-world refueling stations that are involved in the EU 3Emotion project.

## Thermodynamic model of refueling compressed hydrogen tanks

A zero-dimensional thermodynamic model is here presented, the aim of which is to provide a description of the behavior of a hydrogen refueling station during a refueling process from a tank storing high-pressure hydrogen (nominal working pressure 500 bar) to a tank at lower pressure (nominal working pressure 350 bar).

The model is focalized on predicting the gas temperature and pressure evolution within the vessels throughout the whole duration of the refueling, with particular regards to the temperature rise within the vehicle vessels, being constrained by safety limits. The whole refueling is simulated according to SAE TIR J2601/2, which applies to gaseous hydrogen powered heavy-duty vehicles. The performance and safety limits are recalled in Table 1.

**System overview and assumptions**

The station is designed to perform a tank-to-tank refueling, thus comprises one high-pressure storage, the vehicle storage system, both assumed adiabatic and connected through a lamination valve.

Pressure drop are not included since from their calculation was found that do not affect the refueling operation and heat transfer through the piping system is neglected. A sketch of the system is represented in Fig. 1. In both the storage tank, vehicle tank, and in the tank walls is assumed that the gas temperature, pressure, and density are uniform and stagnant condition prevails.

Table 1. SAE J2601/2 safety limits for the refueling of heavy-duty hydrogen vehicles

| **SAE J2601/2 Fueling Process Limits** | |
|---|---|
| Parameter | Limit |
| Ambient temperature range | -40°C-50°C |
| Maximum gas temperature | 85°C |
| Maximum dispenser pressure | 125%NWP |
| Maximum flow rate-normal filling | 0.06 kg/s |
| Maximum flow rate-fast filling | 0.12 kg/s |

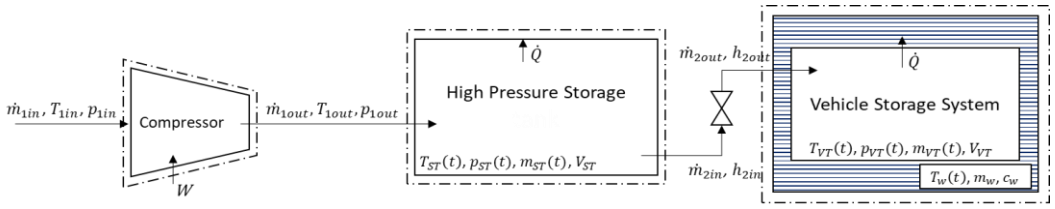


Fig. 1. Schematic representation of the entire station modeled

As a consequence, a lumped parameter approach is used to estimate the overall performance of the systems. For this hypothesis to be accepted, the Biot number, Bi, defined by the dimensionless quantity $\frac{k\delta}{\lambda}$, has to verify the condition Bi<0.1. In the ratio, $k$ is the convection heat transfer coefficient (W/m$^2$ K), $\delta$ is the thickness of the material, and $\lambda$ is the thermal conductivity of the material (W/m K). The type III tanks studied (metallic linear) showed a Bi=0.003, and insofar the lumped system analysis is applicable.

The tanks are dynamic, therefore the model is able of handling and describing the hydrogen migration between them. The refueling is governed by the APRR that describes the desired pressure variation in the vehicle tank, and the feed stream in a function of the temperature and pressure change, which is a significant improvement respect other analyzed models.

**General equations**

For stationary applications the kinetic and potential energies are usually negligible with respect to the enthalpy, heat, and work rates, hence the first law of thermodynamics, otherwise referred to as conservation energy principle, and the conservation of mass applied to an open control volume can be written in the form [1],[8-10] :

$$\frac{dU_{sys}}{dt} = \dot{Q} + \dot{m}_{in}h_{in} - \dot{m}_{out}h_{out} \quad (1)$$

$$\frac{dm}{dt} = \dot{m}_{in} - \dot{m}_{out} \quad (2)$$

$\dot{Q}$ (W) is the rate of heat transfer, $\dot{m}_{in}$ and $\dot{m}_{out}$ (kg/s) and $h_{in}$ and $h_{out}$ (J/kg) are the hydrogen mass flows and specific enthalpies entering and exiting the control volume, respectively.

**Modeling the heat exchange**

In this work, the internal heat transfer from gas to tank wall is considered, whereas it is not the heat exchange from the exterior tank surface to the surroundings since the tanks are well insulated and the refueling is relatively fast.

For the case of filling high-pressure vessels there is not a single standard methodology to calculate how the gas exchanges heat with the tank walls and difficulties are faced in the calculation of the convective heat transfer coefficient, $k_h$ (W/m$^2$K). Therefore, its determination is given to experimental studies and is strongly dependent on geometry, the orientation of the tanks, and the nature of the internal flow. In this study the

correlation for the Nusselt number developed by Bourgeois [12] is applied:

$$Nu_{dint} = 0.14\, Re_{dint}^{0.67} \quad (3)$$

Therefore, the heat exchange is dominated by the forced convection which depends on the dimensionless Rayleigh number calculated at the inlet of the pressure vessel.

For the case of discharging high-pressure vessels, the expression of reference is the correlation developed by Daney [13]. This relation is appropriate for turbulent natural convection in enclosures over the range of the Rayleigh numbers $7x10^8<Ra_H<6x10^{11}$.

$$Nu_H = 0.104\, Ra_H^{0.352} \quad (4)$$

The characteristic length for this equation is the cylinder height, $H$, since the high-pressure tanks in the station are disposed in a vertical position.

**Development of model equations**

From the energy and mass balance equations, the behavior of each component is derived.

*Compressor*

The compressor, for which a quasi-static model based on an isentropic compression transformation is applied, intervenes after the completion of the refueling process in order to restore the nominal pressure in the station's storage. In this works a two-stage reciprocating compressor with intercooling is modeled. Finally, for retrieving hydrogen state points, an external thermodynamic library named CoolProp is adopted.

The equations that allow calculating the electrical compression work and the cooling demand are the following: steady-state conditions ($\dot{m}_{in} - \dot{m}_{out} = 0$), adiabatic compression (Q=0), and no pressure drops.

$$W = W_{ST1} + \dot{W}_{ST2} = \dot{m}_{H2}\,(h_{in} - h_{out})\eta_{el}\eta_{mech} \quad (5)$$

$$Q_{IC} = \dot{m}(h_{int2} - h_{int1}) \quad (6)$$

where $h_{in}$is the specific enthalpy at the inlet conditions of the compressor, $h_{out}$ is the specific enthalpy at the outlet, $h_{int}$ is the specific enthalpy at the outlet of the first stage, $h_{int2}$ is the specific enthalpy at the inlet of the second stage. The assumption of isentropic compression enables the calculation of the unknown thermodynamic properties. For a reciprocating compressor, the isentropic efficiency is given by Eq. (7) [14]. This equation is valid for compression ratios ($r$) between 1.1 and 5:

$$\eta_{is} = 0.1091(\ln r)^3 - 0.5247(\ln r)^2 + 0{,}8577 \ln r + 0.3727 \quad (7)$$

*Compressed hydrogen tanks*

The analysis is based on the modeling presented by Xiao et al. [10], however the hypothesis of constant charge or discharge flow is not accepted here. Indeed, the refueling process is governed by a defined pressure increase established by the APRR. Considering the process of fueling a tank, therefore analyzing a process with positive inflow, the solution of the mass balance Eq.

(2), assuming a constant mass flow at each time is:

$$m = m_0 + \dot{m}t \quad (8)$$

Combining Eq. (8) with the energy balance Eq. (1) and expressing the rate of heat transfer between the gas and the inner tank wall in terms of a convective heat we obtain:

$$(m_0 + \dot{m}t)\frac{du}{dt} + \dot{m}u = \dot{m}h + k_h A(T_w - T) \quad (9)$$

Defining the characteristic temperature $T^*$ (K) as:

$$T^* = \frac{\gamma T_{\text{in}} + \alpha T_w}{1 + \alpha} \quad (10)$$

where $\gamma = c_p/c_v$ is the heat capacity ratio, $T_{\text{in}}$ the temperature of the incoming flow, $T_w$ the wall temperature, and $\alpha$ the dimensionless heat transfer coefficient that represents the ratio between the heat transfer intensity and the total heat capacity change:

$$\alpha = \frac{k_h A}{\dot{m} c_v} \quad (11)$$

The equation that describes the evolution of the temperature of the gas in a tank simplifies to:

$$\frac{dT}{dt} = (1 + \alpha)\frac{T^* - T}{t^* + t} \quad (12)$$

Finally, with the initial conditions $T = T_0$, and equal to the ambient temperature, at $t = 0$ the solution of the differential equation can be found:

$$T = f_g T_0 + \left(1 - f_g\right)T^* \quad (13)$$

$f_g = (m_0/m)^{(1+\alpha)}$, is the fraction of initial mass over total. The same equations can also be applied for a discharging process, changing the sign of the flow.

While in the storage vessel (much larger volumes implemented) the gas temperature variation is minor, for the vehicle vessel (typically of smaller size) the effect of the tank walls and its heating cannot be ignored. The energy balance becomes:

$$\frac{d(m_w c_w T_w)}{dt} = A_{in} k_h (\mathrm{T} - T_w) \quad (14)$$

where $m_w$ and $c_w$ refer respectively to the mass of the tank wall (kg) and the specific heat of the tank wall (kJ/kg K). Solving Eq. (14) with the initial condition $T_w = T_{w0}$ (at the beginning of each refueling the tanks are in thermal equilibrium with the ambient) at $t = 0$ it can be obtained an analytical expression of the temperature rise in the tank walls.

$$T_w = f_w T_{w0} + (1 - f_w)T \quad (15)$$

Here, $f_w = e^{-\tau_w}$ and $\tau_w$is a dimensionless time for the tank walls.

*Reduction valve*

The pressure difference between the high-pressure storage tank and the vehicle tank requires the adoption of a reduction valve that regulates the pressure so that at the outlet the pressure is equal to the identified APRR. Since no work is added, the expansion can be considered adiabatic, and the mass flowing in the valve is conserved, the energy balance for a steady-state process describes an isenthalpic process, i.e. $h_{in} = h_{out}$.

The effect of hydrogen throttling is an increase of the temperature at the outlet of the valve as a result of the Joule-Thomson effect.

**Modeling the real gas equation of state**

A real gas equation is required rather than the ideal gas law due to the high density of hydrogen and the pressure of refueling, therefore a compressibility factor Z must be introduced. In this study, a virial equation is used to define the aforementioned factor [15]:

$$Z = \frac{p\ v}{R_{gas}T} = (1 + \mathrm{B}p) \qquad (16)$$

where $R_{gas}$ is the gas constant, equal to 4.124 kJ/kg K, and $\mathrm{B}$ is a coefficient that depends on temperature according to the relation, $B = B_1/T + B_2/T^2 + B_3/T^3$.

According to the study from Chen et al. [17] in the temperature range 173 K to 393 K Eq. (16) can be truncated at the first term and the fitted value becomes $B_1$=1.9155x10$^{-6}$ K/Pa. As a consequence, the real gas equation is as follows:

$$Z = \frac{p\ v}{R_{gas}T} = \left(1 + \frac{B_1 p}{T}\right) \qquad (17)$$

## Implementation

The thermodynamic model developed in this work has been implemented in MATLAB, and an iterative algorithm has been developed for predicting the evolution of the physical parameters within the components throughout the whole duration of the refueling. Then, an additional functionality to the previous algorithm has been developed to analyze the effect of the speed of the APRR on the refueling duration.

Table 2. Initial filling condition and geometric properties

| **Input parameter** | |
|---|---|
| Vehicle tank volume, $V_{VT}$ | 4x322 L |
| Ambient temperature, $T_{amb}$ | 15 °C |
| Vehicle tank initial pressure, $p_{0,VT}$ | 2 MPa |
| Vehicle tank initial temperature, $T_{0,VT}$ | 15 °C |
| Internal diameter of vehicle tank, $D_{int}$ | 0.49 m |
| Internal diameter of the injector, $d_{int}$ | 0.012 m |
| Storage tank initial mass | 350 kg |
| Storage tank initial pressure | 50 MPa |
| Storage tank volume | 11 m$^3$ |
| Storage tank internal area | 97.47 m$^2$ |

**Algorithms description**

The initial filling conditions and the geometric tank characteristics used in the model are shown in Table 2. The entire refueling is modeled trough an iterative procedure in which the initial conditions are determined based on the initial condition of the tanks and the thermodynamics at each step are found using the information of the preceding iteration. The setting of the APRR allows the determination of the pressure increase in the vehicle tanks. While via the coupling of the energy equation for the gas inside the cylinder Eq. (13) and the real gas equation Eq. (17), the temperature and mass evolution in the vehicle tanks can be found. To obtain those results, the MATLAB function *fsolve* was used.

Due to the mass conservation equation Eq. (2), the mass flow in and out the lamination valve is the same, therefore

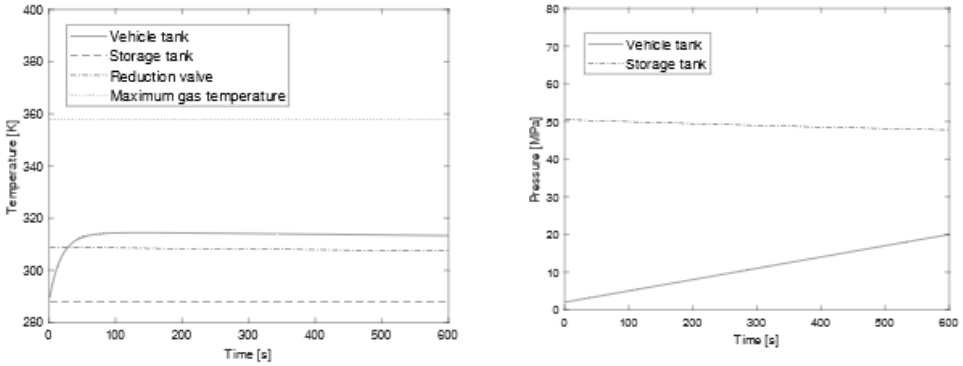


Fig. 2. Thermodynamics of hydrogen refueling process over time: temperature (a) and pressure (b)

it is known the mass depletion inside the storage vessels to which corresponds a variation of the pressure and temperature respect their initial condition.

In the second algorithm the APRR is not fixed, but the code runs for a range of values and it stops when it is reached the specified amount of hydrogen to be dispensed or once any of the fueling parameter safety limits have been exceeded. This enables to perform a parametric study on the most suitable ramp rate that accomplishes the refueling in the shortest time possible.

## Results and discussion

In this section, the numerical results of the model and its variations are presented.

**Vehicle tank refueling process simulation applied to 3Emotion Project**

The first simulation describes the thermodynamic behavior of the station for the refueling of the vehicle tank. The filling time is 600 seconds, and the APRR=0.03 MPa/s.

Fig. 2(a) shows the temperature evolution in the storage tank, the vehicle tank, and at the outlet of the reduction valve. The temperature out of the storage tank decreases as mass is leaving, although the effect is not very marked. Across the reduction valve a temperature increase takes place caused by the reverse Joule-Thomson effect, moreover, the temperature at the outlet decreases as the refueling proceeds as a result of decreasing pressure difference between the storages. Lastly, the temperature in the vehicle tank increases rapidly at the beginning of the refueling when the mass flow entering the system is higher, leading to a more considerable heat of compression than it flattens to a plateau. The temperature increment at the end of the refueling is 25°C. Furthermore, is also displayed the maximum gas temperature limit (358 K) set by the SAE J2601/2 in the dotted line.

Fig. 2(b) shows the pressure variation in the two systems. The pressure out of the storage tank decreases due to mass leaving the tank. Whereas the pressure increases linearly in the vehicle tank at a rate established by the APRR, and at the end of the refueling is reached a pressure of 20

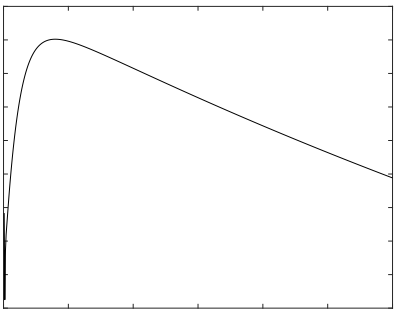

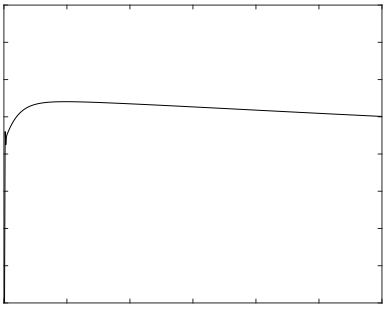

Fig. 3. Mass flow rate profile overtime for the refueling of the vehicle tank

MPa (target pressure). At the end of the refueling the amount of hydrogen dispensed is 17.75 kg.

Fig. 3 shows the mass flow of hydrogen during the charging process. The mass flow is induced by the pressure difference, thus it grows in the first part of the refueling than after a peak it steadily decreases. In this case, the maximum flow rate imposed by the standard for a normal filling (0.06 kg/s) is never exceeded, and the result is comparable with the real data collected from the 3Emotion stations' dataloggers. The curve mean value, 0.026 kg/s, is indeed aligned with the trend of the average flow rate measured for the 18 months of analysis: see Fig. 4.

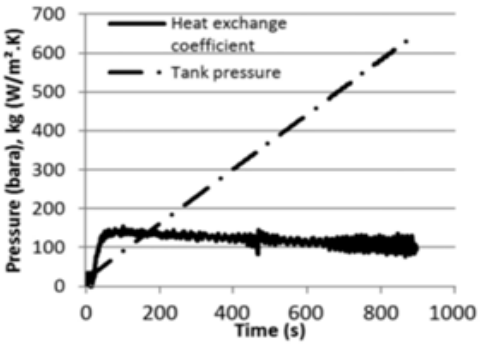


Fig. 5. (a): Heat transfer coefficient profile obtained from the model. (b): Heat transfer coefficient from the study of Bourgeois et. al

*Heat transfer coefficient evolution*

In Fig. 5(a) is plotted the heat transfer coefficient between the gas and tank wall throughout a fill process for the model. Comparatively to what has been predicted in literature [12],[19] the convection coefficient increases rapidly within the first seconds and then declines progressively. Indeed, its evolution is strongly related to

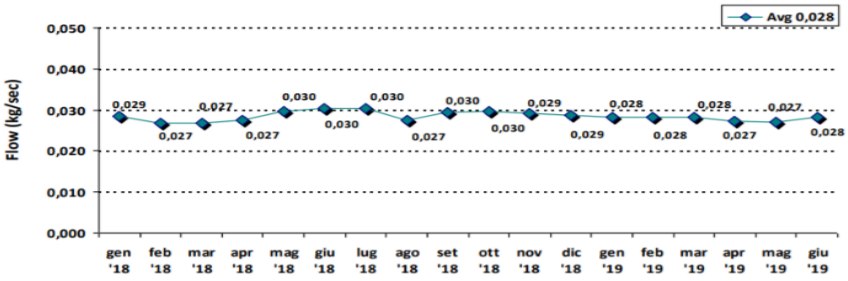


Figure 4. Average flow rate measured in the 3Emotion station for the 18th months of analysis

the rate of mass flow entering the tank; the greater the mass flow rate, the greater is the increase in the coefficient in consequence of higher turbulence at the inlet of the cylinder, that is the cause of the heat exchange. To verify the validity of the heat transfer model, the algorithm has been tested with the data from the study of Bourgeois et al. [12] and the results compared (Fig.5(b)). The resemblance of the two curves is evident, first a quick increase, up to a maximum value of about 157 W/m$^2$K, followed by a nearly linear drop.

**Storage tank refueling process simulation**

A simulation of the storage tank is provided in Fig.6. From the initial condition, i.e., 47.75 MPa and 15°C, to the nominal pressure of 50 MPa the station takes 1911 seconds. The speed of this refilling time strictly depends on the compressor capacity, which is constant and equal to 0.0062 kg/s.

As can be seen in Fig.7 the work performed by the compressor, calculated as expressed in Eq. (5), increases as the

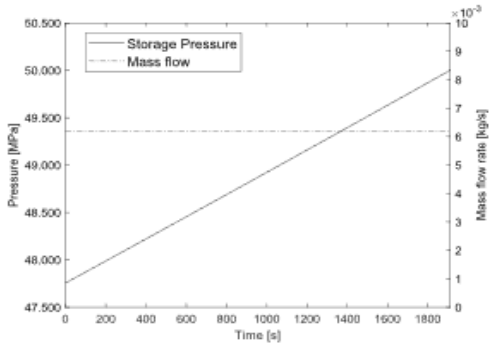


Fig. 6. Pressure evolution in the filling of the storage tank and flow rate at the inlet of the tank.

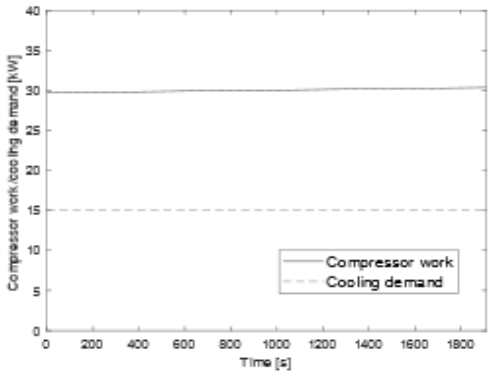


Fig. 7. Compressor work for the filling of the storage tank and consumption of the intercooler

filling advances due to higher pressure ratios in the second stage as the pressure in the tank reaches the nominal value. Instead, the compressor cooling demand is constant ed equal to 15 kW. The reason is that the operating temperatures of the intercooler are fixed, and the mass flow that is suctioned by the compressor is also constant.

**Variation of ambient temperature**

The effects of ambient temperature on the temperature distribution within the cylinder, on the SOC, and on the refueling time is investigated. The initial pressure is 2 MPa, the APRR set to 0.03 MPa/s, while the ambient temperature is varied between 15 and 30 °C. The results are summarized in Table 3. It can be seen that the temperature distributions (Fig. 8) run almost parallel, indeed the temperature difference between the beginning and the end of the refueling process is approximately the same. Moreover, the higher is the ambient temperature the greater is the peak. This is due to a greater

Table 3. Effect of the ambient temperature over the refueling time, SOC, and final vehicle tank temperature. Initial pressure set at 2 MPa

| $T_{amb}$ [°C] | Filling time [s] | SOC [%] | Final temperature vt [K] | ΔT [°C] |
|---|---|---|---|---|
| **15** | 600 | 59.78 | 313.3 | 25.33 |
| **20** | 600 | 59.72 | 318.6 | 25.62 |
| **25** | 600 | 59.66 | 323.8 | 25.88 |
| **30** | 600 | 59.60 | 329.1 | 26.16 |

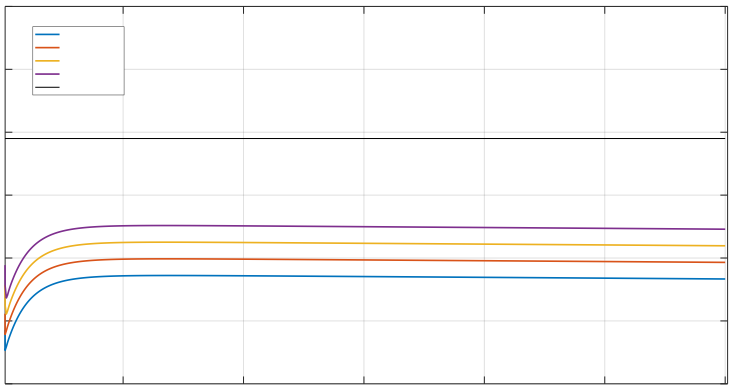

Fig. 8. Gas temperature profile at different ambient temperatures between 15 and 35 °C. APRR=0.03 MPa/s, $p_0$=2 MPa

initial heating of the tank that clearly lead to a higher gas temperature. However, the increase of the ambient temperature has a very limited effect on the SOC, that reaches in any case values close to 60% with equal refueling times.

**Variation of the initial vehicle tank pressure**

In this simulation the initial pressure was varied between 2 MPa and 30 MPa while the ambient temperature is fixed at 15°C. Fig. 9 shows that the refueling from the 2 MPa manifests in a more significant increase in temperature, whereas with 30 MPa the increase is smaller. Therefore, filling with a lower initial pressure yields to a higher overall temperature increment. Table 4 illustrates these relative values, furthermore, shows the variation of the SOC between the refueling beginning and end, which diminishes with increasing initial pressures.

**APRR parametrization study**

In conclusion, the influence of different APRRs for filling the vehicle tank up to its full capacity, that is 30 $kg_{H2}$, is described. The APRR is thus varied between 0.01 MPa/s to 0.08 MPa/s with an increment of 0.01MPa/s, while the selected initial conditions are 15°C and 2 MPa. The aim is to determine which of those APRRs allow to refuel the vehicle in the shortest time

Table 4. Effect of the initial pressure over the refueling time, SOC, and final vehicle tank temperature. Ambient temperature set at 15 °C

| Initial $P_{VT}$ [°C] | Filling time [s] | Initial SOC [%] | Final SOC [%] | Final $T_{VT}$ [K] | ΔSOC [%] |
|---|---|---|---|---|---|
| **2** | 600 | 5 | 59 | 313.3 | 54 |
| **10** | 600 | 27 | 80 | 312.5 | 53 |
| **20** | 547 | 51 | 99 | 310.2 | 48 |
| **30** | 191 | 72 | 99 | 229.6 | 27 |

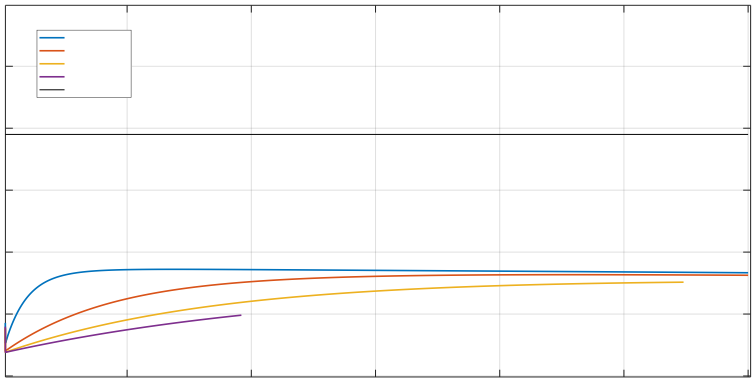

Fig 9. Gas temperature profile at different initial tank pressure between 2 and 30 MPa. APRR=0.03 MPa/s, $T_0$=15°C MPa

possible while maintaining compliance with the SAE J2601/2 guidelines.

Fig. 10 shows the APRRs and their relative refueling time. As might be expected, the higher is the APRR, the lower is the refueling time, despite this correlation is not linear. Although the highest APRR values seem to be the preferred option, they do not respect the mass flow rate limit. In Fig. 11 is shown the mass flow rate over time for each APRR and displays the maximum value allowed by the SAE J2601/2. It is evident that the peaks for the flow rate calculated with APRR=0.07 MPa/s and APRR=0.08 MPa/s overcome the safety limit. Therefore, the quickest way to fill the tank up to 30 kg is to adopt APRR=0.06 MPa/s to which corresponds a refueling of 581 seconds. Finally, a comparison of the thermodynamic behavior between the different cases is presented. Fig.12 shows the gas temperature profiles. For each specified APRR, the gas temperature increases and then flattens, but the greater the APRR, the higher the peak that, in addition, is reached in a shorter time. Furthermore, the curves tend to get nearer because of the predominant influence of the internal forced convection.

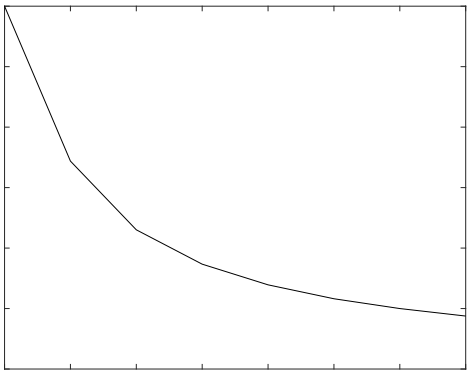

Fig 10. Refueling time reduction as a consequence of higher values of the APRR

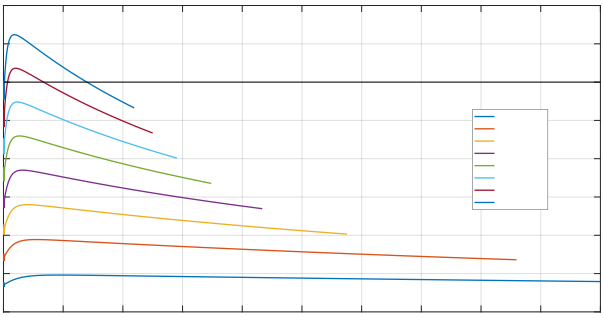

Fig 11. Mass flow rate overtime at different APRR between 0.01 and 0.08 MPa/s. Simulation for the filling to full capacity. $T_0$=15°C MPa/s, $p_0$=2 MPa

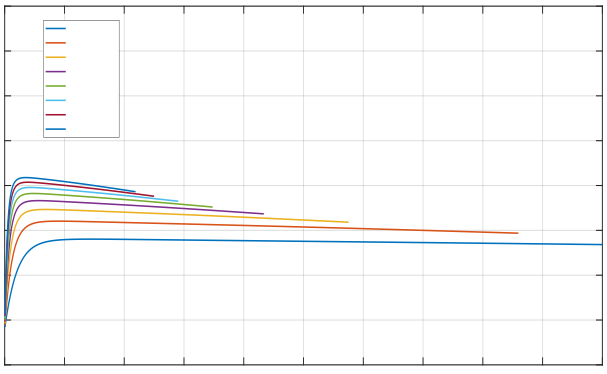

Fig 12. Gas temperature profile overtime at different APRR between 0.01 and 0.08 MPa/s. Simulation for the filling to full capacity. $T_0$=15°C MPa/s, $p_0$=2 MPa

## Conclusions

From this analysis the following conclusions can be drawn:

- Filling the vehicle tank with an APRR=0.03 MPa/s, we are always in a safe condition in which the pressure, temperature, and density limits given by the SAE J2601 are never exceeded. The heating of the gas in the tank follows a non-linear shape and starting from an ambient temperature of 288 K, and an initial pressure of 2Mpa at the end of the refueling, the gas temperature reaches 313.33 K and a final pressure of 20 MPa. The amount of hydrogen dispensed at the end of the process is 17.75 kg.

- The correlation proposed by Bourgeois [12] for the modeling of the heat transfer in horizontal cylinders filled with high-pressure gas seems to apply well to the case under investigation. This is confirmed by the comparable behavior of the heat transfer coefficient profile calculated in the study and the one obtained from the algorithm tested with the data from the literature.

- The effect of varying the initial vehicle tank pressure is more significant than changing the ambient temperature. In general, a higher ambient temperature and a lower tank pressure result in a higher maximum and final temperature. Whereas, for greater initial pressures the refueling time and the SOC considerably decrease.

- The filling time and the refueling speed are strongly correlated: the lowest the first, the highest the second, and hence the APRR that should be set by the station. For the case of filling up the vehicle up to its full capacity the most appropriate APRR is 0.06 MPa/s.

## Future works

In the present thesis, the refueling of fuel-cell buses has been presented from a system perspective and can be considered a preliminary study for this type of application. Further suggestions concern performing an extensive validation of the model and experimental measurements on the various components, improving the modeling of the station including an electrolyzer, a cascade system or simulating several fillings in a row.

# Contents

# List of figures

# List of tables

# Nomenclature

## Roman letters

| | |
|---|---|
| $A_{in}$ | Internal surface area of tank, $m^2$ |
| $c$ | Compressor clearance, % |
| $c_p$ | Constant-pressure specific heat, kJ/kg/K |
| $c_v$ | Constant-volume specific heat, kJ/kg/K |
| $c_w$ | Specific heat of tank wall, kJ/kg/K |
| $d$ | Dimeter of the injector, m |
| $D$ | Tank diameter, m |
| $f$ | Darcy friction factor |
| $f_g$ | Fraction of initial mass over total mass, $f_g=m_0/m$ |
| $g$ | Acceleration of gravity, $m/s^2$ |
| $h$ | Specific enthalpy of hydrogen, kJ/kg |
| $h_{in}$ | Specific enthalpy of inflow hydrogen, kJ/kg |
| $h_{out}$ | Specific enthalpy of outflow hydrogen, kJ/kg |
| $H$ | height of the tank, m |
| $k_h$ | Heat transfer coefficient at inner surface, kW/ $m^2$/K |
| $L$ | Length, m |
| $m$ | Hydrogen mass in tank, kg |
| $m_0$ | Initial mass in tank, kg |
| $\dot{m}_{in}$ | Hydrogen mass inflow rate, kg/s |
| $\dot{m}_{out}$ | Hydrogen mass outflow rate, kg/s |
| $m_w$ | Mass of tank wall, kg |
| $N$ | Compressor speed, 1/s |
| $p$ | Pressure of hydrogen, Mpa |
| $\dot{Q}$ | Heat transfer rate, W |
| $r$ | Compression ratio |
| $R_{gas}$ | Gas constant,$R_{gas}=4.124x10^{-3}$ kJ/K/mol |
| $s$ | Specific entropy, KJ/kg/K |
| $t$ | Time variable, s |
| $t^*$ | Characteristic time, $t^*=m_0/\dot{m}$, s |
| $T$ | Temperature of hydrogen, K |
| $T^*$ | Characteristic temperature, $T^*=(\gamma T_{in}+\alpha T_w)/(1+\alpha)$, K |
| $u$ | Specific internal energy, kJ/kg |
| $v$ | Flow velocity, m/s |
| v | Specific volume, kg/ $m^3$ |
| $V$ | Volume of the tank, $m^3$ |
| $W$ | Work, W |
| $Z$ | Compressibility factor |

## Greek symbols

| | |
|---|---|
| $\alpha$ | Dimensionless heat transfer coefficient, $a=k_hA/(c_v\dot{m})$ |
| $\beta$ | Volumetric thermal expansion coefficient |
| $\gamma$ | Ratio of specific heats, $\gamma=c_p/c_v$ |
| $\delta$ | Thickness, m |
| $\varepsilon$ | Pipe roughness, m |
| $\eta$ | Efficiency |
| $\lambda$ | Thermal conductivity, W/m/K |
| $\mu$ | Dynamic viscosity, Pa s |
| $\nu$ | Kinematic viscosity, $\nu = \mu/\rho$, $m^2/s$ |
| $\rho$ | Density, $kg/m^3$ |
| $\tau$ | Dimensionless time, t/ $t^*$ |

## Acronyms

| | |
|---|---|
| APRR | Average Pressure Ramp Rate |
| BEB | Battery Electric Bus |
| BEV | Battery Electric Vehicle |
| CFD | Computational Fluid Dynamics |

| | |
|---|---|
| CHIC | Clean Hydrogen in European Cities |
| CIRPS | Interuniversity Research Center for Sustainable Development |
| DOE | Department of Energy |
| FCEB | Fuel Cell Electric Bus |
| FCEV | Fuel Cell Electric Vehicle |
| FCH JU | Fuel Cells and Hydrogen Joint Undertaking |
| GHG | Greenhouse Gas |
| HRS | Hydrogen Refueling Station |
| IECV | Internal Combustion Engine Vehicle |
| MAF | Monitoring & Assessment Framework |
| NREL | National Renewable Energy Laboratory |
| NWP | Nominal Working Pressure |
| PMI | Project Management Institute |
| SAE | Society of Automotive Engineers |
| SOC | State of Charge |
| TCO | Total Cost of Ownership |
| TIR | Technical Information Report |

**Subscripts**

| | |
|---|---|
| o | Initial, standard |
| amb | Ambient |
| cyl | Cylinder |
| el | Electrical |
| h | Convective |
| in | Inlet |
| int | Internal |
| is | Isentropic |
| mech | Mechanical |
| out | Outlet |
| sys | System |
| ST | Storage tank |
| ST1 | First stage |
| ST1 | Second stage |
| v | volumetric |
| VT | Vehicle tank |
| w | wall |
| H2 | Hydrogen |

**Dimensionless numbers**

| | |
|---|---|
| Bi | Biot number |
| Nu | Nusselt number |
| Ra | Rayleigh number |
| Re | Reynolds number |

# Chapter 1

# Introduction

The first part of this chapter introduces the reasons why hydrogen is gaining increasing attention in the last decades as an energy transition towards more clean, versatile, and efficient sources are needed to tackle issues like climate change, security of supply, and fossil fuel depletion. Hydrogen can be used for a wide range of applications; this thesis focuses on its employment as an alternative to fossil-based fuels for road transportation vehicles, in particular for heavy-duty applications, such as for large passenger transportation. In the second part, the research objectives and the novelties of the thesis are outlined. It is also illustrated the methodology and the literature inherent to the subject. Ultimately, the structure of the thesis, hence the description of the chapters is presented.

## 1.1 Need for climate action

From the massive bushfires that flared up in Australia for three months to the severe floods that interested Indonesia the last January and China in June until the abnormal heat registered in the Antarctic Peninsula at the beginning of February, when a record temperature of 18.4 °C has been logged, to recall a few of the most recent and extreme events, are all a manifestation -now more than ever- that global warming is seriously putting under threat human and natural systems.

Limiting global warming means to reduce anthropogenic $CO_2$ emissions. The Intergovernmental Panel on Climate Change held in 2018 found that in order to stay below 1.5°C of warming, global net anthropogenic $CO_2$ emissions should decline by around 45% by 2030, from 2010 levels, reaching net-zero by around 2050 [1]. Still, the path towards a low-carbon energy system is far to be achieved with emissions that are rising up [2], hence it is fundamental to reaffirm the need for urgent climate action as agreed in the United Nations Secretary-General's Global Climate Action Summit in September 2019 [3].

Hydrogen could play a vital role in tackling climate change and become a protagonist in the global energy transition. The reason for this is in its vast potential, as an energy carrier, to connect multiple sectors contributing deeply to

their decarbonization. Although the majority of hydrogen produced today is from fossil fuels, hydrogen produced from renewable energy, otherwise known as “green hydrogen”, is a near-zero carbon production route and is rapidly growing interest due to the falling costs of renewable power and to facilitate the integration of a large amount of variable renewable energy [4].

Hydrogen is highly versatile and can be used in a wide range of applications that include: industry, currently the largest share of the hydrogen produced every year in pure form is exploited for ammonia and oil refining production; buildings and power, mixed with natural gas can reduce emissions in end-use sectors; transport as fuel powering Fuel Cell Electric Vehicles (FCEVs) [5]. In this last sector, hydrogen is gaining much attention with 4 000 fuel cell electric cars sold in 2018, registering an increase of 56% respect the previous year [6]. It is a small number compared to one of Battery Electric Vehicles (BEVs), but the advantageous characteristics of having a driving range and refueling time similar to conventional Internal Combustion Engine Vehicles (ICEVs) suggest a potential increase of the FCEVs share in the market. In particular, one of the segments in which this expansion could have a wide development and significant advantages over BEVs is heavy-duty transportation (forklifts, trucks, and buses) [7].

### 1.1.1 Decarbonizing road transport

The sustainability of FCEVs and BEVs in comparison with diesel vehicles is assessed when are investigated the Greenhouse Gas (GHG) emissions, energy efficiency, and the costs. It is straightforward that, on a tank-to-wheel basis, the deployment of fuel cell electric vehicles and battery electric vehicles have a significant impact on the reduction of GHG emissions since, during driving, they do not emit any $CO_2$ or do not generate any other pollutant gas typical of ICVs. However, a complete evaluation requires that also the well-to-tank phase should be considered, thereby the emissions in the fuel path from the production of the energy source to fuel supply (transport to the fuel station) should be examined. The two indexes are a subset of a more comprehensive methodology, defined as well-to-wheel, that tracks the entire energy consumption and GHG emissions of a fuel in the production, supply, and use, and it is the most suitable when different fuels and drivetrains are confronted. FCEVs are the only ones that can potentially operate with zero $CO_2$ emissions along the entire value chain when hydrogen is produced entirely from a renewable source. Whereas if it derives from a carbon source, it is likely to achieve a $CO_2$ reduction of around 40 to 45%. For BEVs it is more difficult

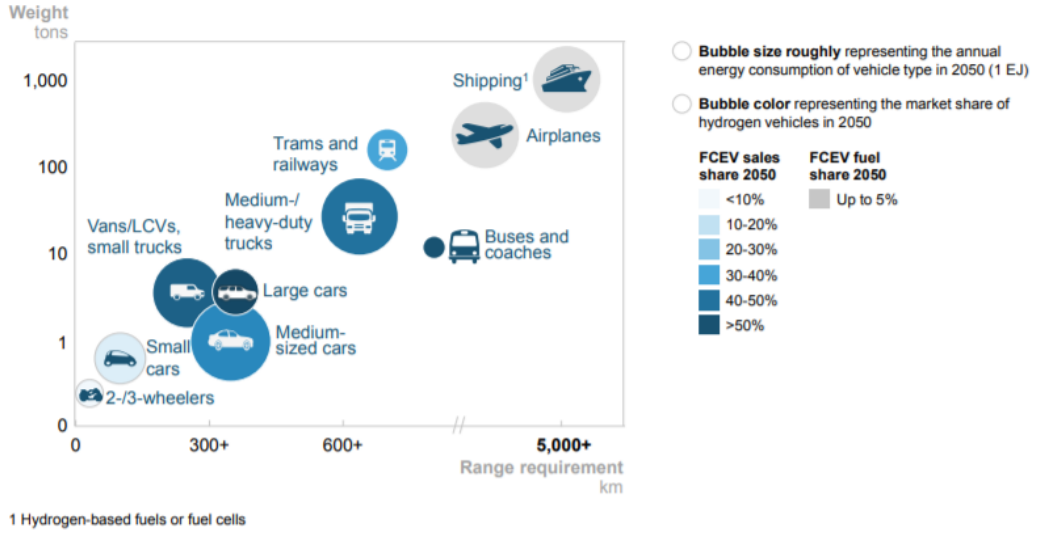


Figure 1.1. Transportation market segmentation by 2050. Source: Hydrogen Council 2017

to uniformly quantify the $CO_2$ reduction potential since the emissions strictly depend on the emission factors related to each countries' power mix, hence vary from where the vehicle is charged.

The main characteristic that distinguishes the BEVs from the other two technologies is the limited travel range due to the low energy density of the batteries. Despite allowing to reach peak power and average power with high efficiency, for long-distance travel BEVs seem to lose competitiveness requiring adequate infrastructure and long charging time. On the contrary, it could be the ideal solution for smaller passenger vehicles where the circulation of FCEVs could suffer because of unfeasible costs and technological issues.

Hydrogen, instead, has a remarkably higher energy density and can be operated likewise the ICVs. In fact, the FCEVs range is comparable and determined by the fuel tank size, and the short refueling times, as well as the necessity of just one daily refill, guarantee high flexibility. These factors, combined with the requirement of large fuel cells to deliver the peak power, makes these vehicles best suited for heavy-duty applications, such as for freight or large passenger transportation [8]. Specifically, the analysis of an average bus duty cycle that consists of 12 to 20 hours a day of operation, with frequent stops, low speeds, high auxiliary loads, highlights the advantages of Fuel Cell Electric Buses (FCEBs) over Full Electric Buses (BEBs) [9]. The Hydrogen Council [10] has estimated the segmentation of the transport sector upon vehicle weight and demanded driving range and for each market share the sales of the FCEVs by 2050 (see Figure 1.1). According to their esteem, FC drivetrains would be employed mainly in the bus

segment, whereas they are less attractive for small cars application. While the progress with heavy-duty commercial freight vehicles has been more limited, FCEBs are being deployed in growing numbers, with China and South Korea the leading countries [11].

To conclude, an accurate cost-based comparison between different vehicle technologies should explore not only the purchasing price but also operating, capital, and downtime costs as well as the social cost of pollution, namely what should be considered is the Total Cost of Ownership (TCO). Due to higher purchasing costs and thus, higher financing costs of the new bus technologies, the TCO for standard diesel buses is lower, although several studies agree that the capital cost and the maintenance cost are expected to decrease significantly in the coming years. The gap will be further reduced moving past the niche market size towards the production-at-scale [12] [13]. These observations suggest that the zero-emission powertrains are complementary, rather than competing technologies and can deeply contribute to the decarbonization of the transport sector.

### 1.1.2 EU bus projects

Many countries worldwide are investing in FCEB technology. Above all, as aforementioned before, China and South Korea that along with Japan, account for more than 55% of all worldwide patents regarding fuel cells and plans the deployment of more than a thousand buses in the next upcoming years [8]. In the US, the State of California was the pioneer in the deployment of low- and zero-emission propulsion technologies, and since 2007 the US Department of Energy's (DOE's) National Renewable Energy Laboratory (NREL) undertakes to publish an annual report on the status and progress from demonstrations of FCEB in the country. Finally, also the EU is pushing in the direction of emissions reductions and is funding several demonstration projects to commercialize electric-drive technologies by way of public-private partnerships supported by the Fuel Cell and Hydrogen Joint Undertaking (FCH JU). Among the most recent, the Clean Hydrogen in European Cities (CHIC) Project brought together a coalition of partners from industry, cities, and research organizations to operate a fleet of 54 FCEBs and hydrogen refueling stations in nine cities across Europe. The project was successfully completed in December 2016, meeting the expectations and demonstrating all the advantages that FCEBs can offer [14].

The High V.LO-City Project plans to implement 14 FCEBs in four regions across the European Union. It has the goal of facilitating the mobilization of FCEBs and the dissemination of clear information on hydrogen bus operations to transport authorities and key decision makers [15].
On a small scale under the HyTransit project were introduced a fleet of six FCEBs in Aberdeen, Scotland, to test the technology on demanding inter-city UK routes [16].

The lessons learned of these previous projects underline the role of the regional and local authorities as one of the most important facilitators of the FCB adoption. Their involvement is one of the most important goals of the 3Emotion (Environmentally friendly Efficient Electric Motion) Project, which aims to bridge the gap between current demonstrations and develop a plan for commercialization [9].

Other more recent projects have been announced (JIVE, JIVE2, MEHRLIN, H2BUS EUROPE) that will lead to volume scaling-up and the mobilization of more than 1,200 buses across Europe in the next years. The scaling-up will make indispensable more effective management of the refueling phase (also with multiple buses fueling simultaneously or back-to-back) that, as it has been described in chapter 1.1.1, represents one of the major advantages of fuel-cell technology. For the first time, this will pose to the station operators the urgency of reducing the refueling operation, both to preserve that advantage distinctive of the technology and to contain the investment costs related to the installation of the refueling stations.

## 1.2 Objectives

This present work aims to develop a thermodynamic model to assess the operational performances of hydrogen refueling stations. The model is compared with aggregate data from real-world refueling stations that are involved in the EU 3Emotion Project.

More specifically, the case of a tank-to-tank refueling is investigated, which is governed by the pressure difference between the high-pressure tank where the hydrogen is stored and the vehicle tank at a lower pressure. The modeling of the entire system includes a high-pressure storage tank, compressor, lamination valve, vehicle storage tank, and the study of the heat transfer provide a description

of hydrogen thermodynamic behavior during refueling. Both the refueling of the vehicle tank and the refilling of the storage tank is performed.

Moreover, a variation of the operating conditions such as different ambient temperature and initial vehicle tank pressure is carried out to assess their influence on the process parameters.

Additionally, attention is paid on refueling time thus it is investigated the optimal refueling rate that minimizes the refueling duration without exceeding the safety limits delineated by the Standard Protocol SAE J2701/2 that has been developed to regulate the refueling. To achieve this, a parametric study on the refueling rates for dispensing a specified amount of hydrogen is performed.

## 1.3 Methodology

The starting point of the present thesis is investigating the thermodynamics of hydrogen refueling stations for fueling heavy-duty vehicles (i.e., buses). The overall station has been modeled in MATLAB, and an iterative algorithm has been developed for predicting the gas temperature evolution and pressure variation within the vessels throughout the whole duration of the refueling. The values of these parameters are determined through a numerical procedure that solves at once the energy balance equation, for which it is applied a lumped parameter model, and the real gas equation. The heat transfer characteristics proper of the vessels involved have been determined through a critical study of the literature concerning light-duty vehicles, for which numerical and empirical studies have been conducted in several studies. Furthermore, the energy consumption of the station compressor for fueling the station storage to restore the pressure is presented. Finally, the influence of the ambient temperature and initial tank pressure on the evolution of the gas temperature during hydrogen refueling, as well as on the refueling time and state of charge are investigated.

To obtain the thermodynamic properties of the hydrogen, an external thermodynamic property database named CoolProp is implemented in the code. The validity of the model results has been assessed by means of the investigation and examination of data regarding real operating stations. Finally, a more in-depth analysis of the operation of the vehicle vessel was performed, and an additional algorithm has been developed to determine the appropriate average pressure ramp rate that minimizes the refueling time within the allowable temperature and pressure limits.

## 1.4 Bibliography review

Many numerical studies have been conducted to predict the temperature behavior of compressed hydrogen during the refueling of storage tanks at high pressure. In some of them a multi-dimensional heat transfer analysis, based on Computational Fluid Dynamics (CFD) is carried out. The multi-dimensional CFD calculations can provide detailed information on the temperature, density, and velocity field within the tank, but the computation requires a high effort level.

In their works Dicken and Mérida develop a CFD model to investigate the temperature distribution in a compressed gas cylinder during refueling with the aim of determining the mean temperature of hydrogen and allowing density calculations depending on temperature and pressure. Their results, validated by a set of experimental data obtained placing 63 thermocouples in a type III tank, showed a non-uniform temperature distribution during the filling [17] [18].

Further researches carried out by Monde et al. demonstrated that there is a consistent trend in the gas temperature distribution and that can be accepted the uniformity assumption [19] [20]. Measured temperatures during fast fill up to 35 and 70 MPa well predicted the estimated values of their model [21].

While Zhao et al. develop a CFD model to discretize the tank and evaluate the temperature distribution with respect to the ambient condition and associated process parameter. The simulation was validated with experimental valuations on a 35 MPa, 150-liter vehicle cylinder and an empirical formula was derived fitting the numerical results. It is found that the maximum temperature increases as the mass filling rate and ambient temperature increase, whereas it decreases with the growth of initial pressure [22].

When the goal is to have a global assessment of the performance of hydrogen storage systems and a fast parameter analysis is required, zero-dimensional thermodynamic models are more suitable. Amongst those who adopted this approach, Striednig et al. propose a model where ideal gas and real gas effect are compared. Moreover, the influence of thermodynamic parameters on the gas temperature is analyzed. Experiments conducted on a type I tank show that the

zero-dimensional model is adequate, and the better fitting of the real gas model as respects the ideal to predict the maximum gas temperature [23].

In their study Hosseini et al. firstly investigate the change in the required compression work with pressure and the percentage of hydrogen low heating value for different processes. Then deals with the filling of hydrogen tanks from the perspective of exergy destruction and exergy efficiency. The analysis demonstrates that the exergy efficiency benefits from the rise of initial tank pressure, which also results in a lower final tank temperature [24].

Xiao et al., applying a lumped parameter model, derived an analytical solution of the temperature and pressure as a function of time. The model assumes ideal gas behavior, constant mass flow rate, and the effect of the wall thickness. The final formula can be used to fit experimental data and to correlate the effects of the process parameters, such as the initial and final masses, initial pressure, mass flow rate, ambient temperature, on the final temperature [25]. The same approach is applied by Yang to estimate the filling time from different refueling parameters [26]. Subsequent work of the authors extends the model also to include the effect of the tank walls [27].

Two main studies focused on analyzing the overall performance of a hydrogen refueling station for refueling vehicles for personal transportation. Omdahl, in her master thesis, developed a dynamic model implemented in MATLAB. The station includes an electrolyzer, compressors, heat exchangers, storage systems, absorption refrigeration systems, and controllers. The model assumes ideal gas, uniform temperature distribution, and neglects heat-exchange. Various conditions as different initial vehicle tank pressures, ambient temperatures, and Average Pressure Ramp Rates (APRRs) were tested [28].

The second one is Rothuizen's Ph.D. thesis, where a numerical library developed in Dymola is used for the modeling of the components. Real gas equations, pressure losses, and heat exchange are considered. The single tank system is compared to a cascade system that comprises 1 to 8 tanks. It is demonstrated that the energy savings are consistent when adopting two tanks instead of one, but the reduction of energy consumption flattens with more than four tanks. Furthermore, the study suggests alternative designs that are compared from the

point of view of thermodynamics, energy consumption, and exergy destruction [29].

A comprehensive study about the techno-economic feasibility for refueling a fleet of hydrogen fuel cell vehicles is the Hydrogen Station Cost Optimization and Performance Evaluation Model (H2SCOPE), developed by Argonne National Laboratory. The laboratory provides highly flexible open-source tools, whose inputs can be modified by the users accordingly to their purposes, that evaluates the cost of hydrogen refueling for various station configurations and demand profiles. Similar tools are the Hydrogen Analysis (H2A) hydrogen production models realized by the NREL with support from the US Department of Energy Fuel Cell Technologies Office.

## 1.5 Novelty

Several studies focused on predicting the compressed hydrogen temperature and pressure rise during a fill process, however the attention was addressed on studying the phenomena over small volumes and high pressure typical of light-duty vehicles (e.g., automotive application). Less known effort has been reported in the literature about the modeling of the hydrogen behavior during the refueling at lower pressure and greater capacity proper of heavy-duty vehicles.

As a result, a proper standardized protocol that establishes safety limits and performance requirements for gaseous hydrogen fuel dispensers has been developed only for light-duty vehicles and is still under development for heavy-duty vehicles (PRHYDE project [30]).

The motivation for the present study is to address this gap in the literature through careful modeling of the thermodynamics of all the components involved in the refueling process with particular attention to the vehicle tank temperature and pressure increase and the refueling rate. The model developed through an iterative algorithm is capable of determining the hydrogen mass flow rate, temperature, and pressure with a timeframe of one second starting from the set initial and boundary conditions (e.g., ambient temperature, initial tank conditions, vehicle tank pressure ramp rate). Furthermore, an additional functionality to the previous algorithm has been developed to allow the identification of the maximum acceptable refueling rate that minimizes the refueling duration within the allowable temperature and pressure limits of the vehicle tank.

## 1.6 Outline of the thesis

The thesis contains 7 chapters whose description is presented below:

- **Chapter 2: Hydrogen refueling stations state-of-art** explains the design and the operation of the hydrogen refueling stations. The problems associated with the refueling with hydrogen and hence the refueling protocol are discussed.

- **Chapter 3: 3Emotion: an introduction** contains a detailed description of the EU project 3Emotion. The project objectives, partnerships, and demonstration sites that are involved are summarized.

- **Chapter 4: Model development** presents the model assumptions and the numerical formulations that are applied to each component for the simulation of a hydrogen refueling system.

- **Chapter 5: Model implementation** presents the physical model that describes the refilling of a high-pressure tank. Furthermore, it focuses on the importance of the refueling time for the scaling up of the technology, hence illustrates a further algorithm that, depending on the initial conditions and on the amount of hydrogen to refill, determines the appropriate ramp rate able to minimize the filling duration.

- **Chapter 6**: **Results and discussion** an analysis of the thermodynamic behavior and the comparison of the results with data collected during the operation of the 3Emotion station are discussed in detail. Then, a simulation for the storage refueling is carried out and analyzed. Finally, the effect of varying the ambient temperature and initial pressure on the refueling time, state of charge, final vehicle tank temperature, and the influence of different pressure ramp rates on the refueling time are investigated.

- **Chapter 7**: **Conclusions** summarizes the conclusions achieved in the present work and provides further suggestions for the development of future works.

# Chapter 2

# Hydrogen refueling stations and relative operation state-of-art

In this chapter a description of the Hydrogen Refueling Stations (HRS) design and their operation is presented. The refueling with hydrogen consists of dispensing high-pressure gas from a station reservoir to a smaller vehicle tank. In practice, the refueling of hydrogen gas is done with two basic principles, either by exploiting the pressure difference between the tanks of the station or by storing the hydrogen at low pressure and then compressing it directly into the vehicle. The station dispenser controls the rate of gas transfer and the rate of pressure rise. As a consequence, the characteristic of hydrogen refueling stations is to be a system where the pressure, temperature, and mass within the components vary over time. The problems that result from this behavior and the risks to which the customers may be subjective encouraged the Society of Automotive Engineers (SAE) to develop a Technical Information Report (TIR) to assure the safety of hydrogen refueling that, at the same time occurs within a period comparable to existing technology.

The protocol used to realize a fast and reliable fueling of a vehicle is named SAE TIR J2601, and its description is discussed in this chapter. Lastly, it is depicted how hydrogen is supplied to the station and which are the storage technologies for compressed gas.

## 2.1 Hydrogen refueling systems and relative operation

There are two methods for refueling a vehicle with hydrogen, either by compressing directly into the tank or by connecting the vehicle to a storage tank at higher pressure, a procedure that is noted as tank-to-tank refueling. In this case the hydrogen goes in the vehicle due to the pressure difference between the storages. The two designs are shown in Figure 2.1.

In tank-to-tank refueling the compression and further expansion due to the pressure difference have as a drawback the wasting of some compression work.

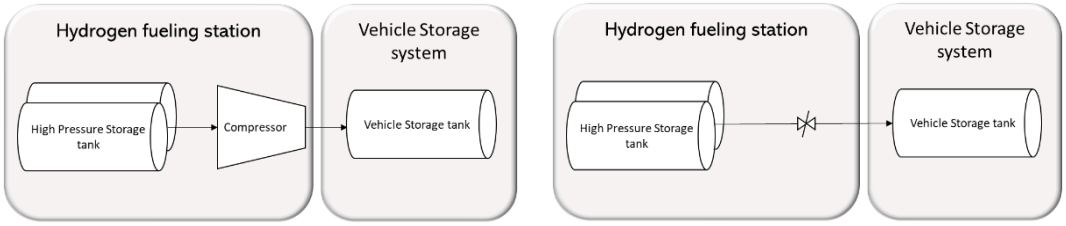


Figure 2.1. Sketch of a hydrogen refueling station. Left: direct compression. Right: Tank-to-tank refueling

Likewise, it has an advantage of occurring at high mass flow, not being limited by the compressor's capacity [28].

Most commonly, there is not a single-tank storage system, but the hydrogen is stored in a cascade system at different pressure levels. When the refueling occurs, the hydrogen flows firstly from a low-pressure level tank until the pressure across a reduction valve, which is located downstream of the storage tank, reaches a specific limit. Then, the station switches the refueling from a storage tank at a higher pressure level up to the end of the fueling. The fueling station is equipped with a compressor to fill up the cascade tanks in order to re-establish the pressure and the mass of the storage vessels, thereby ensuring that the station can successfully accomplish the refueling of another vehicle. The entire process of refueling a vehicle and re-establish the initial conditions in the storage tanks is recognized as a complete refilling cycle. The cascade system is widely used because allows the storage of a considerable amount of hydrogen at high-pressure, thus to dispense the fuel even in case of power unavailability or during maintenance. Moreover, the cascade system has a more straightforward operational strategy and requires a smaller compressor, so it is more favorable from an energy consumption point of view [29]. Figure 2.2 shows the design of a cascade station with three tanks without considering processes upstream of the storage.

### 2.1.1 Problems in hydrogen refueling

The problems that arise during the refueling are related to the physical characteristics of hydrogen. In fact, despite having the highest specific energy content, because of its shallow triple point temperature and low molecular weight, hydrogen has the lowest density among all the elements (i.e., 0.085 kg/m$^3$ at atmospheric pressure and 15 °C [31]). Therefore, to achieve a driving range compared to fossil-fuel vehicles, it would necessitate being stored in large volume

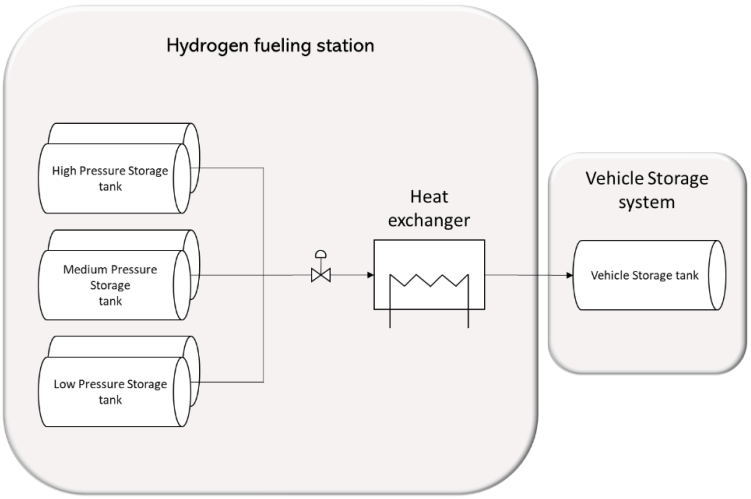


Figure 2.2. Sketch of a tank-to -tank refueling with a cascade system of three storage tanks

tanks or compressed at high pressure. At present, the most practical way is to store hydrogen on-board as a compressed gas at 35 MPa or 70 MPa. Another issue related to hydrogen is that, at the pressures and temperatures at which the refueling usually takes place, it presents a negative Joule-Thomson coefficient, this means that an isenthalpic expansion of the gas from the high-pressure storages through the reduction valve towards the low-pressure vehicle tank results in a temperature increase, affecting the vehicle tank. The Joule-Thomson effect is not the only phenomenon that causes a temperature rise of the gas during filling. A second factor, which is also predominant, is the heat of compression occurring while introducing more and more mass in the vehicle tank [22]. The third one, less effective than the others, is the conversion of kinetic energy to internal energy while fueling a tank. The temperature rise is eased by the heat transfer from the gas to the tank walls and successively transferred towards the external environment.

In order to avoid excessive overheating of the tank and, at the same time, provide a refueling that is acceptable for the customers in terms of duration, the Society of Automotive Engineers (SAE) established a fueling protocol. For a safe dispensing system, it provides criteria for maximum fuel temperature at the dispenser nozzle, the maximum fuel flow rate, the maximum rate of pressure increase, and cooling requirements for each starting conditions (ambient temperature and initial tank pressure). For light-duty vehicles the protocol of reference is denoted SAE TIR J2601/1 and applies for vehicles with Nominal Working Pressure (NWP) of 35 MPa and 70 MPa [32], while for heavy-duty

Table 2.1. SAE J2601/2 safety limits for the refueling of heavy-duty hydrogen vehicles

| **SAE J2601/2 Fueling Process Limits** | |
|---|---|
| Parameter | Limit |
| Ambient temperature range | -40°C-50°C |
| Maximum gas temperature | 85°C |
| Maximum dispenser pressure | 125%NWP |
| Maximum flow rate-normal filling | 0.06 kg/s |
| Maximum flow rate-fast filling | 0.12 kg/s |

vehicles, such as transit buses or trucks, the NWP is 35 MPa and the fueling protocol is the SAE TIR J2601/2 [33].

## 2.2 Refueling protocol limits

A safe refueling means that the limits of temperature, pressure, and density should never be exceeded neither during nor after the fueling period. The SAE J2601 and SAE J2601/2 establish that the ambient temperature must be between -40°C and 50°C, the maximum gas temperature within the vehicle fuel tanks less than or equal to 85 °C and finally, the maximum allowed pressure is 125% NWP, that is 87.50 MPa for a 70 MPa NWP vehicle and 43.75 MPa for a 35 MPa NWP vehicle. A further limitation is specified for the fuel flow rate, which should never exceed 0.06 kg/s or 0.12 kg/s in case of a “fast filling”, namely a way of dispensing hydrogen that permits to reduce even more the refueling duration without potential hazards. Table 2.1 summarizes the tank safety limits for heavy-duty hydrogen vehicles.

As mentioned above, the refueling is characterized by an increase in gas temperature due to the reverse Joule-Thomson effect and the heat of compression, hence to avoid thermal stresses on the vehicle tank, it is common to pre-cool the hydrogen before entering in the tank. This procedure is mostly adopted for light-duty vehicles whose storage capacity -between 2 and 10 kg- is much lower compared to the one of the heavy-duties (e.g., 30 kg) and refueling times are more expedite (<5 min vs. 10-15 minutes), therefore are more interested by the temperature rise. The SAE J2601 details the exact value of the pre-cooling temperature depending on the station types that are rated according to the NWP and the maximum mass capacity of the vehicle storage system.

### 2.2.1 Refueling procedure

The SAE J2601 takes into account vehicles whose refueling can proceed with and without the possibility to communicate with the station. If there is communication, the vehicle exchanges data about pressure and temperature with the station through infrared signals. A representation of the hydrogen fueling system and the signals transferred are shown in Figure 2.3 and Table 2.2. If there is not an initial pressure pulse is sent to determine the initial vehicle tank pressure, then a second pressure pulse is used to measure the vehicle tank volume, thus its mass capacity.

In any case, a safety procedure for the refueling of a vehicle that complies with the SAE J2601 and SAE J2799 (70 MPa Compressed Hydrogen Surface Vehicle Fueling Connection Device and Optional Vehicle to Station Communications) [34] foresees the following phases:

- *Start-up phase*: once a vehicle stops in the settled area, a safe connection is ensured between the vehicle receptacle and the dispenser nozzle. The information about the ambient temperature, initial vehicle tank pressure, the pre-cooling temperature is employed by the station to select the appropriate pressure ramp rate at which the refueling occurs to assure a safe and fast-fill and the target pressure at which the refueling is terminated. While for light-duty vehicles, the SAE contains look-up tables suggesting which value of the pressure rise is to be used. For heavy-duty vehicles, a standardized protocol is currently on the study.

- *Main fueling phase*: in this phase occurs the actual flow of hydrogen to the vehicle. The speed of fueling is established by the Average Pressure Ramp Rate (APRR) that has been calculated in the startup phase. The fueling continues at a constant value of the APRR until the target pressure is reached. The target pressure is the pressure that the vehicle tank should achieve once it has reached the maximum capacity.

- *Fueling termination*: once the dispenser measures the target pressure, the fueling is aborted and the fill ends. Termination also occurs if the safety limits are exceeded (e.g., vehicle tank temperature and pressure and target pressure) or in case of station inability to meet the fueling requirements (e.g., it cannot maintain the desired APRR). The pressure and temperature

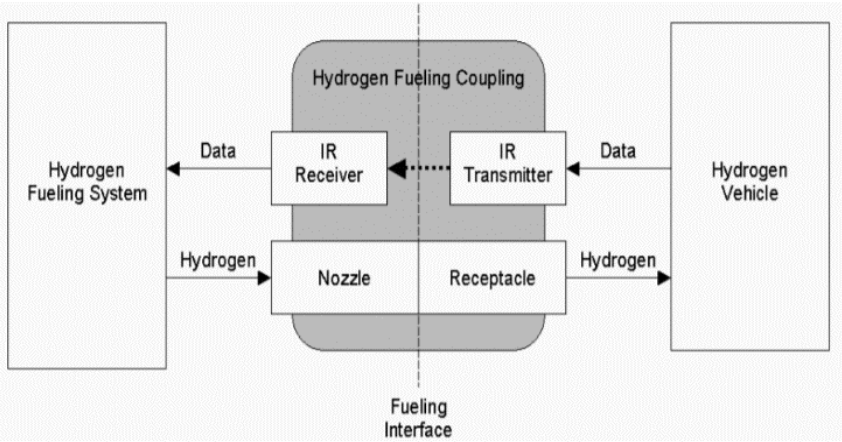


Figure 2.3. Gaseous hydrogen fueling system overview

Table 2.2. Hydrogen fueling system ad hydrogen vehicle signals transferred

| **Data format according to SAE J2799/J2601** | |
|---|---|
| Variable | Unit |
| Protocol Identifier | N/A |
| RDI Software Version Number | N/A |
| Tank Volume | Liter |
| Receptacle Type | N/A |
| Fill Command | N/A |
| Measured Pressure | MPa |
| Measured Temperature | Kelvin |
| Optional Data | 0-74 characters not including "\|" |

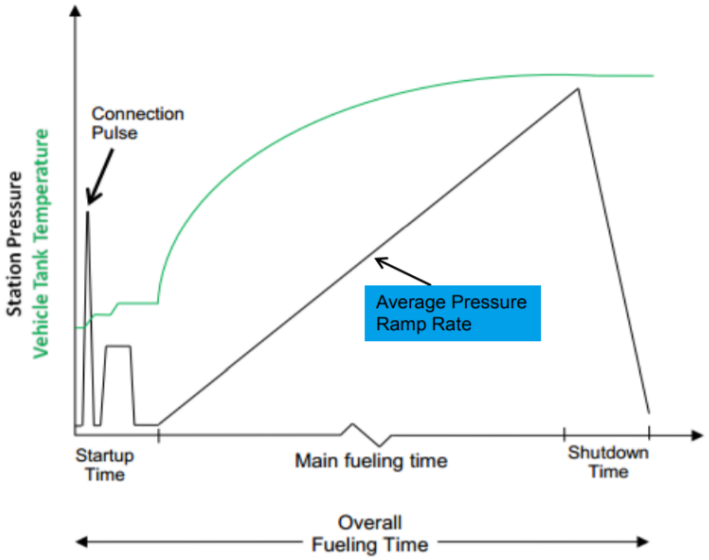


Figure 2.4. Representation of the fueling phases and pressure and temperature development in the vehicle tank

development in the vehicle tank over the overall refueling process are shown in Figure 2.4.

The measurement of the fill level is provided by the state of charge (SOC), which is defined as the ratio between the actual density and the target density, i.e., density calculated at a temperature of 15°C and pressure equal to the NWP and whose expression is:

$$SOC = \frac{\rho(T,p)}{\rho(15°C, NWP)}\ 100\% \qquad (2.1)$$

where $\rho$ is the gas density, T is the temperature, and p is the pressure, whereas the target density for a 35 MPa and 70 MPa vehicle is respectively 24.0 kg/m$^3$ and 40.2 kg/m$^3$. If the density at the end of the refueling is equal to the target density, the SOC is 100%. However, since the fueling is aborted when it is reached the target pressure, which is set on ambient temperature, the SOC could be different than 100%. In fact, a lower initial tank temperature could cause an overfilling because the final temperature is lower than expected. As a consequence, it would result in a higher density, while an initial tank temperature higher than the ambient temperature could lead to an underfilling. Both the phenomena result in undesired or even hazardous conditions.

## 2.3 Hydrogen supply and storage

Alongside the state of the art and procedure of the refueling system it need to be considered the overall complexity of ensuring a constant and reliable source of hydrogen. There are two options for the supply of hydrogen to the HRSs. It can be delivered to the site employing trailer trucks or dispensed directly from a pipeline, or on the contrary, can be produced on-site. Today, local distribution mostly relies on compressed hydrogen, delivered by trucks to the station where it is stored in composite cylinders, typically at 200 to 350 bar and loaded into trailers. This solution is preferred when the distance between the production site and the HRS is not so long. Otherwise, if the distribution distance increases, the pipeline configuration becomes a more cost-effective solution [7]. Pipelines also have the advantage to be able to ensure significant and sustained demand, however the requirement of government support and coordination limits the diffusion of this technology.

Generally, no purification units are provided for these types of plants, therefore the hydrogen should be already delivered with a purity level of 99.99% in accordance with the standard SAE J2719 [35]. Another possibility is the generation of hydrogen on-site. Different methods of production are employed to extract hydrogen from fossil fuels, biomass, or water. Although the steam reforming of natural gas is the most widespread technology, electrolysis, that is the hydrogen produced by water and electricity, is gaining more attention in the scope of zero greenhouse gas emissions technologies. From an operational perspective the on-site generation is more versatile, but the plant grows in complexity requiring a reformer or an electrolyser, purification, compression, and monitoring systems.

### 2.3.1 Compressed hydrogen storage tanks

At the present day, the most common way to store compressed hydrogen is to use gaseous pressure vessels, typically of cylindrical shape. The underlying reason is that at an ambient temperature of 298 K and in the pressure range 300 bar to 700 bar the volumetric density of hydrogen is about 20-40 kg /m$^3$, which is more than twenty times higher than at atmospheric pressure (e.g. $\rho = 0.082$ kg /m$^3$ at 298 K and 1.013 bar). Therefore, if storing 1 kg of hydrogen at ambient conditions requires a tank volume of 12.3 m$^3$, compressing it at 350 bar requires 0.042 m$^3$,

namely 99.6% less storage volume [24]. Besides, the possibility of modularity make them suitable to store a large quantity of hydrogen easily.

Depending on the structural materials, the on-board tanks can be classified into 4 different categories. Stainless steel tanks are called Type I tanks and are applied for stationary applications until a pressure of 300 bar, otherwise with higher pressures, composite tanks are preferred. While type II and type III tanks liner consists of a thin layer of steel or aluminum, with the latter capable of withstanding pressures up to 1000 bar, type IV is comprised of a non-load-bearing polymer liner wrapped with load-bearing high-strength carbon fiber composite.

Despite being limited by the same maximum pressure of the type III tanks, this particular structure provides not only strengths but permits them to be lighter compared to the other pressure vessels. Both these aspects ensure that they are the most widespread in service. Either the type III or type IV, due to their capacity to tolerate high-pressures, is particularly advisable when proceeding with a fast fueling.

In this study the hydrogen supply section is not considered, instead it is expected to be continuously provided to the station at a pressure of 30 bar (which is the typical working pressure of a pressurized low temperature electrolyser).

# Chapter 3

# 3Emotion: an introduction

This chapter provides an overview of the project conducted in cooperation with CIRPS (Interuniversity Research Center for Sustainable Development) and represents the starting point for the thesis. Objectives, composition of the involved partners, and illustration of the engaged locations are described accordingly.

3Emotion Project, which stands for Environmentally friendly Efficient Electric Motion, is the one under consideration. The project started in 2015 as part of the EU Seventh Framework Programme, which carries out for the achievements of its objectives a program called 'Cooperation', via research, technological development, and demonstration activities. Supported by the Fuel Cell and Hydrogen Joint Undertaking (FCH JU), 3Emotion targets to bridge the gap between the current demonstration projects towards large-scale deployment of fuel cell road vehicles and hydrogen refueling infrastructure. Figure 3.1 shows how the project is connected to the Seventh Framework Programme.

The project envisages the establishment of a pan-European consortium of public and private actors among public transport operators, FCB manufacturers, suppliers in the gas industry and technical experts for the deployment of 21 new FCB in addition to 8 existing buses and the realization of 3 new HRSs. The buses and the HRS operate in 5 leading cities: Aalborg (DK), London (UK), Pau (FR), Rotterdam (NL), Versailles (FR). [36]

Finally, the project seems to be managed in compliance with the Project Management Institute (PMI) standard for project management, "A Guide to the Project Management Body of Knowledge" (PMBOK® Guide) [37] and with the ISO 21500 "Guidance on project management" [38].

## 3.1 Project objectives

The 3Emotion Project, as the ultimate goal, is intended to demonstrate to the competent authority the effectiveness of the economic investment in FCB, but in addition to the aforementioned economic advantage, public authorities may also

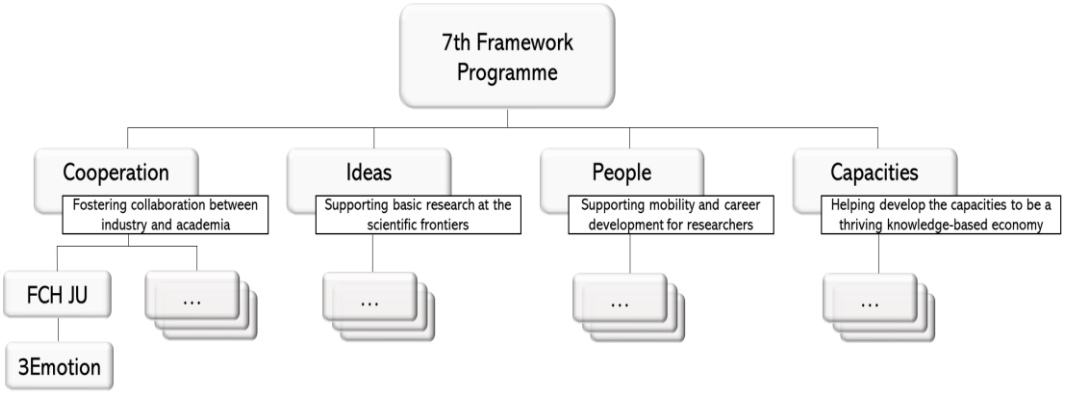


Figure 3.1. Flow chart that shows the framing of 3Emotion within the 7th Framework Programme

consider some positive externalities related to the improvement in the quality of the environment, due to pollution reduction and to the modernization of the transportation infrastructure as a result of the introduction of a new and ecologic technology.

By taking into account the lesson learned from past FCB projects, 3Emotion aims to overcome the last technical and economic barriers and, thanks to its achievements, enhance the number of operators involved paving the way to commercialization as foreseen by the FCH-JU bus Commercialisation Study, 2014. More specifically, the objectives of the project are:

- Lower hydrogen consumption for FCB's to less than 9kg/100km
- Bus capacity 16 $kg_{H2}$/refueling once a day
- Refueling time 10-15 minutes

## 3.2 Project partnerships

Since the project beginning the demonstration sites selected for the operation of the buses and HRSs have changed along with 3Emotion consortium composition. Behind the reasons that caused the withdrawal of some formerly partners there were failures of the procurements of FCBs and lack of co-finances from local authorities since it appeared unfeasible to invest in a new technology still largely unknown that requires extensive initial investments.

New partners joined the project in replacement of the preceding, thus the present consortium composition includes 22 associates from 5 EU-countries, while the demonstration sites are located in 5 different cities: London (UK), Pau (FR), Versailles (FR), Rotterdam and Province of South Holland (NL) and Aalborg (DK).

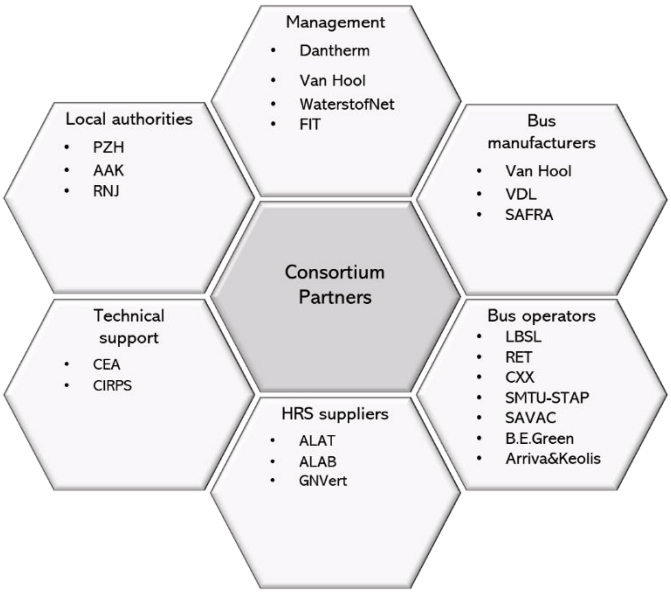


Figure 3.2. Representation of the project consortium partners

The active participation of all the stakeholders involved is essential for the project success and thereby to attain the EU objectives for the commercialization of FCBs. A representation of the consortium is provided in Figure 3.2 with the partners divided into the following categories: **Management**, with the role of ensuring that the project advances as planned. **Bus manufacturers**, to provide the vehicles and assistance during the operation. **Bus transport operators** that, from the achieved results and enlargement of the public acceptance of the technology, are going to sustain the scale-up and commercialization of FCBs and associated HRS within their fleets. **HRS operators**, responsible for developing and implementing the refueling stations. **Technical support**, to evaluate the progress of the equipment performances from the technical and economic viewpoint. **Local authorities**, to ensure institutional support to the project.

## 3.3 Project insight

The project started in 2015 and was expected to be completed in 5 years. During the execution consortium internal problems, delays in the commissioning of the buses and in the license plates certifications process resulted in an extension of the project duration until the end of 2022.

To achieve the project objectives and expected results, 3Emotion has developed an implementation strategy that consists of 6 work packages, the

Table 3.1. 3Emotion implementation strategy

| Work Packages | Objectives |
|---|---|
| **Project Coordination and Management** | Coordination activities, following the project development, and ensuring communication between the partners. |
| **HRS Operation** | Identify the requirements and evaluate the performances of the HRSs. |
| **FCB Operation** | Demonstrate availability and the reliability of FCB technology with the achievements of 3Emotion targets. |
| **Monitoring, integration, and evaluation of impacts** | Evaluation of the technology and its environmental, economic, and social impacts, while making a comparison with other bus technologies. |
| **Transferability process toward an effective FCB commercialization in Europe** | Communication of the results and gather recommendations useful for FCB and HRS commercialization. |
| **Dissemination** | Provide for the diffusion of the project knowledge to the public and develop adequate communication with other project stakeholders. |

objective of which is briefly illustrated in Table 3.1. Within 3Emotion, the latest technologies for fuel cell buses and hydrogen refueling stations are extensively analyzed and studied. Indeed, the involvement in the project of demonstration sites with diverse bus usage characteristics, urban driving, and long-distance routes allow to fully test the hybrid powertrain (a combination of batteries with fuel cells) of the buses in different operational conditions. The insight of the behavior of the system permits to acquire data and gather experience essential for technology development. In parallel, the project focuses on improving and upgrading the existing hydrogen refueling stations, increasing their reliability and hydrogen availability. For both old stations and brand-new stations, efforts are made to evaluate the performance of those refueling infrastructures, to find the best way to increase their capacity and identify a clear scalability approach.

In order to monitor the progress of the equipment performances from a technical and economic viewpoint, the consortium has defined a list of key performance indicators. Measuring, analyzing, and evaluating the performance

represent essential steps to assess the environmental, economic, and social impacts of the project. The compliance of the evaluation with the requirements of the EU projects is certified by the Monitoring & Assessment Framework (MAF) Handbook of HyLights [39].

In the end, in the direction of further mature the technology, the 3Emotion partners are engaged to share the learnings, considerations, recommendations to partners of other projects. These actions, combined with adequate communication and awareness campaigns, are expected to pave the way to commercialization of FCB and to bring forward the change to zero-emission public transport.

## 3.4 Demonstration sites description

As mentioned before, 3Emotion plans the deployment of 29 articulated buses in 5 cities (London, Pau, Versailles, Rotterdam and Province of South Holland, and Aalborg), located in 4 countries (UK, France, Netherlands, and Denmark). According to the site, the buses operate on urban and extra-urban roads, the former characterized by many stops, the latter by a higher mileage intercity with few stops. To the two existing stations located in London and Rotterdam, in 3Emotion three new stations are going to be implemented. Two of them have hydrogen production on-site with electrolysis (Pau and Aalborg), the third one is a trucked-in station. The hydrogen is dispended at 350 bar for the buses, and 700 bar for cars, if the stations are designed for this option. A description of the characteristics of each station is depicted below.

### 3.4.1 London site

In London a hydrogen refueling station was in operation before the beginning of 3Emotion to refuel eight Wrightbus FCB. Under 3Emotion, two additional buses are deployed to be refueled in the same station, while five of the eight Wrightbus received a fuel-cell module refurbishment.

The HRS is a delivery type station, not publicly available that serves the buses of the London transport operator and cars only by appointment. The hydrogen is produced in Rotterdam as blue hydrogen and transported to the station using a liquid trailer, which is equipped with a compression system to allow dispending at 440 bar in the storage tanks permanent on-site. The hydrogen trailer is later used as integrated storage, with a capacity up to 900 kg, in addition to the 350 kg on-

ground permanent storage, for a total capacity of 1250 kg that is stored at 500 bar. Each day the station is capable of dispending 400 kg/day of hydrogen, which is well beyond the one required by the buses, i.e., 160 kg/day.

The actual refueling occurs with a single dispenser in a four-hour overnight window as a result of the pressure difference between the storage at 500 bar and the buses at 350 bar.

### 3.4.2 Dutch site

The Province of South Holland, to which belongs Rotterdam, is engaged in the shift towards a more sustainable mobility for many years. Initiatives to promote hydrogen as an alternative fuel can be traced back to 2013, and nowadays two Dutch transport operators are involved, RET and PZH.

Within 3Emotion four additional buses are deployed by PZH to be added to the two already in operation by RET since 2014. These new buses have a higher capacity due to the fact that they do not cover only urban roads but are used for longer distances in a suburban context.

The buses refuel in the same station situated to the South of Rotterdam that receives hydrogen from the Benelux/France pipeline. The gas leaves the pipeline at 30 bar then is stored in two medium-pressure vessels at 495 bar and in a high-pressure vessel at 877 bar to achieve a total capacity of 250 kg. The station employs two piston compressors in series to fill up the storages, whereas another will be implemented in the upgrading. Since the buses have different performances, the total of almost 200 kg/day of hydrogen delivered to the station serves the PZH buses (about 115 kg/day), the remaining the RET buses.

The station has installed three dispensers, a fourth is planned: one at 700 bar for fast-filling of cars, that requires a heat-exchanger for the gas cooling, a second dispenser for the cars at 350 bar, and one final always at 350 bar for the buses. In Figure 3.3 the station dispenser installed in the site is depicted.

### 3.4.3 Versailles site

In Versailles, a hydrogen refueling station is operative since 2017 to refuel both cars and buses, thus it is a dual pressure 350/700 bar station with a dual flow for the buses. The station uses blue hydrogen produced in two plants situated in northern France and is delivered in a compressed state at 200 bar via tube trailers of approximately 350 kg for a total capacity of 200 kg/day.

Figure 3.3. Photo of the Rotterdam station. Source: 3Emotion D2.11

Figure 3.4. Photo of the Versailles station storage units. Source: 3Emotion D2.12

Figure 3.5. Photo of the fuel cell buses in use in Pau site. Source: 3Emotion D2.12

The trailers constitute part of the storage, which also includes a medium-pressure storage of about 100 kg at 495 bar and a high-pressure storage of about 60 kg at 877 bar.

In total the station is capable of storing nearly 500 kg of hydrogen, which is used today to refuel seven buses, funded within 3Emotion, and 40 light vehicles. Figure 3.4 shows the storage units of the station.

Additionally, the station is equipped with two piston compressors, one heat-exchanger for the refueling at 700 bar and another dispenser not-cooled for the buses, this allows to simultaneously refuel up to 2 buses in a thee hour recompression.

### 3.4.4 Pau site

The city of Pau, located on the northern edge of the Pyrenees in France, was selected for the construction of a locally producing hydrogen refueling station via electrolysis. The station, which is funded in collaboration with other projects, is composed of an electrolyzer, two compressors, a series of low and medium pressure storages, and eight dispensing spots. The electrolyzer has a nominal production of 174 kg/day that can increase up to 268 kg/day, moreover it is foreseen a 200 bar tube trailer for back up in case of maintenance or unavailability of the electrolyzer.

The hydrogen is generated at 20 bar and is stored in a low-pressure vessel at 20 bar, acting as a buffer, and in a medium pressure vessel at 600 bar (in total are stored 860 kg of hydrogen) before being refueled at 350 bar upon demand. The station serves eight articulated buses and the regular operation is to refurbish

them overnight, one by one, from the 7 pm to the 5 am, but when it is necessary, a top-up refilling can take place daytime. The fuel cell buses that are in service are depicted in Figure 3.5.

### 3.4.5 Aalborg site

The city of Aalborg and its partners are the last that joined 3Emotion. The project provides for the deployment of three buses and the realization of a hydrogen refueling station with on-site production through electrolysis. The station is capable of producing 100 kg/day nominally and providing hydrogen pressurized at 35 bar that is stored in storage vessels at 35 bar, 300 bar, and 450 bar (in total 242 kg of hydrogen stored). The balance of plant also includes a single compression system from the pressure at the outlet of the electrolyzer to the pressurized storages.

The dispensing system can refuel at 350 bar the three buses consequently in 2 hours overnight. The refueling time can be reduced if it is carried out the fast filling, for which a cooling system is required.

### 3.4.6 Summary of the sites

In conclusion, to validate the potential value of the hybrid drivetrain technology for a fleet of buses and push forward towards a large-scale deployment, the 3Emotion Project comprehends quite varied configurations. The sites were selected so that the most effective commercialization impact is reached, ensuring the implementation of the hydrogen refueling stations with a different layout to refuel buses of different size fleet and the operation of the same buses under different environmental conditions.

Undoubtedly, the main layout difference lies in the hydrogen supply. On-site production stations respect the delivery stations have more components, however allow for a more compact station footprint. Furthermore, they do not require a national infrastructure and, as a consequence, are easier to manage.

The design capacity is around 100 kg/day to 200 kg/day, except for the station of London, whose experience gained with many years of operation allowed to be improved to refuel up to ten buses, thus has a more significant size. Moreover, some sites were realized with the possibility to refuel cars as well as buses, which entails a variation in the system configuration even higher. A summary of the main characteristics of the sites described in the previous paragraphs is illustrated in Table 3.2.

Table 3.2. Site descriptions summary table

| Site | Hydrogen source | Capacity | Storage capacity | Storage pressure | Bus fleet | Gas pressure |
|---|---|---|---|---|---|---|
| **London** | Trucked-in | 400 kg/day | 1250 kg | 350/500 bar | 10 | 350 bar |
| **RET&PZH** | Pipeline | 200 kg/day | 250 kg | 495/900 bar | 6 | 350/700 bar |
| **Versailles** | Trucked-in | 200 kg/day | 500 kg | 200/495/877 bar | 7 | 350/700 bar |
| **Pau** | On-site electrolysis | 174 kg/day | 860 kg | 200/20/600 bar | 8 | 350 bar |
| **Aalborg** | On-site electrolysis | 100 kg/day | 242 kg | 35/300/450 bar | 3 | 350 bar |

## 3.5 Final remarks

In compliance with the standard guidelines, the monitoring of the project progress is guaranteed by the periodical preparation of project deliverables in the form of reports. To ensure the quality and accuracy of what is stated, the reports are submitted to whom of competence for an internal review. The results are then shared within the involved partners to always allow a productive exchange of information, besides, according to the FCH-JU transferability objective, they are made publicly available. Each completed deliverable contributes to the achievement of the pre-set objectives and to the development of the appropriate expertise that is required in the path towards the commercialization of fuel cell buses and hydrogen refueling stations.

The analysis performed in this thesis is intended to assess the operation of the refueling stations in the five sites, to identify the possible functional and technical improvements and the prospect for scaling-up. The results provide the necessary input for drafting the reports. Furthermore, due to the lack of standardized fueling protocols for heavy-duty vehicles and since the current studies are mainly focused on estimating the hydrogen refueling cost, this thesis aims to contribute to the understanding of the process parameters that characterize the refueling of those vehicles.

# Chapter 4

# Model development

In this chapter a zero-dimensional thermodynamic model is presented, the aim of which is to provide a description of the behavior of an HRS during a refueling process from a tank storing high-pressure hydrogen to a tank at lower pressure.

The whole refueling is simulated according to SAE TIR J2601. The model is focalized on predicting the gas temperature and pressure evolution within the vessels throughout the whole duration of the refueling, with particular regards to the temperature rise within the vehicle vessels, being constrained by safety limits. Furthermore, through the model, it was possible to assess the effect of different refueling operations on the main controlled variables (i.e., temperature, pressure, mass, flow rate, refueling time). In particular, determine the appropriate APRR that minimizes the refueling time, within the allowable temperature and pressure limits.

The station is designed to perform a tank-to-tank refueling, thus comprises one high-pressure storage, the vehicle storage system, both assumed adiabatic and connected through a lamination valve. The compressor, for which a quasi-static model based on an isentropic compression transformation is applied, intervenes after the completion of the refueling process in order to restore the nominal pressure in the station's storage. A sketch of the system is represented in Figure 4.1. The components, for whom are assumed homogeneous gas properties, are modeled according to the first law of thermodynamics, Newton's law of cooling, and the mass conservation equation. The tanks are dynamic, therefore the model is able to handle and describe the hydrogen migration between them.

Hydrogen is considered as a real gas, considering the non-negligible compressibility factors within the analyzed pressure and temperature ranges. The pressure losses were calculated but then not included as they do not affect the HRS from the operation point of view. The heat transfer through the pipelines is neglected.

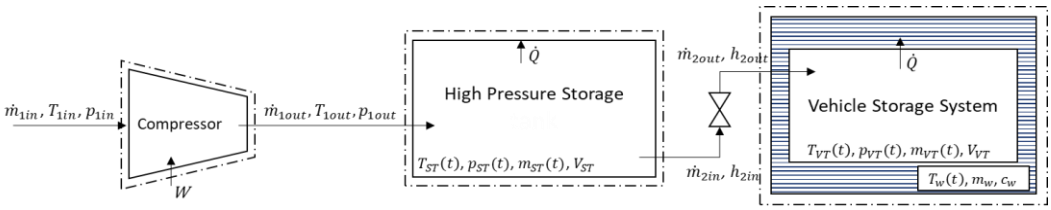


Figure 4.1. Schematic representation of the entire station modeled

## 4.1 Model background

The dynamic physical model developed in this work is able to simulate the refueling of heavy-duty vehicles and to investigate its operational performances. Therefore, it can provide indications for this type of process likely to fill the regulatory gap for that application. As explained in chapter 2.1.1, during the refueling with hydrogen, the gas temperature increases mainly due to two phenomena, namely the heat of compression and the reverse Joule-Thomson effect. Therefore, a correct estimation of the temperature and pressure increase inside the vehicle vessels is of great importance in order to avoid that the critical conditions of the materials are reached and to prevent potential safety hazards.

The model data serve as a base case to understand the physical conditions of all components and subsequently are used in an optimization algorithm to find the maximum refueling speed, and hence the rate of pressure increase in the filling event that reduces the refueling time always respecting the safety requirements. This model also allows to change the boundary conditions (e.g., different ambient temperature and initial vehicle tank pressure) and see the influence of these factors on the refueling.

## 4.2 Energy and mass balance equations

The first law of thermodynamics otherwise referred to as conservation energy principle for any system undergoing any kind of process states that:

$$\frac{dE_{sys}}{dt} = \dot{Q} - \dot{W} + \sum_{in} \dot{m}(PV + u + \frac{v^2}{2} + \mathrm{gz}) - \sum_{out} \dot{m}(PV + u + \frac{v^2}{2} + \mathrm{gz}) \quad (4.1)$$

where the rate of net energy transfer of a flowing fluid in and out of the system, i.e. $dE_{sys}/dt$, has been expressed -on a unit-mass basis - as the sum of flow,

internal, kinetic, and potential energies. The present model applies to a non-reacting open control volume and can be rewritten considering that PV+u is defined as the enthalpy h. For stationary applications the kinetic and potential energies are usually negligible with respect to the enthalpy, heat, and work rates, therefore the rate of net energy transfer coincides with the change in internal energy, i.e. $dU_{sys}/dt$. Upon these considerations for single-stream devices, the energy balance reduces to:

$$\frac{dU_{sys}}{dt} = \dot{Q} - \dot{W} + \dot{m}_{in}h_{in} - \dot{m}_{out}h_{out} \tag{4.2}$$

The different terms in the equation are described. $\dot{Q}$ (W) is the rate of heat transfer. $\dot{W}$ (W) is the power, in particular since we are considering steady flow processes, the only type of work is the shaft work. Lastly, $\dot{m}_{in}$ and $\dot{m}_{out}$ (kg/s) and $h_{in}$ and $h_{out}$ (J/kg) are the hydrogen mass flows and specific enthalpies entering and exiting the control volume, respectively.

A further fundamental principle is the conservation of mass, that applied to a control volume affirms: the net mass transfer to or from a control volume during a time interval is equal to the net change (increase or decrease) of the total mass within the control volume. In formula:

$$\frac{dm}{dt} = \dot{m}_{in} - \dot{m}_{out} \tag{4.3}$$

where $\frac{dm}{dt}$ is the rate of accumulation of mass in the control volume. Under steady-flow conditions the total mass does not change in time, that is, the accumulation term is equal to zero. Therefore, the total amount of mass entering the system is equal to the total mass that goes out. Herein, $\dot{m}_{in}$ refers to a positive quantity $\dot{m}$, which indicates a mass flow entering in a control volume, whereas if exiting, $\dot{m} = -\dot{m}_{out}$.

## 4.3 Compressor model

After hydrogen is removed from the storage tanks, a compressor is activated to restore the refueled hydrogen. This ensures that, if another vehicle must be refueled, the station capacity is not altered. Figure 4.2 shows the control volume around a compressor.

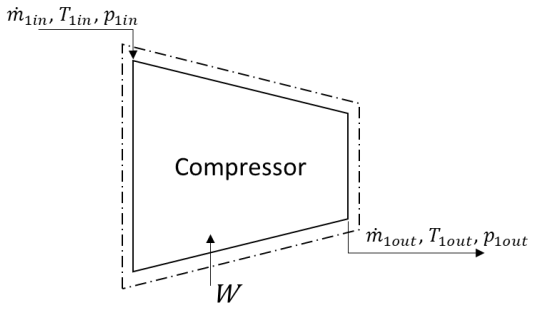


Figure 4.2. Control volume around a compressor

On the market can be found several types of compressors. In hydrogen refueling stations the majority of compressors used nowadays are either positive displacement compressors or centrifugal compressors. The positive displacements, in turn, can be divided into the reciprocating, diaphragm, and ionic compressors. In these machines, the decrease of the volume of the chamber where it is enclosed the gas results in increasing pressure, conversely in centrifugal compressors is the rotation of a wheel at high speed that generates the pressure rise [40].

In this works a reciprocating compressor is going to be modeled. The compression is achieved by moving a piston in a cylinder and can be reached pressures of more than 1000 bar. Even if in reality they work in a discontinuous process is assumed that the gas is delivered continuously, hence the mass flow is constant. Moreover, due to the high compression ratio (i.e.$\frac{p_{out}}{p_{in}}$), the compression is divided into multiple stages (usually two or three stages) with intercooling. Finally, for retrieving hydrogen state points an external thermodynamic library named CoolProp is adopted.

### 4.3.1 Development of model equations

The simulation on the compression process gives us information about the amount of work required to increase the pressure of a unit of hydrogen from the production pressure (assumed, in this case, equal to 30 bar) to the storage pressure (equal to, in this case, 500 bar) and, subsequently, the demand for electric power consumed is calculated. The equations needed are based on the following assumptions: steady-state conditions ($\dot{m}_{in} - \dot{m}_{out} = 0$), adiabatic compression (Q=0), and no pressure drops. Thus, the compression work for each stage reduces to:

$$W_{ST1} = \dot{m}(h_{int1} - h_{in}) \tag{4.4}$$

$$W_{ST2} = \dot{m}(h_{out} - h_{int2}) \tag{4.5}$$

where $h_{in}$is the specific enthalpy at the inlet conditions of the compressor, $h_{out}$ is the specific enthalpy at the outlet, $h_{int1}$ is the specific enthalpy at the outlet of the first stage, $h_{int2}$ is the specific enthalpy at the inlet of the second stage. Therefore, the total work requested is the sum of the work of each stage:

$$W = W_{ST1} + W_{ST2} \tag{4.6}$$

The intercooler is modeled with the assumption that no work is performed (W=0), and only heat is exchanged, for which the energy balance results in:

$$Q_{IC} = \dot{m}(h_{int2} - h_{int1}) \tag{4.7}$$

For a specific compressor, once are known the volume of the compressor cylinders ($V_{cyl}$), the piston strokes per second ($N$), i.e., the compressor speed, and the volumetric efficiency ($\eta_v$) is possible to determine the mass flow rate, as expressed by:

$$\dot{m} = V_{cyl}\, \rho_{in}\, \eta_v\, N \tag{4.8}$$

The volumetric efficiency is defined as the ratio between the actual volumetric flow at inlet temperature and pressure conditions to piston displacement, which is the actual volume of the cylinder swept by the piston per unit of time. This is because the piston does not cover the entire stroke of the cylinder, but when it reaches the end of the stroke, there is always some remaining volume, defined as clearance. The clearance is expressed as a fraction of the piston displacement and typically is in the range from 4% to 30% [41].

Several effects contribute to the reduction of the volumetric efficiency, among these leakages, heating of the gas during admission to the cylinder, and above all, the re-expansion of the remaining gas in the clearance-volume space from the previous stroke [42]. For all these effects, it is difficult for the compressor manufacturers to have correct measurements and provide one single expression

for the calculation of the performances. A general formula that can be used to estimate the volumetric efficiency is:

$$\eta_v = 96 - \mathrm{r} - C\left[\frac{Z_{in}}{Z_{out}} r^{\frac{1}{\gamma}} - 1\right] \tag{4.9}$$

where $r$ is the compression ratio, C the cylinder clearance, $\gamma$ is the heat capacity ratio $c_p/c_v$, $Z_{in}$ and $Z_{out}$ the compressibility factor at the suction and discharge.

### 4.3.2 Compressor analytical solution

Since the compressor works under a high compression duty, having to carry out the gas from the pipeline at low pressure to the pressure of the storages, the overall compression is assumed divided into two stages. According to the station operators, the compressor works with a compression ratio equal to 4 for the first stage, then the second stage compresses the gas up to 500 bar (i.e. nominal pressure of the storage tank).

In order to understand the electricity consumption of the compressor, the enthalpies at the compressor discharge of Eq. (4.4) and Eq. (4.5) have to be determined. Considering that the compression is simulated as adiabatic, the specific entropy during the process is constant (i.e. $s_{in} = s_{out,s}$), hence the isentropic outlet temperature at each stage can be determined knowing the outlet pressure. These two thermodynamic properties are then used to find the isentropic enthalpies, through which we can establish the real enthalpies at the outlet, as expressed by Eq. (4.10):

$$h_{out} = \frac{h_{out,s} - h_{in}}{\eta_{is}} + h_{in} \tag{4.10}$$

For a reciprocating compressor the isentropic efficiency is given by Eq. (4.11) [40].This equation is valid for 1.1< $r$ <5:

$$\eta_{is} = 0.1091(\ln r)^3 - 0.5247(\ln r)^2 + 0{,}8577 \ln r + 0.3727 \tag{4.11}$$

From the real outlet enthalpy and pressure, the outlet temperature can also be found. However, in practice, the compression is not perfectly adiabatic but can be described by a polytropic transformation, which depends on the properties of the

gas and the compressor design. For a polytropic compression $PV^n = \text{constant}$, where $n$ is the polytropic coefficient which can be estimated from [40]:

$$n = \frac{\ln\left(\frac{p_{out}}{p_{in}}\right)}{\ln\left[\frac{\eta_{is}\left(\frac{p_{out}}{p_{in}}\right)}{\eta_{is} - 1 + \left(\frac{p_{out}}{p_{in}}\right)^{\frac{\gamma-1}{\gamma}}}\right]} \tag{4.12}$$

The knowledge of the polytropic efficiency and the inlet and outlet pressure allows for the evaluation of the outlet temperature with Eq. 4.13. These values can be confronted with the one obtained considering an isentropic compression.

$$T_{out} = T_{in}\left(\frac{p_{out}}{p_{in}}\right)^{\frac{n-1}{n}} \tag{4.13}$$

Finally, the electrical power (W) consumed by the compressor motor is obtained as shown in Eq. 4.14, considering the electric motor efficiency $\eta_{el}$ equal to 97% and the mechanical efficiency $\eta_{mech}$ equal to 95%.

$$W_{compr} = \dot{m}\, c_{p,H_2} T_{in}\left(\left(\frac{p_{out}}{p_{in}}\right)^{\frac{n-1}{n}} - 1\right)\eta_{el}\eta_{mech} \tag{4.14}$$

## 4.4 Tank model

As described in Chapter 2.2 exist four types of pressure vessels to store hydrogen. In this study, a type III tank (metallic liner) is analyzed. The control volume around a tank is shown in Figure 4.3.

In both the storage tank and vehicle tank is assumed that the gas temperature, pressure, and density are uniform and stagnant condition prevails. As a consequence, a lumped parameter approach is used to estimate the overall performance of the systems. For this hypothesis to be accepted, the Biot number, Bi, defined by the dimensionless quantity $\frac{k\delta}{\lambda}$, has to verify the condition Bi<0.1. In the ratio, $k$ is the convection heat transfer coefficient (W/m$^2$ K), $\delta$ is the thickness

of the material (for a type III tank $\delta = 3$ mm), and $\lambda$ is the thermal conductivity of the material (W/m K). The type III tanks studied showed a Bi=0.003, and insofar the lumped system analysis is applicable. Even in the tank wall, the temperature and thickness are considered homogenous, and their effect is included in the model.

Since the refueling is a fast process, the tanks are considered adiabatic, hence the heat transfer between the tank wall and the ambient is ignored. Moreover, they are constructed to be resistant and well-insulated, therefore the above hypothesis is further validated. Lastly, it is assumed that at the beginning of each refueling the tanks are in thermal equilibrium with the ambient, and no shaft work is performed. The analysis is based on the modeling presented by Xiao et al. [27], nonetheless rather than considering a constant mass flow, in the present study, the governing equations are a dynamic function of the temperature and pressure change, which is a significant improvement respect to other analyzed models.

### 4.4.1 Development of model equations

Figure 4.2 shows the control volume around a tank. From the lumped parameter model, an analytical solution was developed for solving equation (4.2). Considering the process of fueling a tank, therefore analyzing a process with positive inflow, the solution of the mass balance (4.3), assuming a constant mass flow at each time is:

$$m = m_0 + \dot{m}t \tag{4.15}$$

The conservation of energy (Eq. 4.2) expressed for the refueling of a vehicle yields:

$$\frac{dU_{sys}}{dt} = \frac{d(mu)}{dt} = u\frac{dm}{dt} + m\frac{du}{dt} = \dot{m}h + \dot{Q} \tag{4.16}$$

where u is the specific internal energy (J/kg) and m (kg) the hydrogen mass content of the storage tank. Substituting Eq. (4.15) in Eq. (4.16) and expressing the rate of heat transfer between the gas and the inner tank wall in terms of a convective heat we get:

$$(m_0 + \dot{m}t)\frac{du}{dt} + \dot{m}u = \dot{m}h + k_h A(T_w - T) \tag{4.17}$$

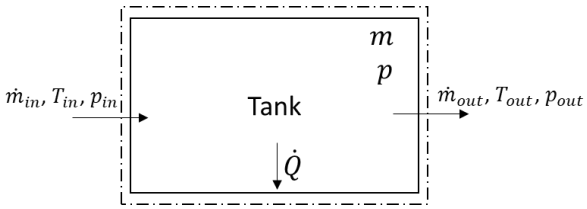


Figure 4.3. Control volume around a tank

where $T_w$ is the wall temperature, T is the temperature of hydrogen in the tank, and $k_h$ (W/m$^2$K) the convective heat transfer coefficient at the inner surface of the tank. Due to the high pressures involved during the refueling, the hydrogen within the tanks cannot be treated with an ideal gas model, as confirmed by the compressibility factor values at those pressures (e.g., Z=1.23 at 288 K and 35 MPa and Z=1.46 at 288 K and 70 MPa). However, for ease of modeling, the specific internal energy u and the specific enthalpy h are determined according to the ideal gas relations, that is: $u = c_v T$ and $h=c_p T_{in}$, where $c_v$ and $c_p$ are determined at the specific operating temperature and $T_{in}$ is the temperature of the incoming flow. Therefore Eq. (4.17) can be written as:

$$(m_0 + \dot{m}t)\frac{d(c_v T)}{dt} + \dot{m}c_v T = \dot{m}c_p T_{\text{in}} + k_h A(T_w - T) \tag{4.18}$$

writing the equation in terms of temperature, after some rearrangements we obtain:

$$\frac{dT}{dt} = \frac{\gamma T_{\text{in}} + \alpha(T_w - T) - T}{t^* + t} \tag{4.19}$$

where $\gamma$ is the heat capacity ratio, $t^*=\frac{m_0}{\dot{m}}$ is the characteristic time (s) and $\alpha$ the dimensionless heat transfer coefficient that represents the ratio between the heat transfer intensity and the total heat capacity change:

$$\alpha = \frac{k_h A}{\dot{m}c_v} \tag{4.20}$$

Defining the characteristic temperature $T^*$ (K) as:

$$T^* = \frac{\gamma T_{\text{in}} + \alpha T_w}{1 + \alpha} \tag{4.21}$$

The equation that describes the evolution of the temperature of the gas in a tank (Eq 4.19) simplifies to:

$$\frac{dT}{dt} = (1+\alpha)\frac{T^* - T}{t^* + t} \tag{4.22}$$

with the initial conditions $T = T_0$ at $t = 0$ , the solution of Eq. 4.22 can be found:

$$\frac{T^* - T}{T^* - T_0} = \left(\frac{1}{1+\tau}\right)^{(1+\alpha)} \tag{4.23}$$

where $\tau = \frac{t}{t^*}$ is a dimensionless time. Writing the term on the right side of Eq. (4.23) as $f_g = \left(\frac{1}{1+\tau}\right)^{(1+\alpha)} = \left(\frac{m_0}{m}\right)^{(1+\alpha)}$ fraction of initial mass over total, and expressing the solution for the hydrogen temperature, we obtain the final solution:

$$T = f_g T_0 + \left(1 - f_g\right)T^* \tag{4.24}$$

Because of incoming mass, the temperature inside the tank increases for the heat of compression and to a smaller extent due to the reverse Joule Thomson effect, as discussed in chapter 2.1 and successive chapter 4.6. The extent of that temperature increment due to compression is provided by Eq. (4.24). Diversely, in the storage tank the solution of the energy balance simulates the temperature decrease as hydrogen flows out of the system.

While in the storage vessel (much larger volumes implemented) the gas temperature variation is minor, for the vehicle vessel (typically of smaller size) the effect of the tank walls and its heating cannot be ignored.

The energy balance applied to the tank wall where the heat transfer from the outer surface of the tank wall to the ambient is not considered[1], i.e., adiabatic vessels becomes:

$$\frac{d(m_w c_w T_w)}{dt} = \mathrm{A}\, k_h(\mathrm{T} - T_w) \tag{4.25}$$

[1] This is a conservative assumption since the ambient – which is at a lower temperature than those reached during refueling – will, during the refueling process, absorb heat from the tank wall surface and coadiuvate the cooling of the tank. Not considering such heat exchange means considering a worst-case condition which is acceptable (if not preferable) from a design point of view

where $m_w$ and $c_w$ refer respectively to the mass of the tank wall (kg) and the specific heat of the tank wall (kJ/kg K). Solving Eq. 4.25 with the initial condition $T_w = T_{w0}$ at $t = 0$ it can be obtained an analytical expression of the temperature rise in the tank walls.

$$T_w = e^{-\tau_w} T_{w0} + (1 - e^{-\tau_w}) T \tag{4.26}$$

where $\tau_w$ is a dimensionless time for the tank walls determined likewise was discussed for the gas equations.

Finally, the real gas equation of state is needed to model the phenomena. A real gas equation is required rather than the ideal gas law due to the high density of hydrogen and the pressure of refueling, therefore a compressibility factor Z must be introduced. In this study, a virial equation is used to define the aforementioned factor [43]:

$$Z = \frac{p\,V}{R_{gas} T} = (1 + \mathrm{B}p) \tag{4.27}$$

where $R_{gas}$ is the gas constant, equal to 4.124 kJ/kg K, and $\mathrm{B}$ is a coefficient that depends on temperature, i.e. $\mathrm{B} = \mathrm{B(T)}$ and can be expressed by equation 4.28:

$$B = \frac{B_1}{T} + \frac{B_2}{T^2} + \frac{B_3}{T^3} \tag{4.28}$$

For the temperature that tends to infinite the compressibility factor assumes the value of 1, proper of the ideal gas state, while in the real gas case values for the coefficient $B_1$, $B_2$, $B_3$ can be obtained by fitting the data, thus a real-gas state equation can be derived. According to the study from Chen et al. [43], in the temperature range 173 K to 393 K Eq. 4.28 can be truncated at the first term and the fitted value becomes $B_1$=1.9155x10$^{-6}$ K/Pa for which the maximum relative errors introduced are 3.8% respect to the National Institute of Standards and Technology (NIST) data [44]. As a consequence, the real gas equation is as follows:

$$Z = \frac{p\,v}{R_{gas} T} = \left(1 + \frac{B_1 p}{T}\right) \tag{4.29}$$

## 4.5 Heat transfer model

In the previous parts have been illustrated in detail the physical phenomena that occur during the refueling, in particular, the distinguishing hydrogen feature of temperature rise as the gas flows into the tanks. It follows that careful modeling of the heat exchanges is critical. In this work, the internal heat transfer from gas to tank wall is considered, whereas it is not the heat exchange from the exterior tank surface to the surroundings as it is assumed that the tank is adiabatic (the explanation was given in chapter 4.4).

For the case of filling high-pressure vessels there is not a single standard methodology to calculate how the gas exchanges heat with the tank walls and difficulties are faced in the calculation of the convective heat transfer coefficient, $k_h$. Therefore, its determination is given to experimental studies and is strongly dependent on geometry, the orientation of the tanks, and the nature of the internal flow. A general approach followed in numerous researches [17], [29], [45] is to apply a correlation based on dimensionless numbers such that:

$$Nu_{Dint} = \frac{D_{int}\, k_h}{\lambda_{gas}} = \mathrm{a}Re_{dint}^{b} + cRa_{Dint}^{d} \tag{4.30}$$

where $Nu_{Dint}$ is the Nusselt number defined as the ratio of the thermal energy convected to the fluid to the thermal energy conducted within the fluid ($\lambda_{gas}$ is the gas thermal conductivity, $D_{int}$ the internal diameter of the pressure vessel). Equation 4.30 suggests that the heat transfer is governed by a mixed convection condition in which the first term is proper of the forced convection and is described by the Reynolds number $Re$ (Eq. 4.31), while the second term represents the natural convection that depends on the Rayleigh number $Ra$ (Eq 4.32).

$$Re_{dint} = \frac{\rho\, v\, d_{int}}{\mu} \tag{4.31}$$

$$Ra_{Dint} = \frac{g\beta(\,T_w - T)D_{int}}{\nu\, a_0} \tag{4.32}$$

where $\rho$ is the gas density, $v$ the velocity, $d_{int}$ the inside diameter of the inlet to pressure vessel, $g$ is the acceleration due to gravity, $\beta$ the volumetric thermal expansion coefficient, $T_w$ the wall temperature, $T$ the gas temperature, $\mu$ the dynamic viscosity, ν is the kinematic viscosity ($\nu = \mu/\rho$), $a_0$ the thermal diffusivity.

The parameters $a$, $b$, $c$, and $d$ are constants whose value is determined upon experimental tests. At present, there are no known published studies regarding the heat transfer measurements during filling with highly-pressurized hydrogen conducted on large volumes such as the one under investigations. Thereby, in this study are applied explicit empirical relations of cases with similar operating conditions. Accordingly to the study of Bourgeois [45], for horizontal cylinders for which a zero-dimensional is valid, the heat exchange is dominated by forced convection, thus the correlation for the Nusselt number becomes:

$$Nu_{dint} = 0.14\, Re_{dint}^{0.67} \tag{4.33}$$

For the case of discharging high-pressure vessels, the expression of reference is the correlation developed by Daney (Eq. 4.34), which studied experimentally the natural convection of cryogenic liquids in vessels of different shapes with nearly uniform wall temperature. This relation is appropriate for turbulent natural convection in enclosures over the range of the Rayleigh numbers $7\text{x}10^8 < Ra_H < 6\text{x}10^{11}$ [46].

$$Nu_H = 0.104\, Ra_H^{0.352} \tag{4.34}$$

The characteristic length for this equation is the cylinder height, $H$, since the high-pressure tanks in the station are disposed in a vertical position.

## 4.6 Reduction valve model

The pressure difference between the high-pressure storage tank and the vehicle tank requires the adoption of a reduction valve (Figure 4.4 shows the reduction valve with the control volume around it) that regulates the pressure so that at the outlet the pressure is equal to the identified APRR. Since no work is added, the expansion can be considered adiabatic, and the mass flowing in the valve is conserved, the energy balance for a steady-state process describes an isenthalpic process, i.e. $h_{in} = h_{out}$.

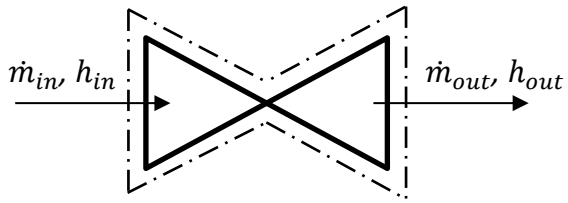


Figure 4.4. Control volume around a reduction valve

The application of CoolProp to the valve enables the determination of the inlet enthalpy knowing the temperature and pressure at the outlet of the storage tanks. Since the process is assumed isenthalpic, the information on the inlet enthalpy and the pressure variation in the vehicle vessels can be used to find the valve outlet enthalpy and thus temperature, through the Coolprop thermodynamic library. This induced change in the gas temperature due to the reduction of pressure between the storages manifests, for hydrogen, in its increase as a result of the Joule-Thomson effect.

In the delineated procedure the pressure losses in the connecting pipelines of the refueling station calculated but finally not considered due to the negligible values which do not affect the HRS from a global operation point of view. To verify wheter this assumption is reasonable, the Darcy-Weisbach equation (Eq. 4.35) has been employed to calculate the pressure drops in the station pipings:

$$\Delta p = f\rho\frac{\Delta L}{D}\frac{v^2}{2} \tag{4.35}$$

where $f$ is the friction factor, $\rho$ is the density of the fluid, $\Delta L$, and $D$ are respectively the length and the inner diameter of the pipe, $v$ the fluid velocity in the tube. The friction factor is a function of the pipe roughness $\varepsilon$ and diameter, and the Reynolds number, that has been defined in the previous paragraph (Eq. 4.31). In case of fully developed internal laminar flow, the friction factor for a circular tube can be calculated as [47]:

$$f = \frac{64}{Re_D} \tag{4.36}$$

For a turbulent flow several equations have been developed for estimating the friction factor, one of these is the Haaland's equation whose formulation is [48]:

$$f = (-1.8\log((\frac{6.9}{Re_D}) + (\frac{3.7\varepsilon}{D})^{1.11}))^{-2} \tag{4.37}$$

In the present case a diameter of 0.008 m and a roughness of $4.6x10^{-5}$ (typical value for commercial steel) have been considered for which the turbulent regime is dominating during the entire simulation.

Upon these considerations for both the pipe segments, that are the tube between the storage vessels and the lamination valve and the tube between this last component and the vehicle vessels, the pressure drops are limited (i.e., the maximum values calculated are 0,2617 MPa/m for the first segment and 0,019 MPa/m for the second).

The entity of such pressure drop is negligible from a global point of view since the HRS system layout accounts relatively short pipings from the storage to the vehicle (<5m generating a maximum pressure drop of 1,31 and 0,09 MPa respectively – summing to below 5% of NWP).

# Chapter 5

# Model implementation

In the previous chapter has been illustrated the theory, and hence the equations that are at the basis of the refueling station model, in which one high-pressure tank is used to fuel a heavy-duty vehicle. The purpose of this chapter is to present the developed algorithm.

Furthermore, within the perspective of hydrogen and fuel-cell technology role to power the future of mobility and the enhancement of the vehicle fleet, the prerequisite for the stations would be to effectively manage the greater flow and hence to improve the refueling phase. Thanks to shorter times, the logistics would be improved, and as a consequence, this would drive down the technology cost. Therefore, an additional functionality to the previous algorithm has been developed to analyze the effect of the speed of refueling, and thus of the APRR to which is related, on the refueling duration.

## 5.1 Model parameters

There are many variables and operating parameters that are involved in the simulation. Table 5.1 shows the input parameters adopted for the thermodynamic analysis of the refueling with compressed hydrogen.

Table 5.1. Input parameters to the model

| Parameter | Description | Unit of measure |
|---|---|---|
| $T_{amb}$ | Ambient temperature | K |
| $p_{0,VT}$ | Vehicle tank initial pressure | MPa |
| $T_{0,VT}$ | Vehicle tank initial temperature | K |
| $V_{VT}$ | Vehicle tank volume | $m^3$ |
| $m_w$ | Mass of tank walls | kg |
| $c_w$ | Specific heat of tank walls | kJ/kg K |
| $T_{0,w}$ | Initial temperature of tank walls | K |
| $D_{int}$ | Internal diameter of vehicle tank | mm |
| $d_{int}$ | Internal diameter of vehicle tank | mm |
| $m_{0,ST}$ | Storage tank initial mass | m |
| $V_{ST}$ | Storage tank volume | $m^3$ |
| $p_{0,ST}$ | Storage tank initial pressure | MPa |
| $A_{int}$ | Internal area of storage tank | $m^3$ |
| $V_{cyl}$ | Compressor cylinder volume | $m^3$ |
| $c$ | Compressor clearance | % |
| $p$ | Compressor inlet pressure | MPa |

## 5.2 Algorithm description

The initial conditions for the model are defined by the initial temperature, pressure, and quantity of the gas within the cylinders, by the geometric characteristics of the cylinders, and by the physical properties of hydrogen. The simulation is run for 600 steps, each timestep lasting 1 second, corresponding to a total refueling duration of 10 minutes. The entire refueling is modeled trough an iterative procedure in which the initial conditions are determined based on the initial condition of the tanks, and the thermodynamics at each step are found using the information of the preceding iteration.

As detailed in chapter 2.2, the refueling phase is controlled by an Average Pressure Ramp Rate (APRR) that defines the speed of filling. Its value is selected by the station for the measured ambient temperature and describes the desired pressure rise in the vehicle tank, which is constant over time.

That is:

$$\frac{dp_{VT}}{dt} = APRR = constant \tag{5.1}$$

The setting of the APRR value allows the determination, at each simulated timestep, of the pressure in the vehicle tanks. Whereas the prerequisite for a correct estimation of the behavior of the other thermal properties, that are the temperature and the dispensed mass of hydrogen, is the study of the heat transfer. In this model, the internal heat transfer from the gas to the cylinder wall is considered, while it is neglected the one from the cylinder wall to the environment for the reasons explained in chapter 4.4. During a charging process of a high-pressure vessel placed horizontally, the heat exchange is dominated by the forced convection, and the heat transfer coefficient can be determined using the Nusselt-correlation of Eq. 4.33 (see chapter 4.5).

Via the coupling of the energy equation for the gas inside the cylinder (Eq. 4.24) and the real gas equation (Eq. 4.29), the temperature and mass evolution in the vehicle tanks can be found. To obtain those results the MATLAB function *fsolve* was used.

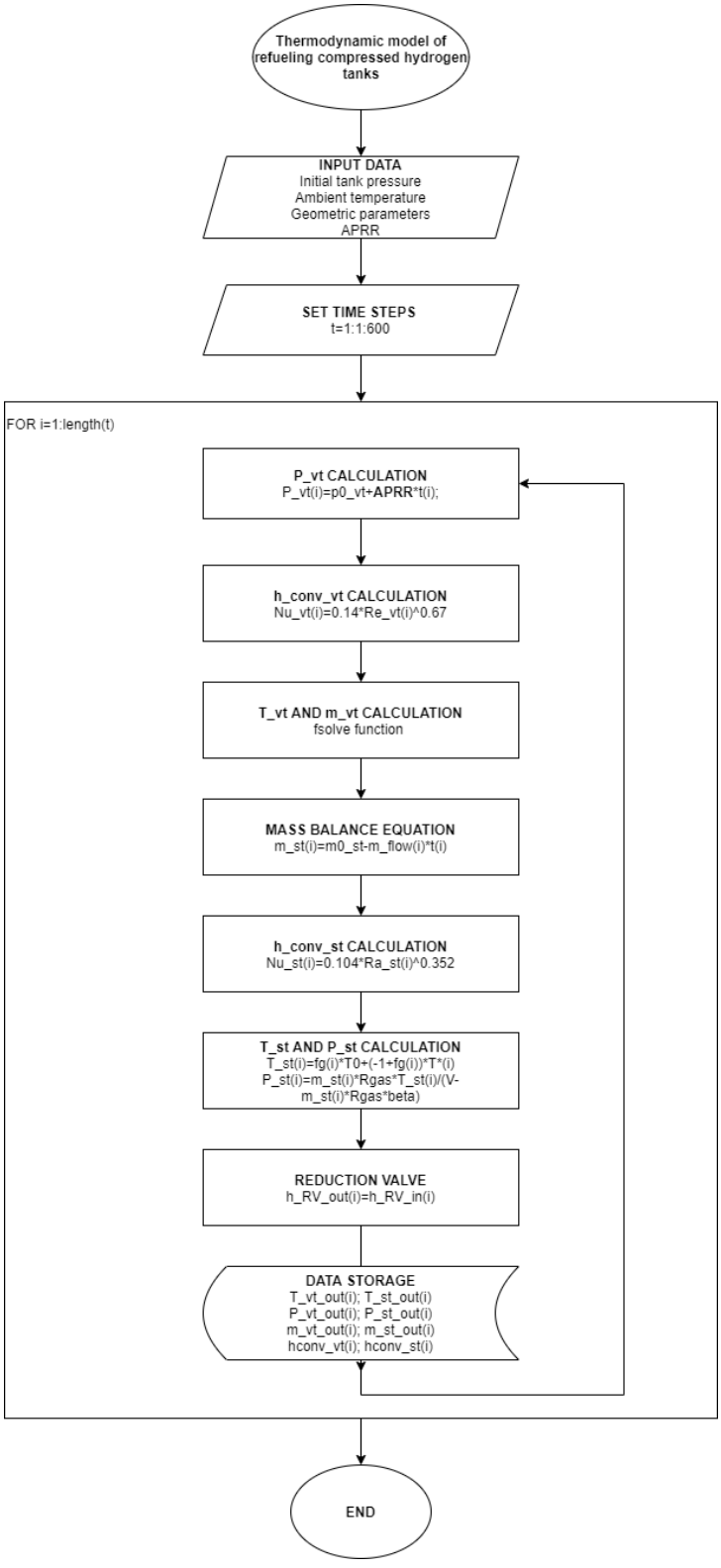


Figure 5.1. Flow chart of the refueling of a heavy-duty vehicle tank

The overall process is controlled by a reduction valve that throttles the gas to the desired pressure altering the mass flow that runs through it. Due to the mass conservation equation (Eq. 4.3), the mass flow in and out the lamination valve is the same, therefore it is known the mass depletion inside the storage vessels to which corresponds a variation of the pressure and temperature respect their initial condition. Also in this case was evaluated the effect of the heat transfer, for which a good approximation is given by the Daney's relation (Eq. 4.34). Thus, the output quantities that are determined of each iteration are: the gas temperature and pressure, the mass flow rate of hydrogen, and the heat transfer coefficients.

The iterative procedure of the algorithm described in this section is illustrated by the flow diagram of Figure 5.1.

## 5.3 The implication of shorter refueling times

The advantages of fuel-cell technology and, in particular, its application for heavy-duty vehicles have been illustrated in detail in the Introduction. Amongst them are recalled the driving range and the short refueling times, that within the perspective of future market expansion and in order to affirm the competitiveness of the technology, are distinctive features respect other types of zero-emission mobility.

In fact, there is no doubt that in the next years we will see a large-scale deployment of hydrogen power and fuel cells for heavy-duty transportation, just in Europe the Jive project aims to deploy nearly 300 FCEBs by the early 2020s. Therefore the refueling time will gain importance, in the first place, to allow higher utilization of refueling stations and hence reduce the investment costs and secondly, to enable that all the transport activities of people or freight are carried out without additional downtime.

From the above descends the objective of this part of the thesis, that can be summed up in the implementation of a dynamic algorithm that, depending on initial conditions and on the amount of hydrogen to refill, determines the appropriate ramp rate able to minimize the refueling time.

## 5.4 APRR parametric study algorithm

In the following algorithm, the value of the APRR is not fixed, but the code runs for a range of values, and it stops when it is reached the specified amount of hydrogen to be dispensed or once any of the fueling parameter safety limits have been exceeded. Indeed, in this code, which is focused on the refueling time reduction, the desired final SOC and so the gas quantity, that might vary according to the time-to-time filling necessity of the bus, is an input data.
Furthermore, reminding what affirmed in chapter 2.2, the SAE J2601 protocol establishes safety limits to ensure a safe refueling, for which the operating gas temperature must stay below 85°C, the maximum allowed pressure is 125% NWP (i.e., 43.75 MPa for a 35 MPa nominal working pressure vehicle), and finally, the flow rate cannot be allowed to go above 0.06 kg/s at any time during the process. This algorithm application enables to perform a parametric study to find the appropriate ramp rate that, respecting all the above-mentioned constraints, accomplishes the refueling in the shortest time possible.

The determination of the thermodynamic properties and the study of the heat transfer follows the same iterative pattern described in chapter 5.2. The flowchart in Fig.6.1 depicts the structure of the algorithm that combines two cycles, one inside the other, on APRR and time.

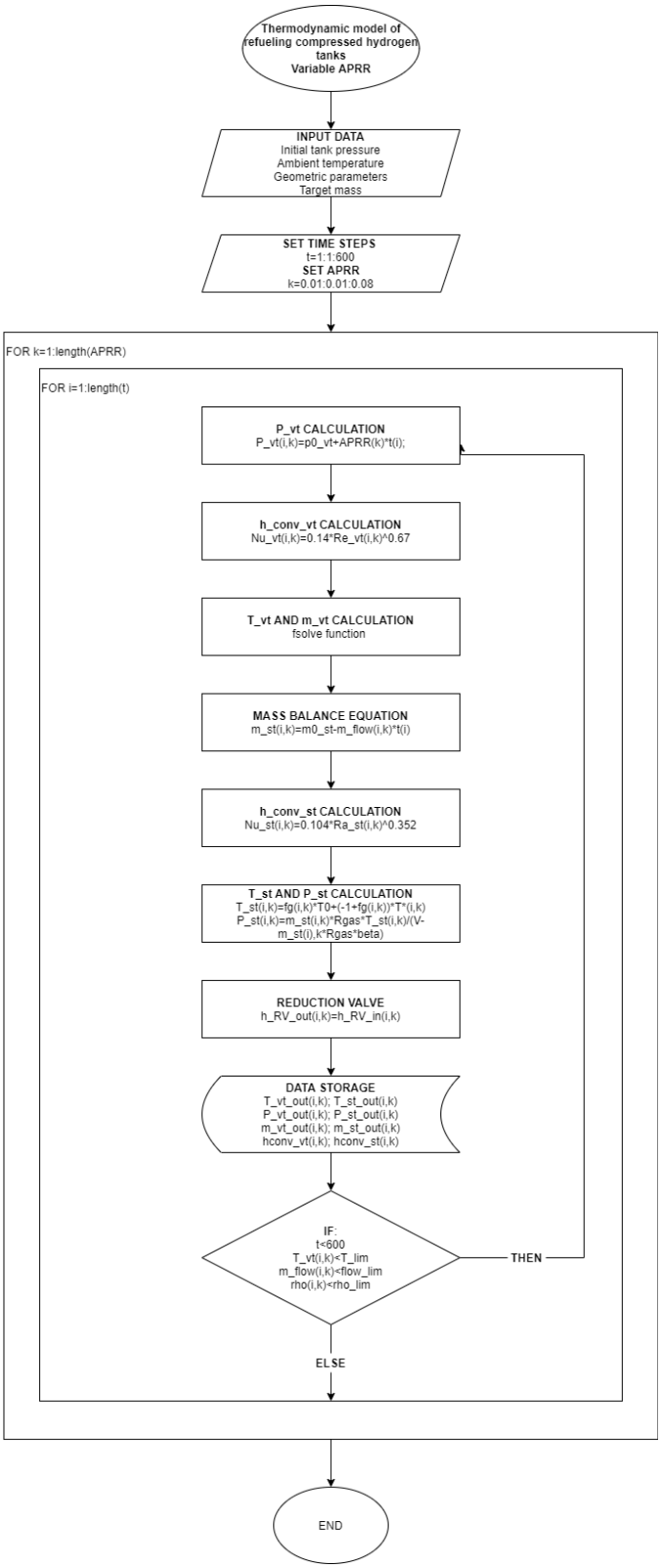


Figure 5.2. Flow chart of the refueling of a heavy-duty vehicle tank with two cycles, on APRR and time

# Chapter 6

# Results and discussion

This chapter presents the numerical results of the model for the analyzed thermodynamic quantities and relative considerations. The station behavior is analyzed, moreover, a simulation of the compressor operation fueling the station's storage and an analysis of the associated electric compression work is discussed. Besides, the influence of the ambient temperature and initial tank pressure on the evolution of the gas temperature during hydrogen refueling, as well as on the refueling time and state of charge are investigated.

To ensure that the model validity, the results are compared with measurements coming from the aggregate data collected during the operation of the 3Emotion stations.

## 6.1 Vehicle tank refueling process simulation

The thermodynamic analysis of the refueling process with compressed gas is described in this section. To enable the comparability of the result, the initial values for the simulation have been chosen in accordance with the on-site measurements and technical references. Table 6.1 shows the filling initial test conditions, while in Table 6.2 are recalled the vehicle tank and storage tank characteristics.

The lack of a standard protocol for heavy-duty hydrogen applications does not make it possible to directly choose the appropriate APRR for different conditions of the ambient temperature and initial pressure in the vehicle tank, as illustrated in chapter 2.2.1.

In this simulation, the speed of fueling, and thus the APRR, has been determined upon the investigation of measured data of real operating stations for a period of 18 months. The measurements in that period of analysis show an average mass flow rate of 0.027 kg/s corresponding to an average ramp rate of 0.03 MPa/s, which is therefore considered the reference value for the model. In the next chapter the attention is focused on refueling duration, and an alternative

Table 6.1. Initial test conditions

| **Test conditions** | |
|---|---|
| Ambient temperature, $T_{amb}$ | 15 °C |
| Dispensed hydrogen pressure, P | 3 MPa |
| Inlet hydrogen flow rate, $\dot{m}$ | 0.0062 kg/s |
| Tanks initial temperature, $T_0$ | 15 °C |
| Initial temperature tank walls, $T_{w0}$ | 15 °C |
| Vehicle tank initial pressure, $p_{in,VT}$ | 2 MPa |
| Storage tank initial pressure, $p_{in,ST}$ | 50 MPa |
| Filling time, t | 600 s |

Table 6.2. Vehicle tank and storage tank specifications

| **Tanks characteristics** | |
|---|---|
| Vehicle tank volume, $V_{VT}$ | 4x322 L |
| Vehicle tank internal length, L | 1.7 m |
| Vehicle tank internal diameter, $D_{int}$ | 0.49 m |
| Internal diameter injector, $d_{int}$ | 0.012 m |
| Full tank capacity, m | 30 kg |
| Mass of tank wall, $m_w$ | 4*300 kg |
| Specific heat of tank wall, $c_w$ | 1494 J/kg K |
| Nominal working pressure, NWP | 35 MPa |
| Storage tank volume, $V_{ST}$ | 11 $m^3$ |
| Storage tank internal area, $A_{int}$ | 97.47 $m^2$ |
| Storage tank initial mass, $m_0$ | 350 kg |
| Nominal working pressure, NWP | 50 MPa |

hypothesis for the APRR is presented. The thermodynamic properties of the fueling event are plotted in Figure 6.1.

With regard to the refueling time, it is presented the behavior of such parameters for a period of 10 minutes. That is because for large tank capacities (larger than 10 kg), proper of heavy-duty vehicles, the target refueling duration of a single bus should not exceed 10 minutes. The confirmation of this comes from the observation of the operational data collected from the 3Emotion stations' dataloggers, which monitor the FCB refueling. The logbooks tables provide the requested qualitative and quantitative data, which indicates a suitable sampling frequency according to the data type. Figure 6.2 shows the probability density function of refueling duration exhibiting a peak of probability for a refueling time of 10 minutes, with a standard deviation of 2.11 minutes.

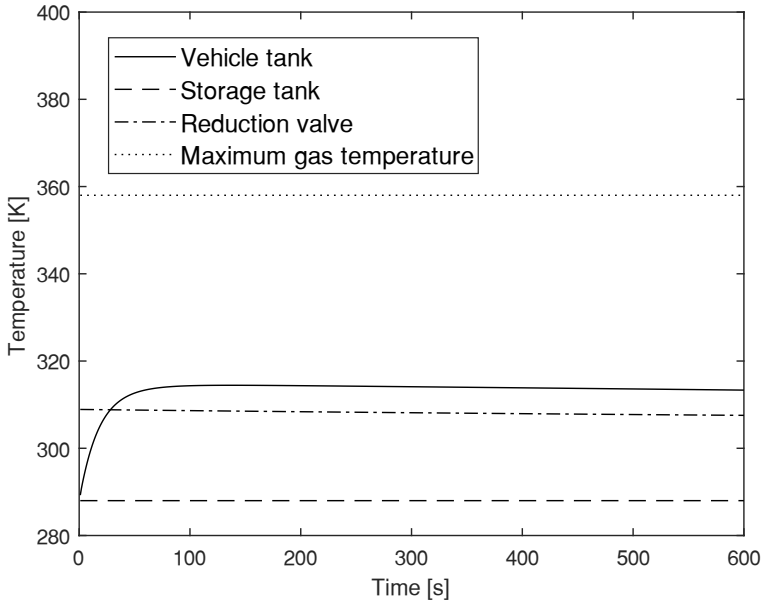


(a) Temperature profile

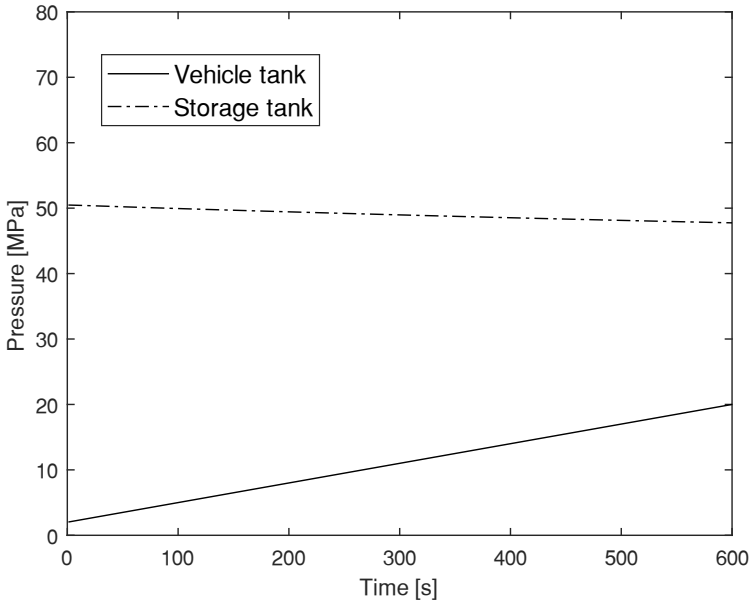


(b) Pressure profile

Figure 6.1. Thermodynamics of hydrogen refueling process overtime: temperature and pressure

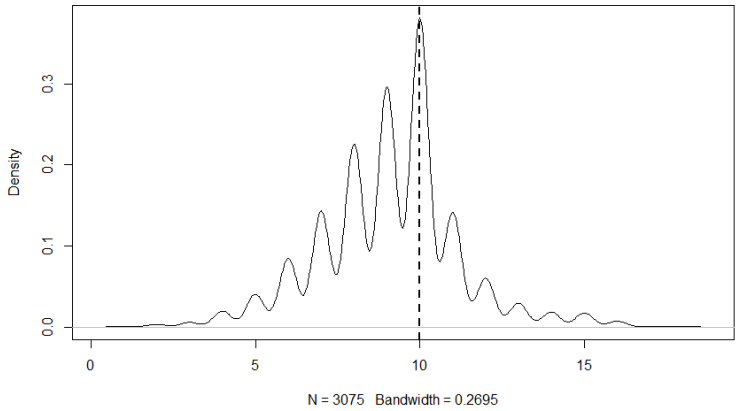


Figure 6.2. Probability density function of refueling duration (min)

Figure 6.1(a) shows the temperature evolution in the storage tank, the vehicle tank, and at the outlet of the reduction valve. The temperature out of the hydrogen refueling station storage tank decreases as mass is leaving, although the effect is not very marked, being these storages characterized by a high mass capacity, and hence the temperature remains close to the ambient temperature during a fill process. Across the reduction valve, a temperature increase takes place caused by the reverse Joule-Thomson effect, moreover the temperature at the outlet decreases as the refueling proceeds as a result of decreasing pressure difference between the storages. Lastly, the temperature in the vehicle tank is non-linear. Indeed, it increases rapidly at the beginning of the refueling when the mass flow entering the system is higher, leading to a more considerable heat of compression than it flattens to a plateau. The temperature increment at the end of the refueling is 25°C.

Furthermore, Fig. 6.1(a) displays the maximum gas temperature limit (358 K) set by the SAE J2601/2 in the dotted line. The limit is never exceeded; actually, the gas temperature is far below, due to a conservative setting used by the stations to prevent any kind of heating problems.

Figure 6.1(b) shows the pressure variation in the two systems. As in the case of the temperature, the pressure out of the HRS storage tank decreases due to mass leaving the tank. Whereas the pressure increases linearly in the vehicle tank at a rate established by the APRR, and at the end of the refueling is reached a pressure of 20 MPa (target pressure).

### 6.1.1 Vehicle tank result validation

By focusing on the filling of the vehicle tank, a comparison between the quantity of hydrogen dispensed into the vehicle tank and the mass flow rate from the storage to the vehicle vessel with the available data can be carried out.

Figure 6.3(a) shows the mass temporal profile during refueling. As pressure increases, the mass grows almost linearly, and at the end of the 10 minutes' refueling is measured a value of 17.75 kg. This result agrees well either with what the fuel cell bus manufacturers declare, namely that the buses refuel approximately 16 $kg_{H2}$/day, and it is also in line with what emerges from the analysis of the operational data. In Figure 6.3(b) is plotted the probability density function of the hydrogen amount dispensed by each registered refueling, in particular, more than 58% of the refueling events dispensed between 15-20 $kg_{H2}$/refueling with a mean value of 15.25 $kg_{H2}$/refueling.

Figure 6.3(c) shows the mass flow of hydrogen during a charging process obtained from the simulation. The mass flow is induced by the pressure difference, thus it grows in the first part of the refueling than after a peak, steadily decreases. In this case, the maximum flow rate imposed by the standard SAE J2601/2 for a normal filling, i.e., 0.06 kg/s, is never exceeded, and the result is comparable with the real data. The curve mean value, 0.026 kg/s (≅1.56 kg/min), is indeed aligned with the trend of the average flow rate measured for the 18 months of analysis: see Figure 6.3(d).

Finally, Figure 6.4 represents the vehicle storage tank state SOC, whose definition was provided in chapter 2.1.1. The SOC is always less than 1, and at the end of the refueling, its value is 60%. This means that the tank is underfilled respect its capacity but is not something unexpected since the buses are typically refueled by half-tank (full tank capacity is around 30 $kg_{H2}$) as it is also obtained from the model.

### 6.1.2 Heat transfer coefficient evolution

Figure 6.5 shows, on the right, the heat transfer coefficient between the gas and tank wall throughout a fill process resulting from the application of the correlations described in chapter 4.4. Comparatively to what has been predicted in literature [18] the convection coefficient increases rapidly within the first seconds and then declines progressively.

Indeed, its evolution is strongly related to the rate of mass flow entering the tank; the greater the mass flow rate, the greater is the increase in the coefficient

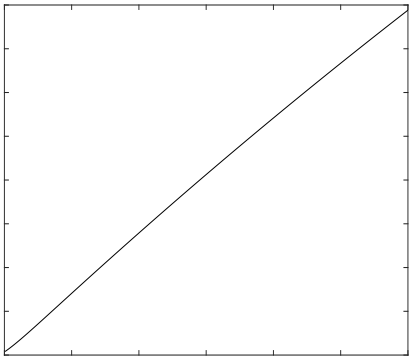

(a) $H_2$ dispensed quantity profile

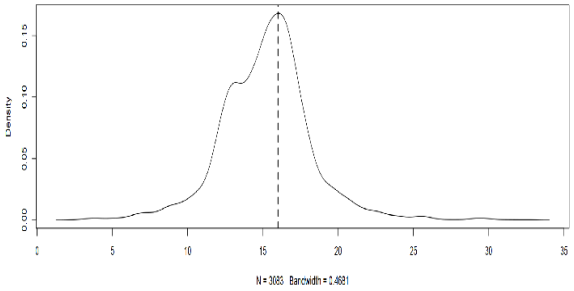


(b) Probability density function of hydrogen (kg) per refueling event

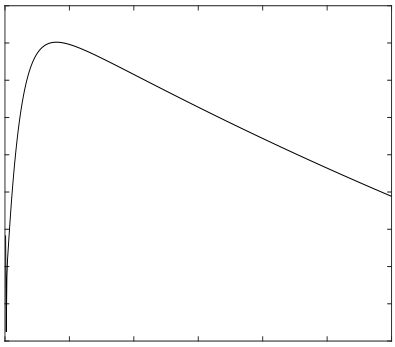

(c) Mass flow rate profile

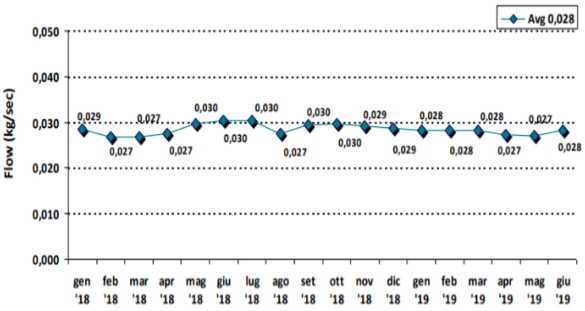


(d) Average flow rate measured in the London station for the 18th months pf analysis

Figure 6.3. Model results for the refueling of the vehicle tank compared with real data collected in the 3Emotion Project

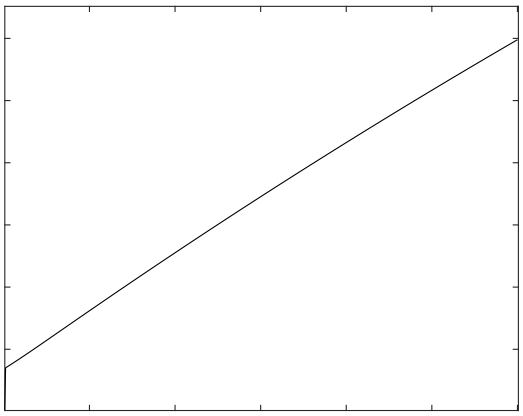

Figure 6.4. Variation of State of Charge (SOC) with time for the refueling of the storage tank

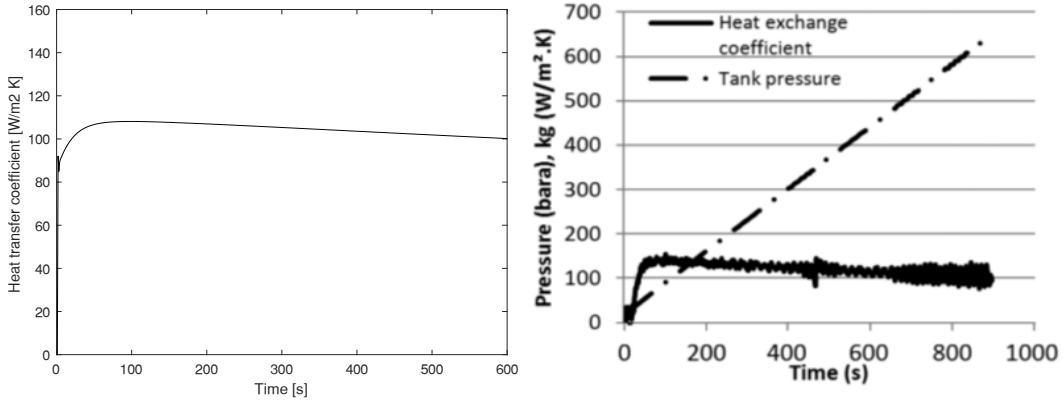


Figure 6.5. Comparison of the heat transfer coefficient profile between the model and the study by Bourgeois et. al

in consequence of higher turbulence at the inlet of the cylinder, that is the cause of the heat exchange.

To verify the validity of the heat transfer model, the algorithm has been tested with the data from the study of Bourgeois et al. [45], and the results have been compared. Indeed, both the models are based on zero-dimensional modeling and the tank orientation, which determines the dominant forces, is the same.

The similarity between the collected data and the run simulation act as a thermodynamics model validity test. For a hydrogen filling conducted at a ramp rate of 0.7 bar/s (0.07 MPa/s) it is calculated an average mass flow rate of 0.037 kg/s, which matches the value reported in the study, i.e., 0.03 kg/s. On the right of Figure 6.5, the heat transfer coefficient as a function of time for the research investigated is showed. The resemblance of the two curves is evident, first a quick increase, up to a maximum value of about 157 $W/m^2K$, followed by a nearly linear drop.

## 6.2 Storage tank refueling process simulation

Once the refueling of the vehicle is terminated the compressor activates to restore the tank nominal pressure so that, in case of several fillings in a row, the station is always capable of providing the service. It is assumed that the gas is provided to the station with a continuous flow at 3 MPa.

A simulation of the storage tank is provided in Figure 6.6. From the initial condition, i.e., 47.75 MPa and 15°C, to the nominal pressure of 50 MPa the station takes 1911 seconds. The speed of this refilling time strictly depends on the

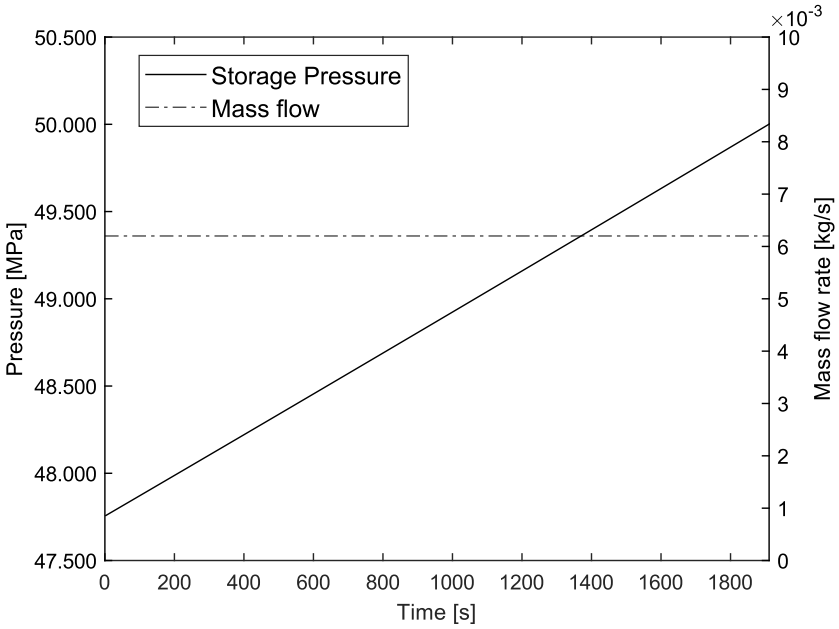


Figure 6.6. Pressure evolution during the refueling of the storage tank and mass flow rate at the inlet of the tank. $T_0$ 15°C, $p_0$=47.75 MPa

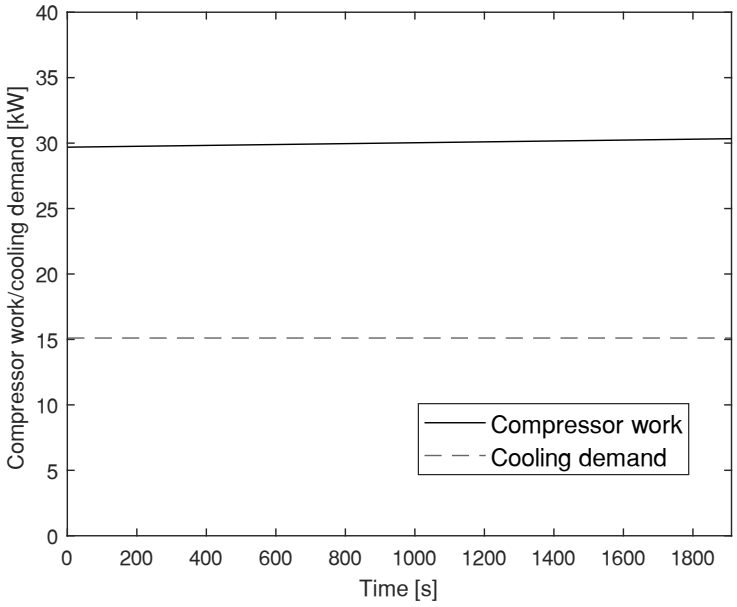


Figure 6.7. Work performed by the compressor for the refueling of the storage tank and consumption of the intercooler

Table 6.3. Comparison of the compressor intermediate and outlet temperatures with an isentropic compression or polytropic compression

| | **Isentropic compression** | **Polytropic compression** |
|---|---|---|
| $\boldsymbol{T_{int}}$ | 454.71 K | 458.05 K |
| $\boldsymbol{T_{out}}$ | 459.68 K | 464.34 K |

compressor capacity, which is constant and equal to 0.0062 kg/s, that for Eq. 4.8 corresponds to about 7 strokes per second (420 rpm). During the process, the gas slightly heats up, however since the refilling is slow, no compression within the storage tank occurs, and the effect has not an appreciable impact.

Figure 6.7 shows the compressor electrical work and cooling demand. The work performed by the compressor, calculated as expressed in Eq. 4.14, increases as the filling advances due to higher pressure ratios in the second stage as the pressure in the tank reaches the nominal value. Instead, the compressor cooling demand is constant ed equal to 15 kW. The reason is that the operating temperatures of the intercooler are fixed, and the mass flow that is suctioned by the compressor is also constant.

In chapter 4.3 are described the equations that allow calculating the power required by the compressor and are presented two processes that model the gas compression. In fact, the compression can either be assumed to follow an isentropic process, thus an isentropic efficiency is introduced (Eq. 4.11) or a polytropic process, which coefficient is estimated from Eq. (4.12). The effect of both the process on the compressor outlet temperature of the first stage, $T_{int}$, and on the second stage, $T_{out}$ are illustrated in Table 6.1. We can conclude that there is no significant difference between the two methods, hence the isentropic assumption implemented in this model well approximates the compression process.

## 6.3 Initial parameter variation

The effects of the ambient temperature and the initial tank pressure on the temperature distribution within the cylinder, on the SOC, and on the refueling time are investigated below. For all the simulations, the APRR was set at 0.03 MPa/s and are respected the limitations imposed by the SAE J2601/2.

Table 6.4. Effect of the ambient temperature over the refueling time, SOC, and final vehicle tank temperature. Initial pressure set at 2 MPa

| Ambient temperature [°C] | Refueling time [s] | SOC [%] | Final temperature vt [K] | Final temperature vt [°C] | ΔT [°C] |
|---|---|---|---|---|---|
| **15** | 600 | 0.5978 | 313.33 | 40.33 | 25.33 |
| **20** | 600 | 0.5972 | 318.61 | 45.61 | 25.62 |
| **25** | 600 | 0.5966 | 323.88 | 50.88 | 25.88 |
| **30** | 600 | 0.5960 | 329.16 | 56.16 | 26.16 |

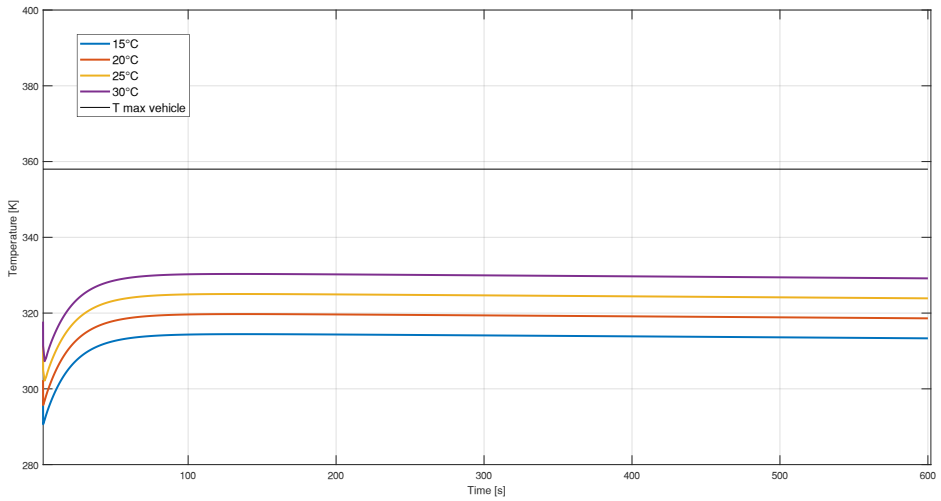


Figure 6.8. Gas temperature profile at different ambient temperatures between 15 and 35 °C. APRR=0.03 MPa/s, $p_0$=2 MPa

### 6.3.1 Effect of ambient temperature

Figure 6.8 shows the gas temperature profile at an initial pressure of 2 MPa and for an ambient temperature varied between 15 and 30 °C, while in Table 6.2 are also summarized the effect on the SOC and on the final gas temperature.

It can be seen that the temperature distributions run almost parallel, indeed the temperature difference between the beginning and the end of the refueling process is approximately the same. Moreover, the higher is the ambient temperature, the greater is the peak. This is due to the more extensive initial heating of the tank that clearly leads to higher gas temperatures. However, the increase of the initial ambient temperature has a very limited effect on the SOC that reaches, in any case, values close to 60% with equal refueling times.

Table 6.5. Effect of the initial pressure over the refueling time, SOC, and final vehicle tank temperature. Ambient temperature set at 15 °C

| Initial pressure [MPa] | Refueling time [s] | Initial SOC [%] | Final SOC [%] | Final temperature vt [K] | ΔSOC [%] |
|---|---|---|---|---|---|
| **2** | 600 | 5 | 59 | 313.33 | 54 |
| **10** | 600 | 27 | 80 | 312.52 | 53 |
| **20** | 547 | 51 | 99 | 310.28 | 48 |
| **30** | 191 | 72 | 99 | 299.63 | 27 |

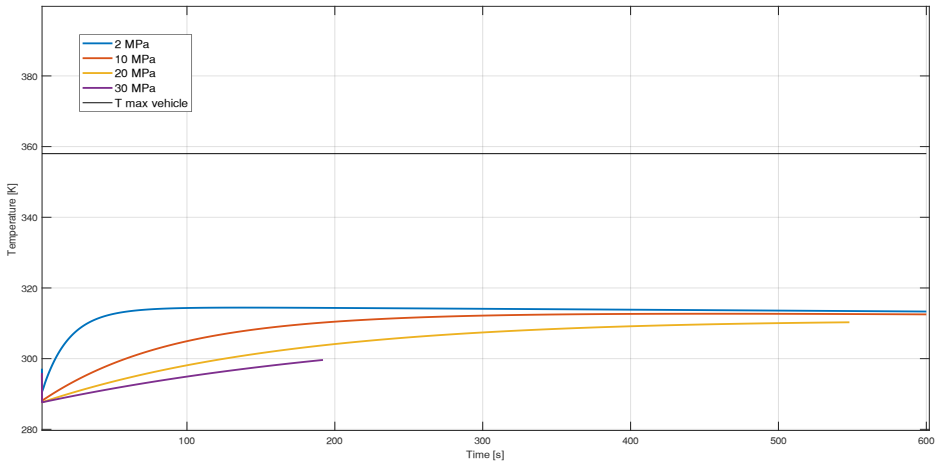


Figure 6.9. Gas temperature profile at different initial tank pressure between 2 and 30 MPa. APRR=0.03 MPa/s, $T_0$=15°C MPa

### 6.3.2 Effect of initial pressure

In this simulation, the initial pressure was varied in the range between 2 MPa and 30 MPa while the ambient temperature is fixed at 15°C. Figure 6.9 shows that the refueling from the 2 MPa manifests in a more significant increase in temperature, whereas with 30 MPa, the increase is smaller. Therefore, filling with a lower initial pressure yields to a higher overall temperature increment. The reason is attributable to the greater quantity of hydrogen that is dispensed when starting from a smaller pressure. Table 6.3 illustrates these relative values, furthermore shows the variation of the SOC between the refueling beginning and end that diminishes with increasing initial pressures.

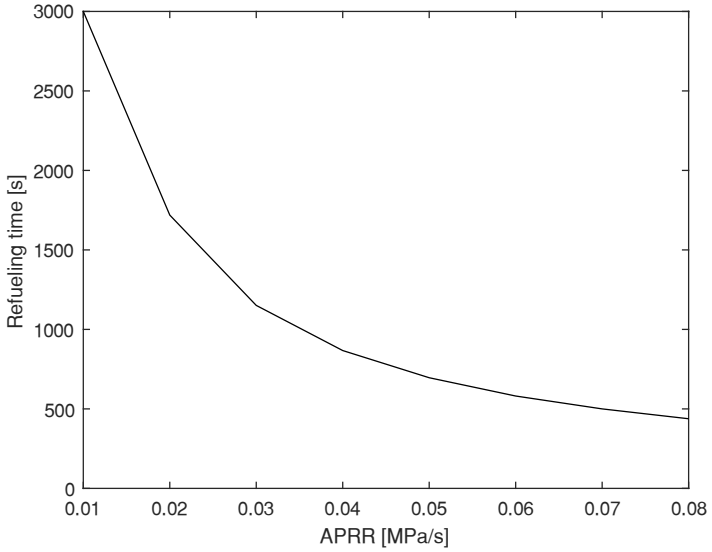


Figure 6.10. Refueling time reduction as a consequence of higher values of the APRR

## 6.4 APRR impact on refueling duration

Due to its dynamicity, the model is able to simulate very different initial and boundary conditions. In chapter 6.3 has been illustrated the effect of changing the ambient temperature and the initial pressure, while in this chapter the influence of different APRRs for filling the vehicle tank to its full capacity is described.

The APRR is thus varied between 0.01 MPa/s to 0.08 MPa/s with an increment of 0.01MPa/s, while the selected initial conditions are 288 K and 2 MPa, which correspond to an almost empty tank. The objective is to determine which of those APRRs allow to refuel the vehicle in the shortest time possible while maintaining compliance with the SAE J2601/2 guidelines.

Figure 6.10 shows the APRRs and their relative refueling time. As might be expected, the higher is the speed of refueling, so the APRR, the lower is the refueling time despite this correlation is not linear. Although the highest APRR values seem to be the preferred option, they do not respect the mass flow rate limit. In Figure 6.11 is showed the mass flow rate over time for each APRR and is displayed the maximum value allowed by the SAE J2601/2. It is evident that the peaks for the flow rate calculated with APRR=0.07 MPa/s and APRR=0.08 MPa/s overcome the safety limit. Therefore, the quickest way to fill the tank up to 30 kg is to adopt APRR=0.06 MPa/s to which corresponds a refueling of 581 seconds.

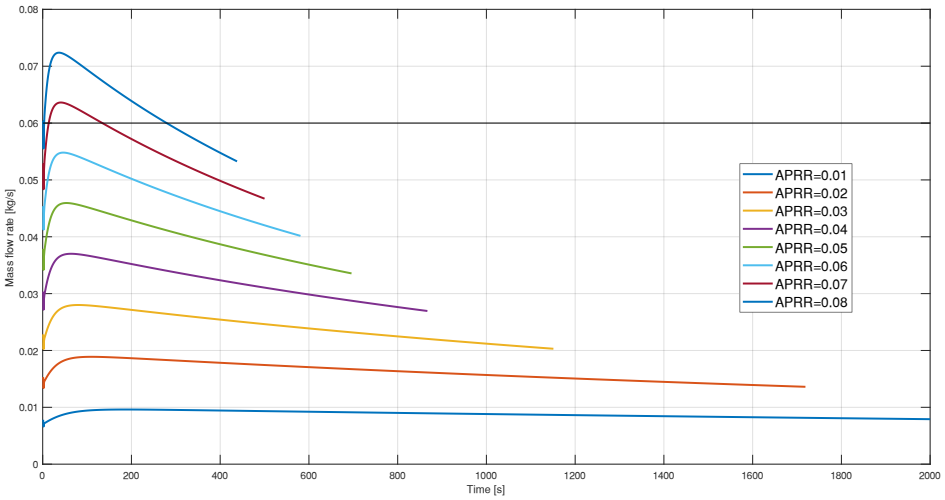


Figure 6.11. Mass flow rate over time at different APRR between 0.01 and 0.08 MPa/s. Simulation for the filling to full capacity. $T_0$=15°C MPa/s, $p_0$=2 MPa

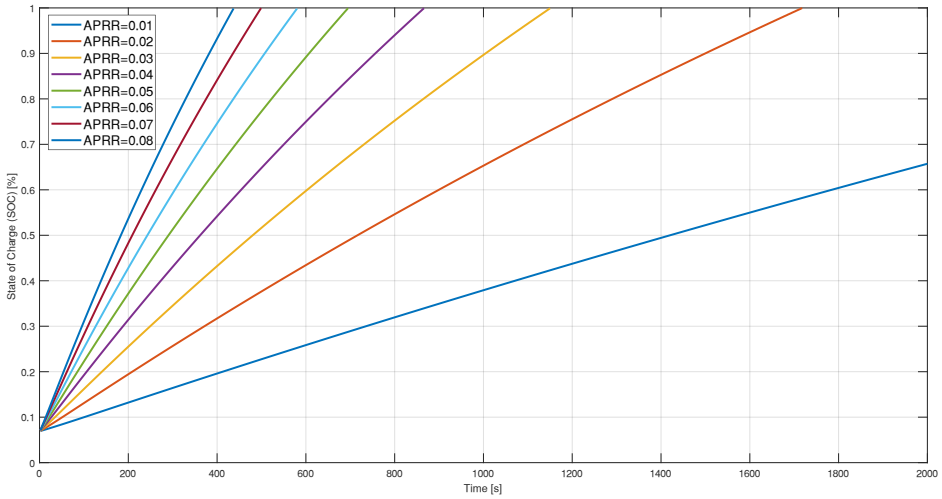


Figure 6.12. State of Charge over time at different APRR between 0.01 and 0.08 MPa/s. Simulation for the filling to full capacity. $T_0$=15°C MPa/s, $p_0$=2 MPa

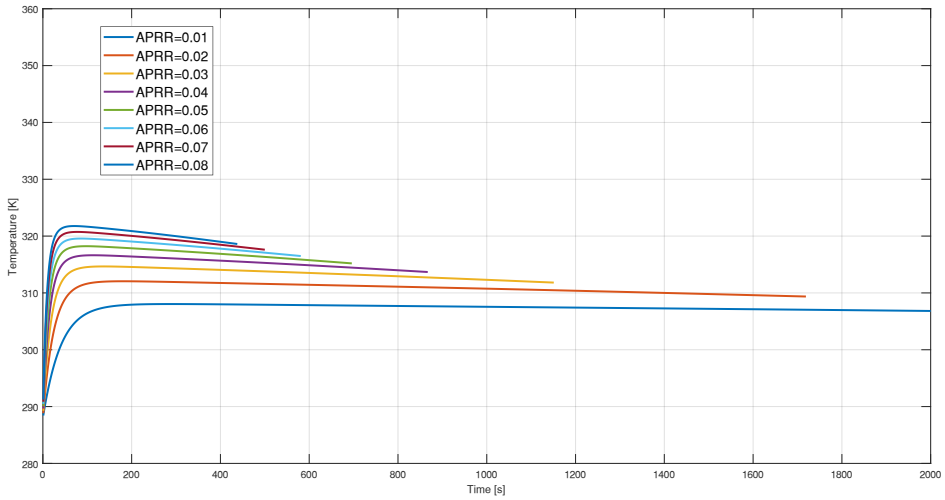


Figure 6.13. Gas temperature profile over time at different APRR between 0.01 and 0.08 MPa/s. Simulation for the filling to full capacity. $T_0$=15°C MPa/s, $p_0$=2 MPa

Figure 6.12 illustrates the various SOC. The refueling for the most performing ramp rate ends at a target pressure of 36.86 MPa that corresponds to a SOC of 99%.

Finally, a comparison of the thermodynamic behavior between the different cases is presented. Figure 6.13 shows the gas temperature profiles. For each specified APRR, the gas temperature increases and then flattens, but the greater the APRR, the higher the peak that, in addition, is reached in a shorter time. Furthermore, the curves tend to get nearer because of the predominant influence of the internal forced convection.

### 6.4.1 APRR parametrization study applied on 3Emotion case study

In conclusion, the same parametric approach can be applied to the vehicle tank simulation presented in chapter 5.2. In that case, the simulation was run for an APRR=0.03 MPa/s upon the investigation of the HRSs operating conditions. Figure 6.14 shows an inverse and decreasing correlation between the APRR and the refueling time. In fact, varying the first can be seen that the latter rapidly decreases by setting a slightly higher value. More specifically, from 0.03 to 0.04 MPa/s the refueling duration is reduced by 25%. The same conclusions can be derived from analyzing Figure 6.15, where the SOC is plotted over time for different APRR (0.03-0.08 MPa/s). By fixing the target SOC, the ending conditions are reached first for higher APRR values.

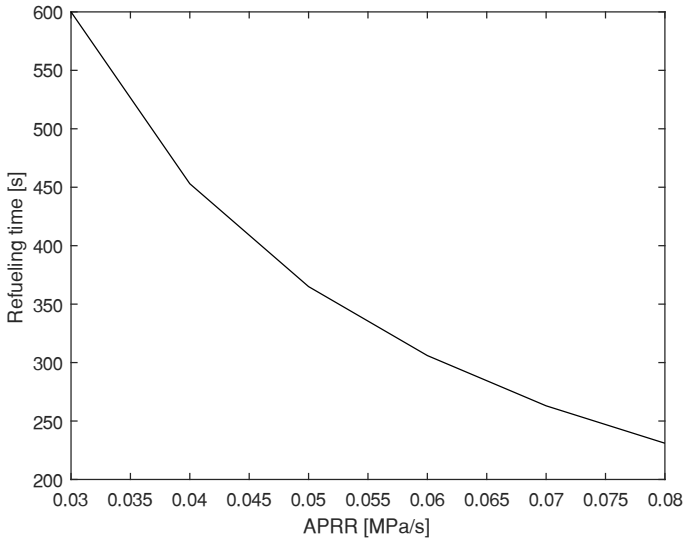


Figure 6.14. Refueling time reduction as a consequence of higher values of the APRR. 3Emotion case study

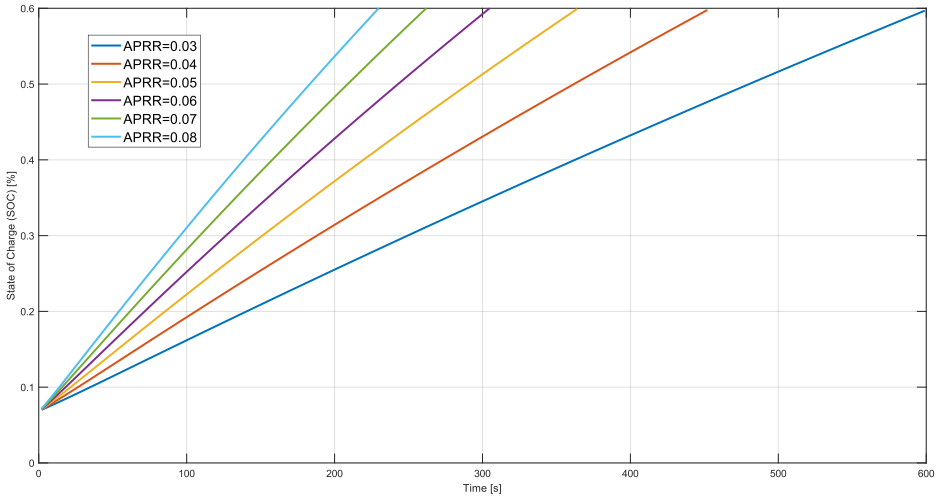


Figure 6.15. State of Charge over time for different APRR between 0.03 and 0.08 MPa/s 3Emotion case study. $T_0$=15°C MPa/s, $p_0$=2 MPa

In conclusion, the most appropriate ramp rate to fill the tank as fast as possible, without exceeding the permissible limits concerning temperature, pressure, flow rate as well as state of charge is 0.06 MPa/s. Even in this case, the limiting condition for a safe refueling is represented by the mass flow rate. With this condition, the refueling time is reduced by 62% from which derive all the advantages illustrated up to now.

# Chapter 7

# Conclusions

If the study of the thermodynamic behavior of compressed hydrogen refueling stations, and in particular, the filling of small scale application vehicle storage tanks, as well as computational fluid dynamic calculations of the temperature distribution inside the tank from the numerical and experimental point of view, have been carried out in the last decades, the application on large volumes, such the one of buses or trucks, is relatively recent and yet widely unexplored.

In this thesis, a thermodynamic model of a hydrogen refueling station for the refilling of fuel-cell buses has been developed and implemented in MATLAB. The main components that are modeled are a compressor, a high-pressure storage tank, a reduction valve, and a vehicle tank. The heat transfer between the gas and the tank walls is also included and modeled dynamically following the change of the gas properties during the refueling process. Both a refilling of a vehicle tank and a refueling of the storage tank are simulated. The results are then compared with measurements coming from the observation of the operation of the 3Emotion stations. Additionally, the influences of ambient temperature, initial pressure on the gas temperature during the filling procedure, on the SOC, and on the refueling time are investigated.

Furthermore, given the relevance attributed to the refueling time for the competitiveness of the hydrogen and fuel-cell technology and its deployment and cost-effectiveness on large-scale, this work presents a method for the determination of the most suitable pressure ramp rate value that minimizes it.

The following conclusions can be drawn:

- Filling the vehicle tank with an APRR=0.03 MPa/s, we are always in a safe condition in which the pressure, temperature, and density limits given by the SAE J2601 are never exceeded. The heating of the gas in the tank follows a non-linear shape and starting from an ambient temperature of 288 K, and an initial pressure of 2MPa at the end of the refueling the gas temperature reaches 313.33 K and a final pressure of 20 MPa.

- From the simulation of 10 minutes refueling with an APRR=0.03 MPa/s, the amount of hydrogen dispensed at the end of the process is 17.75 kg. This value is aligned with what results from the analysis of the operational performances of the 3Emotion hydrogen station sites. Nevertheless, it does not correspond to a complete filling level but to a SOC=60%, therefore to an underfilling. Indeed those conditions do not allow to achieve the full tank capacity, which is 30 $kg_{H2}$.

- The correlation proposed by Bourgeois [45] for the modeling of the heat transfer in horizontal cylinders filled with high-pressure gas seems to apply well to the case under investigation. This is confirmed by the comparable behavior of the heat transfer coefficient profile calculated in the study and the one obtained from the algorithm tested with the data from the literature.

- From the simulation of the storage tank refueling, the time required to restore the initial tank condition is 32 minutes. There is no substantial difference in modeling the compression as an isentropic or polytropic process.

- The effect of varying the initial vehicle tank pressure is more significant than changing the ambient temperature. In general, a higher ambient temperature and a lower tank pressure result in a higher maximum and final temperature. Whereas, for greater initial pressures the refueling time and the SOC considerably decrease.

- The filling time and the refueling speed are strongly correlated: the lowest the first, the highest the second, and hence the APRR that should be set by the station. For the case of filling up the vehicle up to its full capacity the most appropriate APRR is 0.06 MPa/s to which corresponds a SOC=99%. Furthermore, adopting an APRR=0.06 MPa/s when are dispensed 17.75 $kg_{H2}$ the refueling time is reduced by 62%.

## 7.1 Recommendations for further work

In the present thesis, the refueling of fuel-cell buses has been presented from a system perspective and can be considered a preliminary study for this type of application. Further suggestions for a more refined study can be:

- To conduct an extensive validation of the model with point and not aggregate data. This could involve direct experimental measurements on the various components or the acquisition of more precise data provided by the station operators.

- To perform an experimental investigation to further analyze the temperature distribution while filling the vehicle tank and so refine the correlations for the convective heat transfer coefficient used in this study.

- To further improve the modeling of the station including an electrolyzer, a cascade system, and multiple compressors. In this way a more comprehensive and realistic refueling system is modeled and it could be studied the configuration that optimizes at best the station design.

- To investigate the behavior of the station when several vehicles refuel in a row and with back-to-back fills. In this case the storage refilling time, the time between refuelings and the refueling daily load profile should be carefully examined.

# Bibliography

[1] IPCC, «Global Warming of 1.5°C. An IPCC Special Report on the impacts of global warming of 1.5°C above pre-industrial levels and related global greenhouse gas emission pathways, in the context of strengthening the global response to the threat of climate change,,» Geneva, Switzerland, 2018.

[2] UNEP, "The Emissions Gap Report," 2019.

[3] «Climate Action Summit,» in *Report of the Secretary-General on the 2019 Climate Action Summit and the way forward 2020*, 2019.

[4] IRENA, «Hydrogen: a rewable energy perspective,» 2019.

[5] «Hydrogen from Renewable Power: Technology Outlook for the Energy Transition.,» International Renewable Energy Agency (IRENA), Abu Dhabi, 2018a.

[6] *AFC TPC,* 2019.

[7] *IEA, 2019a,* Paris: International Energy Agency.

[8] «Hydrogen Roadmap Europe: A sustainable pathway for the European Energy Transition,» *The Fuel Cells and Hydrogen 2 Joint Undertaking,* 2019.

[9] «3Emotion. Proposal Part B (FCH-JU-2013-2)».

[10] Hydrogen Council, «Hydrogen scaling up, A sustainable pathway for the global energy transition,» *Hydrogen Roadmap Europe,* 2017.

[11] K. Chandler, L. Eudy e C. Gikakis, «Fuel Cell Buses in US Transit Fleets: Current Status 2018 (No. NREL/TP-5400-72208),» *National Renewable Energy Laboratory (US),* 2018.

[12] J. P. Stempien e S. H. Chan, «Comparative study of fuel cell, battery and hybrid buses for renewable energy constrained areas,» *Journal of Power Sources,* pp. 340, 347-355, 2017.

[13] H. Ammermann, Y. Ruf, S. Lange, D. Fundulea e A. Martin, «Fuel Cell Electric Buses – Potential for Sustainable Public Transport in Europe,» *The Fuel Cells and Hydrogen Joint Undertaking,* 2015.

[14] «Clean hydrogen in European cities fuel cell electric buses: a proven zero-emission solution key facts, results, recommendations,» *The Fuel Cell and Hydrogen Joint Undertaking,* 2016.

[15] «HIGH V.LO CITY,» The Fuel Cells and Hydrogen Joint Undertaking, [Online]. Available: http://highvlocity.eu/2012/about/high-vlo-city-vision-and-objectives/.

[16] «HyER,» [Online]. Available: http://hyer.eu/.

[17] W. Mérida e C. J. B. Dicken, «Measured effects of filling time and initial mass on the temperature distribution within a hydrogen cylinder during refuelling,» *Journal of Power Sources,* pp. 165(1), 324-336, 2007.

[18] W. Mérida e C. J. B. Dicken, «Modeling the Transient Temperature Distribution within a Hydrogen Cylinder during Refueling,» Vol. %1 di %2Numerical Heat Transfer, Part A: Applications, pp. 53:7, 685-708, 2007.

[19] P. L. Woodfield, M. Monde e T. Takano, «Heat transfer characteristics for practical hydrogen pressure vessels being filled at high pressure,» *Journal of Thermal Science and Technology,* pp. 3(2), 241-253, 2008.

[20] P. L. Woodfield, M. Monde e Y. Mitsutake, «Measurement of averaged heat transfer coefficients in high-pressure vessel during charging with hydrogen, nitrogen or argon gas,» *Journal of Thermal Science and Technology,* pp. 2(2), 180-191, 2007.

[21] M. Monde, P. Woodfield, T. Takano e M. Kosaka, «Estimation of temperature change in practical hydrogen pressure tanks being filled at high pressures of 35 and 70 MPa,» *International journal of hydrogen energy,* pp. 37(7), 5723-5734, 2012.

[22] L. Zhao, L. Yanlei, J. Yang, Y. Zhao, J. Zheng, H. Bie e X. Liu, «Numerical simulation of temperature rise within hydrogen vehicle cylinder during refueling,» *International journal of hydrogen energy, 35(15),* pp. 8092-8100, 2010.

[23] M. Striednig, S. Brandstätter, M. Sartory e M. Klell, «Thermodynamic real gas analysis of a tank filling process,» *International journal of hydrogen energy, 39(16),* pp. 8495-8509, 2014.

[24] M. Hosseini, I. Dincer, G. F. Naterer e M. A. Rosen, «Thermodynamic analysis of filling compressed gaseous hydrogen storage tanks,» *International journal of hydrogen energy, 37(6),* pp. 5063-5071, 2012.

[25] J. Xiao, P. Bérnard e R. Chahine, «Charge-discharge cycle thermodynamics for compression hydrogen storage system,» *International Journal of Hydrogen Energy 41.12,* pp. 5531-5539, 2016.

[26] X. Zhou, T. Yang, J. Xiao, P. Bénard e R. Chahine, «Estimation of filling time for compressed hydrogen refueling,» *Energy Procedia,* pp. 158, 1897-1903, 2019.

[27] J. Xiao, X. Wang, X. Zhou, P. Bénard e R. Chahine, «A dual zone thermodynamic model for refueling hydrogen vehicles,» *International Journal of Hydrogen Energy,* pp. 44(17), 8780-8790, 2019.

[28] N. Omdahl, «Modeling of a Hydrogen Refueling Station,» Master's thesis, Norwegian University of Science and Technology, 2014.

[29] E. Rothuizen, «Hydrogen Fuelling Stations. A Thermodynamic Analysis of Fuelling Hydrogen Vehicles for Personal Transportation.PhD thesis,» Danmarks Tekniske Universitet, 2013.

[30] «Refueling Protocols for Medium and Heavy-Duty Vehicles,» [Online]. Available: https://cordis.europa.eu/project/id/874997.

[31] «National Institute of Standards and Technology, NIST Chemistry WebBook,» 2018. [Online]. Available: http://webbook.nist.gov/chemistry.

[32] *Fueling Protocols for Light Duty Gaseous Hydrogen Surface Vehicles,* Society of Automitive Engineers (SAE International), 2010.

[33] *Fueling Protocol for Gaseous Hydrogen Powered Heavy Duty Vehicles,* Society of Automitive Engineers (SAE International), 2014.

[34] *70 MPa Compressed Hydrogen Surface Vehicle Fueling Connection Device. J2799_200705,* Society of Automitive Engineers (SAE International).

[35] *Hydrogen Fuel Quality for Fuel Cell Vehicles. J2719_202003,* Society of Automotive Engineers (SAE International).

[36] «3Emotion,» [Online]. Available: https://3emotion.eu/.

[37] ANSI/PMI, The Standard for Project Management - Sixth Edition, IPG, 2017.

[38] ISO 21500: Guidance on project management, 2012.

[39] *Hylights: Monitoring & Assessment Framework (MAF) Handbook at Demonstration Project Level for Large-Scale Road Transportation*

*Demonstration Projects on "Hydrogen for Transport" under FP7/JTI,* Report Date: 23 October 2008.

[40] R. Smith, Chemical process: design and integration, John Wiley & Sons, 2005.

[41] A. Ken e M. Stewart, «Reciprocating Compressors,» in *Surface Production Operations: Design of Gas-Handling Systems and Facilities (Second Edition)*, 1999, pp. 286-326.

[42] B. Guo, «Gas Lift,» in *Petroleum Production Engineering (Second Edition)*, 2017, pp. 549-601.

[43] H. Chen, J. Zheng, P. Xu, L. Li, Y. Liu e H. Bie, «Study on real-gas equations of high pressure hydrogen,» *International journal of hydrogen energy 35.7,* pp. 3100-3104, 2010.

[44] «National Institute of Standards and Technology,» [Online]. Available: https://webbook.nist.gov/chemistry/.

[45] T. Bourgeois, F. Ammouri, M. Weber e C. Knapik, «Evaluating the temperature inside a tank during a filling with highly-pressurized gas. 40(35),» *International journal of hydrogen energy,* pp. 11748-11755, 2015.

[46] D. E. Daney, «Turbulent natural convection of liquid deuterium, hydrogen and nitrogen within enclosed vessels. 19(4),» *International journal of heat and mass transfer,* pp. 431-441, 1976.

[47] T. L. Bergman, F. P. Incropera, D. P. DeWitt e A. S. Lavine, Fundamentals of heat and mass transfer, John Wiley & Sons, 2011.

[48] I. V. Lienhard e H. John, A heat transfer textbook, phlogiston press, 2005.

[49] M. Boles e Y. Cengel, An Engineering Approach, New York: McGraw-Hil l Education, 2014.

# Appendix

## MATLAB code

```
%%%%%%%%%%REFUELING OF VEHICLE TANK MODEL%%%%%%%%%

clc; clear;

%data H2
Ru=8.314; %universal gas constant [J/K mol]
MM_H2=2.016*1e-3; %H2 molecular mass [kg/mol]
Rgas=Ru/MM_H2; %[J/K kg]
beta=1.9155; %real gas equation parameter [K/MPa]

%%%%%%%%%%%%%%%%%%%%VEHICLE TANK DATA%%%%%%%%%%%%%%%%%%%%
V_vt=1.288; %volume vehicle tank [m3]
mw=300*4; %mass of tank wall [kg]
cw=1494; %specific heat of tank wall [J/kg/K]
T0=288; %initial temperature [K]
p0_vt=20*1e-1; %initial pressure [MPa]
T8=288; %inlet flow temperature [K]
Tw0=288; %initial temperature of tank wall [K]
m0=2.14; %initial mass in vehicle tank (Tin=288K,pin=20bar) [kg]
A_in=12; %internal surface area of the vt [m2]
D_int=0.49;  %internal diameter [m]
d_int=0.012; %diameter of the injector of the tank [m]
A_cross=pi*d_int^2/4; %cross section area [m2]
H=3.07; %height of storage tanks [m]
g=9.81; %gravitational accelaration [m/s2]

%%%%%%%%%%%%%%%%%%%%STORAGE TANK DATA%%%%%%%%%%%%%%%%%%%%
V_st=11; %volume storage tank [m3]
p0_st=500*1e-1; %initial pressure [MPa]
m0_st=350; %initial mass in storage tank  [kg]
A_in_st=97.47; %internal surface area of the st [m2]
mflow_in=0.0062; %mass flow from the compressor [kg/s]

t=1:1:600;
APRR=0.03:0.01:0.08;
```

```
%%%%allocation of profiles%%%%%
cp_vt=zeros(length(APRR),length(t))';
cv_vt=zeros(length(APRR),length(t))';
gamma_vt=zeros(length(APRR),length(t))';
m_vt=zeros(length(APRR),length(t))';
m_flow=zeros(length(APRR),length(t))';
T_vt=zeros(length(APRR),length(t))';
Tb=zeros(length(APRR),length(t))';
P_vt=zeros(length(APRR),length(t))';
Tw=zeros(length(APRR),length(t))';

rho_vt=zeros(length(APRR),length(t))';
mu_vt=zeros(length(APRR),length(t))';
ni_vt=zeros(length(APRR),length(t))';
rho_in=zeros(length(APRR),length(t))';
mu_in=zeros(length(APRR),length(t))';
k_vt=zeros(length(APRR),length(t))';
a_vt=zeros(length(APRR),length(t))';
v_in=zeros(length(APRR),length(t))';
Re_vt=zeros(length(APRR),length(t))';
cp=zeros(length(APRR),length(t))';
b_vt=zeros(length(APRR),length(t))';
Ra_vt=zeros(length(APRR),length(t))';
Nu_vt=zeros(length(APRR),length(t))';
h_conv_vt=zeros(length(APRR),length(t))';
SOC=NaN(length(APRR),length(t))';

cp_st=zeros(length(APRR),length(t))';
cv_st=zeros(length(APRR),length(t))';
gamma_st=zeros(length(APRR),length(t))';
m_st=zeros(length(APRR),length(t))';
T_st=zeros(length(APRR),length(t))';
P_st=zeros(length(APRR),length(t))';
alpha_st=zeros(length(APRR),length(t))';
T_star_st=zeros(length(APRR),length(t))';
fg_st=zeros(length(APRR),length(t))';
tau_st=zeros(length(APRR),length(t))';
t_star_st=zeros(length(APRR),length(t))';
Tb1=zeros(length(APRR),length(t))';

rho_st=zeros(length(APRR),length(t))';
mu_st=zeros(length(APRR),length(t))';
ni_st=zeros(length(APRR),length(t))';
```

```
k_st=zeros(length(APRR),length(t))';
a_st=zeros(length(APRR),length(t))';
cp1=zeros(length(APRR),length(t))';
b_st=zeros(length(APRR),length(t))';
Ra_st=zeros(length(APRR),length(t))';
Nu_st=zeros(length(APRR),length(t))';
h_conv_st=zeros(length(APRR),length(t))';

h_RV_in=zeros(length(APRR),length(t))';
h_RV_out=zeros(length(APRR),length(t))';
T_RV_out=zeros(length(APRR),length(t))';

%maximum allowed values
rho_lim=24;
T_lim=358;
flow_lim=0.06;
massa_lim=17.75;

for k=1:length(APRR)

    for i=1:length(t)

%%%%%%%%%%%%%%%%%%%%VEHICLE TANK MODEL%%%%%%%%%%%%%%%%%%%%
        P_vt(i,k)=p0_vt+APRR(k)*t(i);

        if i==1
            %determine wall temperature
         Tw(i,k)=exp(-h_conv_vt(i,k)*A_in/(mw*cw))*Tw0+(1-exp(-
h_conv_vt(i,k)*A_in/(mw*cw)))*T0;

            %to calculate hydrogen mass and temperature in vt
   cp_vt(i,k)=CoolProp.PropsSI('C', 'P', p0_vt*1e6, 'T', T0, 'H2');
   cv_vt(i,k)=CoolProp.PropsSI('O', 'P', p0_vt*1e6, 'T', T0, 'H2');
   gamma_vt(i,k)=cp_vt(i,k)/cv_vt(i,k); %heat capacity ratio

            %write the two functions
            F = @(x) [P_vt(i,k) * V_vt - x(1) * Rgas* 1e-
6*x(2)*(1+beta*P_vt(i,k)/x(2));
                x(2)-(m0/x(1))^(1+ h_conv_vt(i,k)*A_in/((x(1)-
m0)*cv_vt(i,k)))*T0-...
                (1-(m0/x(1))^(1+ h_conv_vt(i,k)*A_in/((x(1)-
m0)*cv_vt(i,k))))*(gamma_vt(i,k)*T8+Tw(i,k)*h_conv_vt(i,k)*A_in/((x(
1)-m0)*cv_vt(i,k)))/...
```

```
                (1+ h_conv_vt(i,k)*A_in/((x(1)-m0)*cv_vt(i,k)))];

            x0 = [2.15;288];
            options=optimset('Display','off','TolX', 1e-
4,'MaxFunEvals',20000);

            [x,fval] = fsolve(F,x0,options);
            m_vt(i,k)=x(1);
            T_vt(i,k)=x(2);
            m_flow(i,k)=m_vt(i,k)-m0;

 %%%%%%%%%%%%%%%%%STORAGE TANK MODEL%%%%%%%%%%%%%%%%%%%
            %to calculate hydrogen mass during refueling
            m_st(i,k)=m0_st-m_flow(i,k)*t(i);

            %to calculate hydrogen temperature and pressure in st
  cp_st(i,k)=CoolProp.PropsSI('C', 'P', p0_st*1e6, 'T', T0, 'H2');
  cv_st(i,k)=CoolProp.PropsSI('O', 'P', p0_st*1e6, 'T', T0, 'H2');
  gamma_st(i,k)=cp_st(i,k)/cv_st(i,k); %heat capacity ratio

alpha_st(i,k)=h_conv_st(i,k)*A_in_st/(m_flow(i,k)*cv_st(i,k));
%dimensionless heat transfer coefficient
            T_star_st(i,k)=-
(gamma_st(i,k)*T8+alpha_st(i,k)*Tw0)/(1+alpha_st(i,k));
%characteristic temperature
            t_star_st(i,k)=m0_st/m_flow(i,k); %characteristic time
            tau_st(i,k)=1/t_star_st(i,k); %dimensionless time
            fg_st(i,k)=(1/(1-tau_st(i,k)))^(1+alpha_st(i,k));
%fraction of initial mass over total mass

            T_st(i,k)=fg_st(i,k)*T0+(-1+fg_st(i,k))*T_star_st(i,k);
            P_st(i,k)=m_st(i,k)*Rgas*1e-6*T_st(i,k)/(V_st-
m_st(i,k)*Rgas*1e-6*beta);  %[MPa]

 %%%%%%%%%%%%%%%%%%%%REDUCTION VALVE%%%%%%%%%%%%%%%%%%%
            h_RV_in(i,k)=CoolProp.PropsSI('H', 'P', P_st(i,k)*1e6,
'T', T_st(i,k), 'H2');
            h_RV_out(i,k)=h_RV_in(i,k); %isenthalpic throttling
            T_RV_out(i,k)=CoolProp.PropsSI('T', 'H', h_RV_out(i,k),
'P', P_vt(i,k), 'H2'); %gas outlet temperature from the valve

        else
```

```
 %%%%%%%%%%%%%%%%%%%%VEHICLE TANK MODEL%%%%%%%%%%%%%%%%%%%%
            %determine internal convective heat transfer
(forced+natural convection)
            rho_in(i,k)=CoolProp.PropsSI('D', 'P', P_vt((i-
1),k)*1e6, 'T', T_RV_out((i-1),k), 'H2');
            mu_in(i,k)=CoolProp.PropsSI('V', 'P', P_vt((i-
1),k)*1e6, 'T', T_RV_out((i-1),k), 'H2'); %dynamic viscosity [Pa s]
            v_in(i,k)=m_flow((i-1),k)/4*1/(A_cross*rho_in(i,k));
%fluid velocity [m/s]
            Re_vt(i,k)=rho_in(i,k)*v_in(i,k)*d_int/mu_in(i,k);
%Reynolds number
            Tb(i,k)=(T_vt((i-1),k)+Tw((i-1),k))/2; %bulk
temperature [K]
            rho_vt(i,k)=CoolProp.PropsSI('D', 'P', P_vt((i-
1),k)*1e6, 'T', Tb(i,k), 'H2');
            k_vt(i,k)=CoolProp.PropsSI('L', 'P', P_vt((i-1),k)*1e6,
'T', Tb(i,k), 'H2'); %thermal conductivity [W/m K]
            cp(i,k)=CoolProp.PropsSI('C', 'P', P_vt((i-1),k)*1e6,
'T', Tb(i,k), 'H2');
            a_vt(i,k)=k_vt(i,k)/(rho_vt(i,k)*cp(i,k)); %thermal
diffusivity [m2/s]
            mu_vt(i,k)=CoolProp.PropsSI('V', 'P', P_vt((i-
1),k)*1e6, 'T', Tb(i,k), 'H2');
            ni_vt(i,k)=mu_vt(i,k)/rho_vt(i,k); %kinematic viscosity
[m2/s]
            b_vt(i,k)=1/(Tb(i,k)+beta*P_vt((i-1),k)); %isobaric
expansion coefficient approximation
            Ra_vt(i,k)=g*b_vt(i,k)*(T_vt((i-1),k)-Tw((i-
1),k))*D_int^3/(ni_vt(i,k)*a_vt(i,k)); %Rayleigh number
            Nu_vt(i,k)=0.14*Re_vt(i,k)^0.67+0.0*Ra_vt(i,k)^0.352;
%Nusselt number
            h_conv_vt(i,k)=Nu_vt(i,k)*k_vt(i,k)/D_int; %convective
heat transfer [W/m2 K]

            %determine wall temperature
            Tw(i,k)=exp(-h_conv_vt(i,k)*A_in/(mw*cw))*Tw0+(1-exp(-
h_conv_vt(i,k)*A_in/(mw*cw)))*T_vt((i-1),k);

            %to calculate hydrogen mass and temperature in vt
            cp_vt(i,k)=CoolProp.PropsSI('C', 'P', P_vt((i-
1),k)*1e6, 'T', T_vt((i-1),k), 'H2');
            cv_vt(i,k)=CoolProp.PropsSI('O', 'P', P_vt((i-
1),k)*1e6, 'T', T_vt((i-1),k), 'H2');
```

```
            gamma_vt(i,k)=cp_vt(i,k)/cv_vt(i,k); %heat capacity
ratio

            %write the two functions
            x0 = [x(1)+0.01;x(2)];
            options=optimset('Display','off','TolX', 1e-4,
'MaxFunEvals', 20000);

            F = @(x) [P_vt(i,k) * V_vt - x(1) * Rgas*1e-
6*x(2)*(1+beta*P_vt(i,k)/x(2));
                x(2)-(m0/x(1))^(1+h_conv_vt(i,k)*A_in/((x(1)-
m_vt((i-1),k))*cv_vt(i,k)))*T0-...
                (1-(m0/x(1))^(1+h_conv_vt(i,k)*A_in/((x(1)-m_vt((i-
1),k))*cv_vt(i,k))))*(gamma_vt(i,k)*T_RV_out((i-
1),k)+Tw(i,k)*h_conv_vt(i,k)*A_in/((x(1)-m_vt((i-
1),k))*cv_vt(i,k)))/...
                (1+h_conv_vt(i,k)*A_in/((x(1)-m_vt((i-
1),k))*cv_vt(i,k)))];

            [x,fval] = fsolve(F,x0,options);
            m_vt(i,k)=x(1);

            %break mass
            if (m_vt(i,k)>massa_lim), break, end
            %break temperature
            T_vt(i,k)=x(2);
            if (T_vt(i,k)> T_lim), disp('superato il valore massimo
di temperatura'), end
            m_flow(i,k)=m_vt(i,k)-m_vt((i-1),k);
            %break mass flow
            if (m_flow(i,k)> flow_lim), disp('superato il valore
massimo di portata'), end
            %break density
            if (rho_vt(i,k)> rho_lim), disp('superato il valore
massimo di densità'), break, end

            %determine state of charge
      rho_target=CoolProp.PropsSI('D', 'P', 35*1e6, 'T', T0, 'H2');
      SOC(i,k)=rho_vt(i,k)/rho_target; %state of charge

 %%%%%%%%%%%%%%%%%%%%%%STORAGE TANK MODEL%%%%%%%%%%%%%%%%%%%%
            %to calculate hydrogen mass during refueling
            m_st(i,k)=m0_st-m_flow(i,k)*t(i);
```

```
            %determine internal convective heat transfer (discharge)
             Tb1(i,k)=(T_st((i-1),k)+Tw0)/2; %bulk temperature [K]
             rho_st(i,k)=CoolProp.PropsSI('D', 'P', P_st((i-
1),k)*1e6, 'T', Tb1(i,k), 'H2');
             k_st(i,k)=CoolProp.PropsSI('L', 'P', P_st((i-1),k)*1e6,
'T', Tb1(i,k), 'H2'); %thermal conductivity [W/m K]
             cp1(i,k)=CoolProp.PropsSI('C', 'P', P_st((i-1),k)*1e6,
'T', Tb1(i,k), 'H2');
             a_st(i,k)=k_st(i,k)/(rho_st(i,k)*cp1(i,k)); %thermal
diffusivity [m2/s]
             mu_st(i,k)=CoolProp.PropsSI('V', 'P', P_st((i-
1),k)*1e6, 'T', Tb1(i,k), 'H2');
             ni_st(i,k)=mu_st(i,k)/rho_st(i,k); %kinematic viscosity
[m2/s]
             b_st(i,k)=1/(Tb1(i,k)+beta*P_st((i-1),k)); %isobaric
expansion coefficient approximation
             Ra_st(i,k)=g*b_st(i,k)*(Tw0-T_st((i-
1),k))*H^3/(ni_st(i,k)*a_st(i,k)); %Rayleigh number
             Nu_st(i,k)=0.104*Ra_st(i,k)^0.352; %Nusselt number
             h_conv_st(i,k)=Nu_st(i,k)*k_st(i,k)/H; %convective heat
transfer [W/m2 K]

             %to calculate hydrogen temperature and pressure in st
             cp_st(i,k)=CoolProp.PropsSI('C', 'P', P_st((i-
1),k)*1e6, 'T', T_st((i-1),k), 'H2');
             cv_st(i,k)=CoolProp.PropsSI('O', 'P', P_st((i-
1),k)*1e6, 'T', T_st((i-1),k), 'H2');
 gamma_st(i,k)=cp_st(i,k)/cv_st(i,k); %heat capacity ratio

alpha_st(i,k)=h_conv_st(i,k)*A_in_st/(m_flow(i,k)*cv_st(i,k));
%dimensionless heat transfer coefficient
             T_star_st(i,k)=-
(gamma_st(i,k)*T8+alpha_st(i,k)*Tw0)/(1+alpha_st(i,k));
%characteristic temperature
             fg_st(i,k)=(m0_st/m_st(i,k))^(1+alpha_st(i,k));
%fraction of initial mass over total mass
             t_star_st(i,k)=m0_st/m_flow(i,k); %characteristic time
             tau_st(i,k)=1/t_star_st(i,k); %dimensionless time
             fg_st(i,k)=(1/(1-tau_st(i,k)))^(1+alpha_st(i,k));
%fraction of initial mass over total mass
```

```
            T_st(i,k)=fg_st(i,k)*T0+(-1+fg_st(i,k))*T_star_st(i,k);
%[K]
            P_st(i,k)=m_st(i,k)*Rgas*1e-6*T_st(i,k)/(V_st-
m_st(i,k)*Rgas*1e-6*beta);  %[MPa]

 %%%%%%%%%%%%%%%%%%%%REDUCTION VALVE%%%%%%%%%%%%%%%%%%%
            h_RV_in(i,k)=CoolProp.PropsSI('H', 'P', P_st(i,k)*1e6,
'T', T_st(i,k), 'H2');
            h_RV_out(i,k)=h_RV_in(i,k); %isenthalpic throttling
            T_RV_out(i,k)=CoolProp.PropsSI('T', 'H', h_RV_out(i,k),
'P', P_vt(i,k), 'H2'); %gas outlet temperature from the valve

        end
    end
 end

 %%%%%%%%%%REFUELING OF STORAGE TANK MODEL%%%%%%%%%%%%

 %data
 V_st=11; %volume storage [m3]
 p0_st=47.75; %final pressure after refueling vehicle [MPa]
 T0=287.99; %final temperature after refueling vehicle [K]
 m0_st=335.67; %initial mass  [kg]
 T8=288; %inlet flow temperature [K]
 Tw0=288; %initial temperature of tank wall [K]
 A_in=97.47; %internal surface area  [m2]
 mflow_in=0.0062; %mass flow from the compressor [kg/s]

 t=1:1:2500;

 %%%%%allocation of profiles%%%%%%%%
 cp_st=zeros(1,length(t))';
 cv_st=zeros(1,length(t))';
 gamma_st=zeros(1,length(t))';
 alpha_st=zeros(1,length(t))';
 T_star_st=zeros(1,length(t))';
 fg_st=zeros(1,length(t))';
 rho_st=zeros(1,length(t))';
 m_st=zeros(1,length(t))';
 T_st=zeros(1,length(t))';
 P_st=zeros(1,length(t))';
 tau_st=zeros(1,length(t))';
 t_star_st=zeros(1,length(t))';
```

```
 rho=zeros(1,length(t))';
 mu=zeros(1,length(t))';
 k_st=zeros(1,length(t))';
 a_st=zeros(1,length(t))';
 b_st=zeros(1,length(t))';
 Ra_st=zeros(1,length(t))';
 ni_st=zeros(1,length(t))';
 Nu=zeros(1,length(t))';
 h_conv_st=zeros(1,length(t))';

 P_out=zeros(1,length(t))';
 beta_2st=zeros(1,length(t))';
 beta_tot=zeros(1,length(t))';
 F_out=zeros(1,length(t))';
 T_out_is=zeros(1,length(t))';
 T_out=zeros(1,length(t))';
 h_out_is=zeros(1,length(t))';
 h_out=zeros(1,length(t))';

 for i=1:length(t)

     %to calculate hydrogen mass during refueling
     m_st(i)=m0_st+mflow_in*t(i);

     if i==1

     cp_st(i)=CoolProp.PropsSI('C', 'P', p0_st*1e6, 'T', T0, 'H2');
     cv_st(i)=CoolProp.PropsSI('O', 'P', p0_st*1e6, 'T', T0, 'H2');
     gamma_st(i)=cp_st(i)/cv_st(i); %heat capacity ratio
     alpha_st(i)=h_conv_st(i)*A_in/(mflow_in*cv_st(i));
%dimensionless heat transfer coefficient

T_star_st(i)=(gamma_st(i)*T8+alpha_st(i)*Tw0)/(1+alpha_st(i));
%characteristic temperature
     t_star_st(i)=m0_st/mflow_in; %characteristic time
     tau_st(i)=1/t_star_st(i); %dimensionless time
     fg_st(i)=(1/(1+tau_st(i)))^(1+alpha_st(i)); %fraction of
initial mass over total mass

         %to calculate hydrogen temperature and pressure in st
         T_st(i)=fg_st(i)*T0+(1-fg_st(i))*T_star_st(i);
```

```
        P_st(i)=m_st(i)*Rgas*1e-6*T_st(i)/(V_st-m_st(i)*Rgas*1e-
6*beta);  %[MPa]

    else

        cp_st(i)=CoolProp.PropsSI('C', 'P', P_st(i-1)*1e6, 'T',
T_st(i-1), 'H2');
        cv_st(i)=CoolProp.PropsSI('O', 'P', P_st(i-1)*1e6, 'T',
T_st(i-1), 'H2');
        gamma_st(i)=cp_st(i)/cv_st(i); %heat capacity ratio

        %determine convective heat transfer (Tb=Tgas)
       rho(i)=CoolProp.PropsSI('D', 'P', P_st(i-1)*1e6, 'T',
T_st(i-1), 'H2');
        mu(i)=CoolProp.PropsSI('V', 'P', P_st(i-1)*1e6, 'T',T_st(i-
1), 'H2');
        k_st(i)=CoolProp.PropsSI('L', 'P', P_st(i-1)*1e6,
'T',T_st(i-1), 'H2');
        a_st(i)=k_st(i)/(rho(i)*cp_st(i)); %thermal diffusivity
[m2/s]
        ni_st(i)=mu(i)/rho(i); %kinematic viscosity [m2/s]
        b_st(i)=1/(T_st(i-1)+beta*P_st(i-1)); %isobaric expansion
coefficient approximation
        Ra_st(i)=g*b_st(i)*(Tw0-T_st(i-1))*H^3/(ni_st(i)*a_st(i));
%Rayleigh number
        Nu(i)=0.104*Ra_st(i)^0.352; %Nusselt number
        h_conv_st(i)=Nu(i)*k_st(i)/H; %convective heat transfer
[W/m2 K]

        %to calculate hydrogen temperature and pressure in st
        alpha_st(i)=h_conv_st(i)*A_in/(mflow_in*cv_st(i));
%dimensionless heat transfer coefficient
        T_star_st(i)=(gamma_st(i)*T_out(i-
1)+alpha_st(i)*Tw0)/(1+alpha_st(i)); %characteristic temperature
        t_star_st(i)=m0_st/mflow_in; %characteristic time
        tau_st(i)=1/t_star_st(i); %dimensionless time
        fg_st(i)=(1/(1+tau_st(i)))^(1+alpha_st(i)); %fraction of
initial mass over total mass

        %to calculate hydrogen temperature and pressure in st
        T_st(i)=fg_st(i)*T0+(1-fg_st(i))*T_star_st(i); %[K]
P_st(i)=m_st(i)*Rgas*1e-6*T_st(i)/(V_st-m_st(i)*Rgas*1e-6*beta);
%[MPa]
```

```
    end
end

%%%%%%%%%%%%%%%%%%%%%%%%%COMPRESSION%%%%%%%%%%%%%%%%%%%
%parameters
V_cyl=4.25*1e-4; %cylinder volume [m3]
c=10; %clearance [%]
%input
T_in=288; %inlet temperature [K]
P_in=3; %inlet pressure [MPa]
beta_1st=4; %compression rario 1st stage
P_int=P_in*beta_1st; %intermediate pressure
eta_el=0.97;
eta_mech=0.95;

t=1:1:2500;

P_out=zeros(1,length(t))';
beta_2st=zeros(1,length(t))';
beta_tot=zeros(1,length(t))';
F_out=zeros(1,length(t))';
T_out_is=zeros(1,length(t))';
T_out=zeros(1,length(t))';
h_out_is=zeros(1,length(t))';
h_out=zeros(1,length(t))';
dH2_st=zeros(1,length(t))';
dH_tot=zeros(1,length(t))';
W2=zeros(1,length(t))';
Wtot=zeros(1,length(t))';
Z_out=zeros(1,length(t))';
eta_v=zeros(1,length(t))';

%thermodynamic data initial conditions
cp=CoolProp.PropsSI('C', 'P', P_in*1e6, 'T', T_in, 'H2');
cv=CoolProp.PropsSI('O', 'P', P_in*1e6, 'T', T_in, 'H2');
gamma=cp/cv;
h_in=CoolProp.PropsSI('H', 'P', P_in*1e6, 'T', T_in, 'H2');
s_in=CoolProp.PropsSI('S', 'P', P_in*1e6, 'T', T_in, 'H2');
rho_in=CoolProp.PropsSI('D', 'P', P_in*1e6, 'T', T_in, 'H2');
Z_in=CoolProp.PropsSI('Z', 'P', P_in*1e6, 'T', T_in, 'H2');

%isentropic compressions
s_int1_is=s_in; %fist stage
```

```
 s_int2=CoolProp.PropsSI('S', 'P', P_int*1e6, 'T', T_in, 'H2');
 s_out_is=s_int2;

 %%% 1st STAGE at fixed beta %%%
 %Find isentropic temperature and enthalpy intermidiate stage
 options=optimset('Display','final','TolX', 1e-4);
 F_int=@(x) CoolProp.PropsSI('S', 'P', P_int*1e6, 'T', x, 'H2')-
s_in;
 T_start=T_in;
 T_int1_is=fsolve(F_int,T_start,options);
 h_int1_is=CoolProp.PropsSI('H', 'P', P_int*1e6, 'T', T_int1_is,
'H2');

 %Find real temperature and enthalpy intermidiate stage
 eta_is=@(P1,P2) 0.1091*log(P2/P1)^3-
0.5247*log(P2/P1)^2+0.8577*log(P2/P1)+0.3727;
 h_int1=h_in+(h_int1_is-h_in)/eta_is(P_in,P_int);
 T_int1=CoolProp.PropsSI('T', 'P', P_int*1e6, 'H', h_int1, 'H2');
 rho_int1=CoolProp.PropsSI('D', 'P', P_int*1e6, 'T', T_int1, 'H2');

 %%%IC%%%%
 h_int2=CoolProp.PropsSI('H', 'P', P_int*1e6, 'T', T_in, 'H2');
 Q_ic=mflow_in*(h_int1-h_int2)/1000; %[kW]

 for i=1:length(t)

     %compression ratios
     P_out(i)=P_st(i); %total outlet pressure [MPa]
     beta_tot(i)=P_out(i)/P_in; %compression ratio tot
     beta_2st(i)=beta_tot(i)/beta_1st; %compression ratio second
stage

     %%%2nd STAGE%%%
     %Find isentropic temperature and enthalpy outlet
     F_out=@(x) CoolProp.PropsSI('S', 'P', P_out(i)*1e6, 'T', x,
'H2')-s_int2;
     T_out_is(i)=fsolve(F_out,T_start,options);
     h_out_is(i)=CoolProp.PropsSI('H', 'P', P_out(i)*1e6, 'T',
T_out_is(i), 'H2');

     %Find real temperature and enthalpy outlet/last stage
     h_out(i)=h_int2+(h_out_is(i)-h_int2)/eta_is(P_int,P_out(i));
```

```
    T_out(i)=CoolProp.PropsSI('T', 'P', P_out(i)*1e6, 'H',
h_out(i), 'H2');

    %convert to specific energy consumption [kWh/kg]
    dH1_st=(h_int1-h_in)*(1/3600000);
    dH2_st(i)=(h_out(i)-h_int2)*(1/3600000);
    dH_tot(i)=dH1_st+dH2_st(i)*(1/3600000);

    %compression work
    W1=mflow_in*(h_int1-h_in)/1000; %kW
    W2(i)=mflow_in*(h_out(i)-h_int2)/1000; %kW
    Wtot(i)=(W1+W2(i))*eta_el*eta_mech; %[kW]

    %volumetric efficiency
    Z_out(i)=CoolProp.PropsSI('Z', 'P', P_out(i)*1e6, 'T',T_out(i),
'H2');
    eta_v=@(P1,P2) (100-(P2/P1)-c*(Z_in/Z_out(i)*(P2/P1)^(1/gamma)-
1))*1e-2;
    %speed (piston strokes per second)
    speed=@(eta,rho) mflow_in/(V_cyl*rho*eta);  %[1/s]
    N=speed(eta_v(P_in,P_int), rho_in);
 end
```